



**INVESTIGATION OF DOUBLE-BLADED
DARRIEUS TURBINE POWER PERFORMANCE
BY USING UNSTEADY CFD**

**2024
MASTER THESIS
MECHANICAL ENGINEERING**

Yasser Abbas Ali AL-SUDANI

**Thesis Advisor
Assist. Prof. Dr. Mehmet BAKIRCI**

**INVESTIGATION OF DOUBLE-BLADED DARRIEUS TURBINE POWER
PERFORMANCE BY USING UNSTEADY CFD**

Yasser Abbas Ali AL-SUDANI

Thesis Advisor

Assist. Prof. Dr. Mehmet BAKIRCI

T.C.

Karabük University

Institute of Graduate Programs

Department of Mechanical Engineering

Prepared as

Master Thesis

KARABÜK

December 2023

I certify that in my opinion the thesis submitted by Yasser Abbas Ali AL-SUDANI titled "INVESTIGATION OF DOUBLE-BLADED DARRIEUS TURBINE POWER PERFORMANCE BY USING UNSTEADY CFD" is fully adequate in scope and quality as a thesis for the degree of Master of Science.

Assist. Prof. Dr. Mehmet BAKIRCI
Thesis Advisor, Department of Mechanical Engineering

This thesis is accepted by the examining committee with a unanimous vote in the Department of Mechanical Engineering as a Master of Science thesis. 14 12, 2023

Examining Committee Members (Institutions) Signature

Chairman : Assoc. Prof. Dr. Okan ÜNAL (KBU)

Member : Assoc. Prof. Dr. Battal DOĞAN (GU)

Member : Assist. Prof. Dr. Mehmet BAKIRCI (KBU)

The degree of Master of Science by the thesis submitted is approved by the Administrative Board of the Institute of Graduate Programs, Karabük University.

Assoc. Prof. Dr. Zeynep ÖZCAN
Director of the Institute of Graduate Programs

“I declare that all the information within this thesis has been gathered and presented in accordance with academic regulations and ethical principles and I have according to the requirements of these regulations and principles cited all those which do not originate in this work as well.”

Yasser Abbas Ali AL- SUDANI

ABSTRACT

M. Sc. Thesis

INVESTIGATION OF DOUBLE-BLADED DARRIEUS TURBINE POWER PERFORMANCE BY USING UNSTEADY CFD

Yasser Abbas Ali AL- SUDANI

Karabük University

Institute of Graduate Programs

The Department of Mechanical Engineering

Thesis Advisor:

Assist. Prof. Dr. Mehmet BAKIRCI

December 2023, 132 pages

Wind speed and direction are key factors in selecting a wind turbine. Different designs are required for different wind conditions. Vertical- axis wind turbines are preferred, especially in frequently changing wind directions. There are different types of Darius turbines among these vertical turbines. They are classified according to their straight or spiral structure and the number of blades. The performance of the Darrieus turbines and the effects of design changes are examined through CFD analysis. In this study, a single-blade design and three new designs with the addition of second blades for a three-blade Darius turbine were presented. The performance of these new designs and standard Darius turbines was compared. The performance of these four designs was measured and analyzed in different wind conditions. CFD analyzes examined the flow characteristics in detail and contributed to the design development. Unsteady-state CFD analyzes and visualizes how flow characteristics affect turbine performance.

The CFD analysis revealed the operational conditions for four designs. Design 1 achieved its highest C_p value of 0.272 at a TSR value of 5. Design 2 was not successful because DWT had no performance improvement. For Design 3, the peak C_p of 0.213 occurred at a TSR of 3.25, while Design 4 reached its highest C_p value of 0.110 at a TSR of 1. Additionally, all designs produced a negative torque value at a TSR of 10.

Key Words : Darrieus, Double Blade, Unsteady, CFD.

Science Code : 91441

ÖZET

Yüksek Lisans Tezi

ÇİFT ROTORLU DARRIEUS TÜRBİN GÜÇ PERFORMANSININ ZAMANA BAĞLI CFD İLE İNCELENMESİ

Yasser Abbas Ali AL-SUDANI

Karabük Üniversitesi

Lisansüstü Eğitim Enstitüsü

Makina Mühendisliği Anabilim Dalı

Tez Danışmanı:

Dr. Öğr. Üyesi Mehmet BAKIRCI

Aralık 2023, 132 sayfa

Rüzgâr hızı ve yönü, bir rüzgâr türbini seçiminde kritik faktörlerdir. Farklı rüzgâr koşulları için farklı tasarımlar gereklidir. Özellikle doğrultusu sık değişen rüzgâr için dikey eksenli rüzgâr türbinleri tercih edilmektedir. Bu dikey türbinlerden biri de farklı tasarımlara sahip Darrieus türbinleridir. Bu türbinler, düz veya spiral yapılarına ve kanat sayılarına göre sınıflandırılırlar. Literatürde, Darrieus türbinlerinde yapılan tasarım değişikliklerin, türbin güç performansını nasıl etkilediğini Hesaplamalı Akışkanlar Dinamiği (HAD) ile inceleyen birçok çalışma bulunmaktadır. Bu mevcut çalışmada, üç kanatlı standart Darrieus türbin kanatlarına, rotor merkezine daha yakın olacak şekilde ikinci kanatların eklendiği üç yeni tasarım sunulmuştur. Bu yeni tasarımların ve standart Darrieus türbinin performansları farklı uç hız oranlarında HAD ile analiz edilmiştir. CFD analizi dört tasarım için çalışma koşullarını ortaya koymuştur. Tasarım 1, 5 TSR değerinde en yüksek C_p değeri olan 0,272'ye ulaşmıştır. Tasarım 2 başarılı olamamıştır çünkü DWT performans artışı sağlamamıştır. Tasarım

3 için 0,213'lük en yüksek Cp değeri 3,25 TSR değerinde gerçekleşirken, Tasarım 4 en yüksek Cp değeri olan 0,110'a 1 TSR değerinde ulaşmıştır. Ayrıca, tüm tasarımlar 10 TSR değerinde negatif tork değeri üretmiştir.

Anahtar Kelimeler : Darrieus, Çift Kanatlı, Zamana bağlı HAD.

Bilim Kodu : 91441

ACKNOWLEDGMENT

In the name of Allah, the beneficent, the merciful

Praise be to Allah, Lord of the Worlds, and prayers and peace be upon those who do not have a prophet after him. We praise and thank him for giving us the strength and determination to complete my master's thesis. Thanks to my father, may Allah have mercy on him, who instilled in me the love of excellence and achievement. thanks and gratitude to my mother; may Allah Almighty protect her for her constant prayers and support for me; and thanks go to my beloved brother and sisters and their husbands who supported me in all circumstances.

I would also like to express my sincere gratitude to my direct supervisor, Assist. Prof. Dr. Mehmet BAKIRCI, for the support he has provided me through his continuous guidance, helpful advice, patience, and support throughout the writing of this dissertation.

CONTENTS

	<u>Page</u>
APPROVAL.....	ii
ABSTRACT.....	iv
ÖZET.....	vi
ACKNOWLEDGMENT.....	viii
CONTENTS.....	ix
LIST OF FIGURES	xii
LIST OF TABLES	xvi
SYMBOLS AND ABBREVIATIONS	xvii
PART 1	1
INTRODUCTION	1
1.1. BACKGROUND.....	1
1.2. ENERGY RESOURCES.....	1
1.3. WIND ENERGY	2
1.4. WIND TURBINE.....	3
1.4.1. Horizontal Axis Wind Turbine (HAWT)	5
1.4.2. Vertical Axis Wind Turbine (VAWT).....	6
1.4.2.1. Savonius VAWT.....	7
1.4.2.2. Darrieus VAWT	8
1.5. MOTIVATION	9
1.6. PROBLEM STATEMENT	10
1.7. OBJECTIVES OF THE PRESENT WORK	11
1.8. THESIS LAYOUT	11
PART 2	12
LITERATURE REVIEW.....	12
2.1. BACKGROUND.....	12
2.2. DARRIEUS VAWT AIMS AND LIMITATIONS.....	13
2.3. BLADE SHAPE OF DVAWT	14

	<u>Page</u>
2.3.1. H- Blade.....	15
2.3.2. Twisted Blade	16
2.3.2. Helical Blade	17
2.4. VERTICAL AXIS WIND TURBINE PERFORMANCE	17
2.4.1. The Significance of Blade Number	19
2.4.2. Tip Speed Ratio	21
2.4.3. Aspect Ratio.....	23
2.5. ENVIRONMENTAL IMPACT	24
2.5.1. Sound and Visual Influence.....	25
2.5.2. Impact on Animals and Birds	26
2.5.3. Climate Change	27
2.6. SUMMARY OF PREVIOUS STUDIES	28
2.7. ORIGINAL POINTS OF PRESENT WORK	29
PART 3	30
WIND TURBINE MODELING	30
3.1. INTRODUCTION.....	30
3.2. ANALYSIS PARAMETERS OF A WIND TURBINE.....	30
3.2.1. Power Coefficient (C_p)	31
3.2.2. Tip Speed Ratio (TSR)	32
3.2.3. The Swept Area (A_s).....	33
3.2.4. Number of Blades (N_b)	33
3.2.5. Chord Length of The Blade (c).....	33
3.2.6. Solidity (σ).....	34
3.2.7 Initial Attack Angle (α)	35
3.3. DVAWT ANALYSIS	35
3.3.1. Actuator Disk Method	37
3.3.2. Double Actuator Disk Procedure.....	39
3.3.3. The Rotor Disk Procedure	39
3.3.4. Theory of Blade-Element/Momentum (BEM)	40
3.3.5. Method of Double Multiple Streamtube (DMS)	40
3.3.6. The Vortex Method.....	41
3.3.7. Computational Fluid Dynamics (CFD)	42

	<u>Page</u>
3.4. NUMERICAL MODELING	42
3.4.1. The Boundary Conditions.....	43
3.4.2. Turbulence Models	44
3.4.3. Mesh Dependency	46
3.4.4. Orthogonal Mesh Quality	47
3.5. VALIDATION CASE STUDY.....	50
PART4	61
RESULTS AND DISCUSSION	61
4.1. INTRODUCTION.....	61
4.2. PRESENT CASE STUDIES	61
4.3. NUMERICAL RESULTS	64
4.3.1. Wind Turbine Torque History	64
4.3.2. Power Coefficient	75
4.3.3. Velocity Field	78
4.3.4. Velocity Stretched Swirling Strength	81
4.3.5. Turbulent Kinetic Energy	85
4.3.6. Turbulence Intensity	89
4.3.7. Total Pressure Distribution	93
4.3.8. Turbulence Eddy Dissipation	97
4.3.9. Velocity Invariant Q	101
4.3.10. Velocity Swirling Strength	105
PART 5	111
CONCLUSIONS AND RECOMMENDATIONS	111
5.1. CONCLUSIONS	111
5.2. RECOMMENDATIONS	112
REFERENCES.....	113
APPENDIX A. TABLES	125
APPENDIX B. CONTOUR FIGURES FOR DESIGNS.....	128
RESUME	132

LIST OF FIGURES

	<u>Page</u>
Figure 1.1. Wind turbines classifications	5
Figure 2.1. Displaying the aerodynamic efficiency of a Vertical Axis Wind Turbine (VAWT) is crucial in assessing its performance	18
Figure 2.2. The trajectory of efficiency for a Vertical Axis Wind Turbine (VAWT).....	18
Figure 2.3. Pictorial Depiction of a Steady and Robust Vertical Axis Wind Turbine (VAWT) with Varied Blade Count.	19
Figure 3.1. Flow chart of Wind Turbine Design Parameters.	31
Figure 3.2. Airfoil (DU06W200) cross-section	34
Figure 3.3. Nomenclature of airfoil.....	35
Figure 3.4. Forces and velocities of the blades of DWT.....	36
Figure 3.5. Flowchart of wind turbine analysis.....	37
Figure 3.6. The control volume for the model.	38
Figure 3.7. Schematic of two-actuator disk.....	39
Figure 3.8. Illustration of the velocity field for the actuator disk theory in the DMS approach.....	41
Figure 3.9. The 2D computational domain for the DVAWT model.....	44
Figure 3.10. Rotational domain for the DVAWT model.	45
Figure 3.11. Mesh generation for CFD domains with different views.	46
Figure 3.12. Mesh Orthogonal Quality Generation for CFD.....	48
Figure 3.13. Mesh generation technique in the present study.....	49
Figure 3.14. The 2D computational domain for DVAWT model according to.....	51
Figure 3.15. Rotational domain for the DVAWT model.	51
Figure 3.16. Mesh generation for CFD domains with different views.	52
Figure 3.17. Power Coefficient (C_p) versus Tip Speed Ratio.	53
Figure 3.18. Torque variation of Darrieus for the present CFD study.	53
Figure 3.19. Velocity field contour.....	54
Figure 3.21. Turbulent kinetic energy contour.....	56
Figure 3.22. Turbulence intensity contour.	57
Figure 3.23. Total pressure contour.	57
Figure 3.24. Turbulence eddy dissipation contour.....	58

	<u>Page</u>
Figure 3.25. Velocity invariant Q contour.	59
Figure 3.26. Velocity swirling strength contour.	60
Figure 4.1. Design studies of present research.	62
Figure 4.2. Boundary condition of velocity vector profile at the inlet.	63
Figure 4.3. Boundary condition of the non-uniform velocity profile at the inlet.	63
Figure 4.4. Wind turbine torque history for Design 1, TSR=0.5.	65
Figure 4.5. Wind turbine torque history for Design 1, TSR=1.	65
Figure 4.6. Wind turbine torque history for Design 1, TSR=3.25.	66
Figure 4.7. Wind Turbine torque history for design 1, TSR=5.	66
Figure 4.8. Wind turbine torque history for Design 1, TSR=10.	66
Figure 4.9. Wind turbine torque history for Design 2, TSR=3.25.	67
Figure 4.10. Wind turbine torque history for Design 3, TSR=0.5.	68
Figure 4.11. Wind turbine torque history for Design 3, TSR=1.	68
Figure 4.12. Wind turbine torque history for Design 3, TSR=3.25.	69
Figure 4.13. Wind turbine torque history for Design 3, TSR=5.	69
Figure 4.14. Wind turbine torque history for Design 3, TSR=10.	69
Figure 4.15. Wind turbine torque history for Design 4, TSR=0.5.	70
Figure 4.16. Wind turbine torque history for Design 4, TSR=1.	71
Figure 4.17. Wind turbine torque history for Design 4, TSR=3.25.	71
Figure 4.18. Wind turbine torque history for Design 4, TSR=5.	71
Figure 4.19. Wind turbine torque history for Design 4, TSR=10.	72
Figure 4.20. Torque history for Design 1, TSR=5 for nonuniform velocity profile at inlet.	74
Figure 4.21. Torque history for Design 3, TSR=3.25 for nonuniform velocity profile at inlet.	74
Figure 4.22. Torque history for Design 4, TSR=1 for nonuniform velocity profile at inlet.	75
Figure 4.23. Power coefficient vs. TSR for Design 1.	76
Figure 4.24. Power coefficient vs. TSR for Design 3.	76
Figure 4.25. Power coefficient vs. TSR for Design 4.	76
Figure 4.26. Power coefficient vs. TSR for different Designs.	77
Figure 4.27. Velocity contour in stn frame after four cycles for Design 1.	78
Figure 4.28. Velocity contour in stn frame after four cycles for Design 2.	79
Figure 4.29. Velocity contour in stn frame after four cycles for Design 3.	80

	<u>Page</u>
Figure 4.30. Velocity contour in stn frame after four cycles for Design 4.	80
Figure 4.31. Velocity stretched swirling strength contour after four cycles for Design 1.	82
Figure 4.32. Velocity stretched swirling strength contour after four cycles for Design 2.	82
Figure 4.33. Velocity stretched swirling strength contour after four cycles for Design 3.	83
Figure 4.34. Velocity Stretched Swirling Strength contour after four cycles Design 4.	84
Figure 4.35. Turbulent kinetic energy contour after four cycles for Design 1.....	86
Figure 4.36. Turbulent kinetic energy contour after four cycles for Design 2.....	87
Figure 4.37. Turbulent kinetic energy contour after four cycles for Design 3.....	88
Figure 4.38. Turbulent kinetic energy contour after four cycle Design1.....	88
Figure 4.39. Turbulence intensity contour after four cycles Design 1.....	90
Figure 4.40. Turbulence intensity contour after four cycles Design 2.....	91
Figure 4.41. Turbulence intensity contour after four cycles Design 3.....	92
Figure 4.42. Turbulence intensity contour after four cycles Design 4.....	92
Figure 4.43. Total pressure contour after four cycles Design 1.....	95
Figure 4.44. Total pressure contour after four cycles Design 2.....	95
Figure 4.45. Total pressure contour after four cycles Design 3.....	96
Figure 4.46. Total pressure contour after four cycles, Design 4.....	97
Figure 4.47. Turbulence eddy dissipation contour after four cycles Design 1.	98
Figure 4.48. Turbulence eddy dissipation contour after four cycles.....	99
Figure 4.49. Turbulence eddy dissipation contour after four cycles Design 3.	99
Figure 4.50. Turbulence eddy dissipation contour after four cycle Design 4.....	100
Figure 4.51. Velocity invariant Q contour after four cycles Design 1.....	102
Figure 4.52. Velocity invariant Q contour after four cycles Design 2.....	103
Figure 4.53. Velocity invariant Q contour after four cycles Design 3.....	104
Figure 4.54. Velocity invariant Q contour after four cycles design 4.....	104
Figure 4.55. Velocity swirling strength contour, Design1.....	107
Figure 4.56. Velocity swirling strength contour Design 2.....	108
Figure 4.57. Velocity swirling strength contour Design 3.....	109
Figure 4.58. Velocity swirling strength contour Design 4.....	109
Figure Appendix B1. Streamlines contours, Design 1.....	129
Figure Appendix B2. Streamlines contours, Design 3.....	129

	<u>Page</u>
Figure Appendix B3. Streamlines contours, Design 4.....	130
Figure Appendix B4. Time step contour at 1.02102 seconds, Design 4.....	130
Figure Appendix B5. Time step contour at 3.06305 seconds, Design 4.....	131
Figure Appendix B6. Time step contour at 7.85049 seconds, Design 4.....	131

LIST OF TABLES

	<u>Page</u>
Table 2.1. Comparing Design Features of a Two-Blade vs. Three-Blade Turbine ...	21
Table 2.2. Summary of VAWT airfoil development.	28
Table 3.1. Grid optimization (Design 3, TSR=3.25)	47
Table 3.2. Validation case study details.....	50
Table 4.1. The wind turbine parameters and power coefficient for Design 1.....	72
Table 4.2. The wind turbine parameters and power coefficient for Design 3.....	72
Table 4.3. The wind turbine parameters and power coefficient for Design 4.....	73

SYMBOLS AND ABBREVIATIONS

SYMBOLS

T	: Torque (Nm.)
t	: Flow time (s)
N	: Rotational speed (m/s)
D	: Diameter (m)
ω	: Angular velocity (rad/s)
P_A	: Available power of wind (Watt)
V_t	: Tangential velocity (m/s)
P_{actual}	: Power Actual (Watt)
A_s	: Surface area of panel (m ²)
E	: Kinetic energy (J)
m	: Mass of air (kg)
\dot{m}	: Mass flow rate (kg/s)
P	: Power of wind (Watt)
C_p	: Power Coefficient
ρ	: Air density (kg /m ³)
u	: Wind speed(m/s)
C	: Chord length
α	: Angle of inclination of the blades
C_l	: lift coefficient
C_c	: Instantaneous lift coefficient
C_d	: Drag coefficient

ABBREVIATIONS

WT	: Wind Turbine
CFD	: Computational Fluid Dynamics

VAWT : Vertical Axis Wind Turbine
TSR : Tip Speed Ratio
HAWT : Horizontal Axis Wind Turbine
URANS : Unsteady Reynolds Averaged Navier-Stokes
2D : 2 Dimensions
3D : 3 Dimensions
DVAWT : Darrieus Vertical Axis Wind Turbine
NACA : National Advisory Committee for Aeronautics
AOA : Angle of Attack
TEDC : Turbulence Eddy Dissipation Contour
Ti : Turbulence Intensity
AEO : Yearly Energy Output Annual,
VSSS : Velocity Stretched swirling strength
DDVAWT : Darrieus Double-blade Vertical Axis Wind Turbine

PART 1

INTRODUCTION

1.1. BACKGROUND

Today, we are following an unsustainable path with energy sources obtained from fossil fuels. However, renewable energy sources, especially wind energy, have significant potential to meet our energy needs. Wind energy is increasingly preferred because it is infinitely renewable as a natural resource and does not harm the environment. The development of this technology plays an important role in meeting energy needs worldwide. With the establishment of wind energy facilities, many benefits are provided, such as reducing carbon emissions, increasing energy security, and supporting economic development. With increasing investments in renewable energy sources, resources such as wind energy may be able to meet a large part of our energy needs in the future. Therefore, this growing interest and investments in renewable energy sources can form the basis of a sustainable future in the energy sector and around the world[1].

1.2. ENERGY RESOURCES

Energy options include using the Earth's reserves, although this may last for thousands of years. This applies to fission (next-generation reactors) and fusion as a nuclear energy source. As for the sources of nuclear fusion, which are not currently available due to the inability to properly control the energy released, the availability of “fuel” would cover the world’s energy needs many times over. Furthermore, renewable refers to all sources that replenish themselves or are replenished in a relatively short period with the same amount consumed; therefore, it is inexhaustible at the human level. This large family includes a variety of energy sources, including hydroelectricity, wind energy, solar energy, ocean waves, ocean thermal gradients, geothermal energy, and biomass[2].

1.3. WIND ENERGY

Sunlight is the primary source for wind energy production. When the sun's beams strike the earth's surface, its outer layer heats up, forming irregular winds. The wind's kinetic energy can be useful in the rotation and operation of wind turbines, but the power output is primarily dependent on wind speed. Wind speeds between six and eight meters per second are generally considered optimal for energy applications. There are very few open-land regions where winds of this speed are prevalent. If this were feasible, wind energy would be the dominant source of energy. Wind energy is one of the most cost-effective renewable energy sources and has become one of our generation's fastest-growing energy production sources. Forecasts for future wind power generation indicate a technical potential comparable to forty times the current electricity demand or five times the present global energy usage.

Wind energy is one manifestation of the kinetic energy of airflow. It can be transformed into another form of energy, such as electrical energy, by converting it to mechanical energy or employing it directly to pump water or grind grain.

The kinetic energy (E) for air mass moving may be calculated as follows:

$$E = \frac{1}{2}mu^2 \quad (1.1)$$

Wind power (P) can be determined by differentiating the wind's kinetic energy with respect to time.

$$P = \frac{dE}{dt} \quad (1.2)$$

Thus,

$$P = \frac{1}{2} \frac{dm}{dt} u^2 \quad (1.3)$$

The wind turbine blades will rotate when the wind flow pushes the blades of a wind turbine, so the mass flow rate (\dot{m}) is:

$$\frac{dm}{dt} = \dot{m} = \rho A_s u \quad (1.4)$$

Substituting Eq. (1.4) into Eq. (1.3) gives

$$P_A = \frac{1}{2} \rho A_s u^3 \quad (1.5)$$

Where P_A is the available power from wind. According to Eq. (1.5), because wind power is proportional to the cube of the wind speed, even modest variations in wind speed can noticeably impact the amount of energy generated. Additionally, the wind power will grow with an increase in the swept area of a wind turbine (diameter, height, or both)[3].

1.4. WIND TURBINE

Recently, wind turbines have experienced significant developments with the advancement of technology. Great progress has been made, especially in the efficiency and power production of turbines. Thanks to high-efficiency propellers, more efficient generators, and smarter control systems, wind turbines can produce more energy and operate even at lower wind speeds. However, along with these developments, some problems also emerged. There are concerns about the impact of large-scale wind farms on ecosystems and, in some cases, the habitat of creatures such as birds or bats. Additionally, turbines appear to create aesthetic and visual pollution and, in some cases, cause controversy among local communities. For these reasons, it is important to consider the environmental impacts and social acceptance of wind turbines, along with their technological development. In order to solve these problems, efforts are being made to develop more innovative and environmentally friendly designs and more careful approaches to site selection and installation processes [4].

Wind turbines come in different types and designs, and each has its own unique features. Types of these turbines include models such as lift and drag type turbines, horizontal axis and vertical axis wind turbines, savonius and darrieus. While horizontal-axis turbines are generally more widely used, vertical-axis turbines are preferred, especially in areas where the wind direction changes frequently[5].

The power efficiency values, operating ranges, and number of blades of each turbine type vary. For example, vertical-axis turbines generally perform better at lower wind speeds, while horizontal-axis turbines may be better suited for higher wind speeds. However, self-starting problems may occur in vertical axis turbines, which may affect wind energy production. Recently, new designs and efficiency improvement efforts have aimed to make turbines operate with higher efficiency and be effective over wider wind speed ranges. In addition to making turbines perform better, these efforts are also moving towards reducing their environmental impact and increasing social acceptance [6].

Vertical-axis wind turbines do not have as high-power efficiency as horizontal-axis wind turbines. However, vertical axes are more suitable in regions where the wind speed direction changes frequently. There are two main types of vertical-axis wind turbines: Savinous and Darrieus. While Savinous turbines are drag-type, Darrieus turbines operate with lift. Therefore, Darrieus turbines have better performance than ravenous turbines. Classification of wind turbines, as shown in Figure 1.1[7].

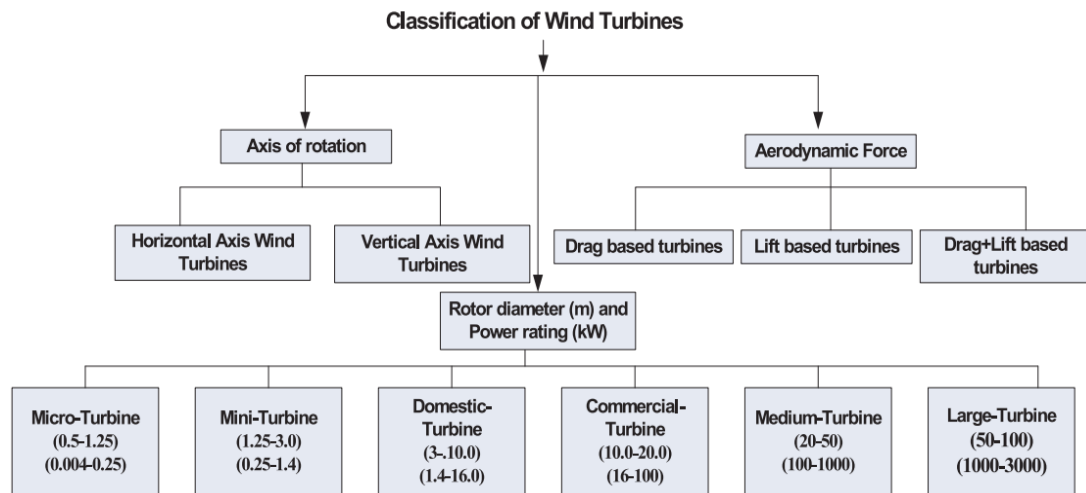


Figure 1.1. Wind turbines classifications [7].

1.4.1. Horizontal Axis Wind Turbine (HAWT)

The highly usual kind of wind turbine has a horizontal axis. They are the turbines, where the rotor shaft is oriented towards the wind, there are choices for wind turbines with one, two, or three blades. Aerodynamically, design blades rotate due to the force's aerodynamic lift. Where the pressure difference occurs in the turbine blades' upper and lower faces. Front blade surface produced a low-pressure zone while the back-blade side developed a high-pressure zone, The airflow moved from high-pressure zone to low-pressure zone provide an aerodynamic force. This relationship, known as Bernoulli's relation, predicts that a fluid's speed will be low where pressure is high. The turbine's blades connect to the electrical generator's rotor. HAWT is more effective and may capture stronger winds[7].

By rotating, the rotor transforms wind energy into mechanical energy, which can power a generator. The wind flow crosses the blade surfaces with an airfoil form. However, it moves more quickly across the upper surface, making a low-pressure zone on the airfoil. The pressure difference between the upper and lower sides generates lift force. A wind turbine's hub is the center of motion for the blades, which rotate around the hub due to lift force. Rotor rotation is hampered by the drag force perpendicular to the lift force. And, the WT design's primary goal is to have a high ratio of lift/drag, and such ratio varies alongside the blade for maximizing the power output from turbine

at various speeds of wind. HAWT offers the following advantages as well as the drawbacks[8][9], as depicted in Table 1.1.

Table 1.1. Advantages and Disadvantages of HAWT.

Advantages		• Disadvantages
I.	The output power is significantly higher than that of the vertical-axis wind turbine.	I. HAWTs are only available in large capacities, and their use in distributed generation is challenging.
II.	High efficiency.	II. Due to their big size and weight, they are difficult to transport from one location to another.
III.	IV. It has a higher rotational speed and is more dependable	III. A stronger construction is needed to support a large generator as well as gearbox mounting at nacelle, which adds to the intricacy and the overall structure cost.
IV.	wind shear profile along the tall tower gets more wind.	IV. The HAWT produces more noise than other wind turbines.
V.	High reliability	V. The development and production of a HAWT need the use of large machinery.
VI.	The turbine's blades may be bent using a gearbox to provide the optimal flow attack angle, improving performance in windy circumstances.	
VII.	During storms, the rotor's blades may tilt.	

1.4.2. Vertical Axis Wind Turbine (VAWT)

Vertical-axis wind turbines have self-starting capability even at low wind speeds, especially Savonius-type turbines. On the other hand, although Darrieus turbines are more efficient, they may encounter self-starting problems[10]. In terms of cost, in some cases, vertical-axis turbines may provide advantages over horizontal-axis turbines, especially under certain conditions. While large-scale wind turbines with horizontal axes are generally preferred in the oceans, it is thought that vertical-axis turbines also have the potential to be used in the oceans in the future. Among the reasons why vertical axis turbines are preferred are their advantages in wide usage areas. Therefore, better understanding vertical axis turbines and increasing their efficiency by developing different designs constitute an important research and development area in the wind energy sector. These efforts represent an important step towards providing more effective and sustainable solutions by increasing diversity in

the field of wind energy. VAWT has an advantages and disadvantages as shown in table 1.2.

Table 1.2. VAWT Advantages and Disadvantages[11][12].

Advantages		• Disadvantages	
I.	In comparison to a HAWT, it has significantly small vibrations and is little noise level.	I.	A VAWT's efficiency is lower than a HAWT's.
II.	Because the direction of the blades is perpendicular to the order in which the wind is blowing, there is no need for a specific orientation, nor is there a requirement for a yaw control device.	VII.	Because the rotor is near to ground and less air being accessible owing to the drag from the surface of ground, it produces less energy than a HAWT of the same height.
III.	It can generate power even at moderate wind speeds.		
IV.	Installation and maintenance are simple.	II.	Since the blades are positioned over the generator and gearbox, replacing and maintaining parts might be challenging if the structure needs to be properly constructed.
V.	Due to its often-smaller size and lower noise level, it is favoured for distributed generation.		
VI.	VAWTs are visually appealing.		

1.4.2.1. Savonius VAWT

Savonius is a VAWT of the drag kind. Sigurd Johannes Savonius, a Finnish engineer, was discovered in 1922. It is the most basic kind of wind turbine. The Savonius turbine has two, three, or more blades; from the top, it has an S-shaped cross-section. These blades are curved, with one side concave and the other convex. The drag effect is lessened when the blade is moving against the wind. This turbine transforms the wind energy into torque on the revolving shaft. Self-starting is an option for this turbine. Modern Savonius models are more efficient and vibrate less than earlier models. Savonius turbines come in various designs, including those with two, three, four, and even more blades and stages [13].

There are significant performance differences between different types of wind turbines. For example, drag-type turbines such as Savonius have lower efficiency than

lift-type turbines such as Darrieus. Tip speed ratio ranges for Savonius and Darrieus turbines differ. Generally, the tip speed range for Savonius turbines is between 0 and 2, while for Darrieus turbines, this range can be considered as 1 to 6. On the other hand, the amount of power to be obtained in Darrieus turbines is closely related to design parameters such as the number of blades, solidity, dimensions, and the tip speed ratio range. Increasing the number of blades can generally increase the performance of Darrieus turbines, but other important criteria such as stability, cost, and vibration are also taken into account. The amount of power obtained in Darrieus turbines is shaped by a number of variables, such as the number of blades, airfoil, angle of attack, rotor angular period speed, tangential speed, and relative wind speed. The tangential force acting on the blades and changing over time, and the torque value it causes, have a critical role in understanding the working mechanism of Darrieus turbines. A detailed study of these factors is considered an important step in increasing the efficiency of wind turbines[14].

1.4.2.2. Darrieus VAWT

Darrieus is a VAWT of the lift kind. French aviation engineer Georges Jean Marie Darrieus discovered and created it in 1926. Studies in the literature on the design and development of Darrieus turbines continue to analyze the effects of a number of design parameters on power efficiency. In particular, the effects of parameters such as the number of blades, solidity ratio, changing pitching applications, airfoil selection, airfoil dimensions, rotor radius, and height ratios on power efficiency, stability, vibration problems, and sound problems are investigated. These studies play an important role in understanding the structural problems of turbines and increasing their efficiency. Additionally, hybrid designs combining the features of Savonius and Darrieus turbines are thought to be a potential way to develop new-generation turbines. These hybrid designs may have the potential to offer improved performance in areas such as higher efficiency and less vibration or noise. Studies are ongoing showing that these new designs may be a promising method to increase the efficiency of wind turbines and reduce structural problems [15].

Tip speed ratio and maximum power coefficient (C_p) values may differ for the operating range of Savonius and Darrieus wind turbines. Savonius turbines are generally effective at low speeds, and type speed ratios generally vary between 1 and 2. The maximum power coefficient can generally be between 0.2 and 0.35. Savonius turbines are generally found to perform better at low rotational speeds and constant speeds. Increasing the number of blades may lower the starting threshold of the turbine, but it does not significantly affect performance [16].

Darrieus turbines are more efficient at higher speeds, and type speed ratios can generally vary between 3 and 5. The maximum power coefficient can generally be between 0.35 and 0.45. Darrieus turbines generally perform better at higher speeds. Increasing the number of blades can generally lower the starting threshold at lower speeds and provide better performance at lower speeds[17][18].

When comparing the power efficiency between Savonius and Darrieus turbines, Darrieus turbines generally have higher power coefficients and are more efficient at higher speeds. However, Savonius turbines can perform better at lower speeds and are generally noted for their simpler construction. Which turbine is more suitable will depend on the wind conditions, energy needs, and other factors of the environment in which it will be used [19]

1.5. MOTIVATION

There are many theoretical and experimental studies in the literature on the improvement of Darrieus turbines. The development of computer-assisted fluid dynamics (CFD) technology is constantly advancing and making significant contributions to studies in this field. With the use of CFD, a wider set of parameters can be analyzed more quickly and economically compared to theoretical and experimental studies. While theoretical studies can generally focus on limited and simple geometries, analysis of more complex and realistic geometries is possible thanks to CFD. However, unlike experimental studies, CFD also has some limitations. Especially in CFD, it can be difficult to analyze a wide range of parameters with the same precision as in experimental studies. However, the development and use of CFD

make significant contributions to research in this field by enabling more comprehensive and detailed analyses of the design and improvement of Darrieus turbines [20].

CFD studies in the literature focusing on Darrieus turbines address a number of important issues. These studies generally include CFD analyses of Darrieus turbines and focus on specific issues. These include topics such as flow separation, dynamic stall, the interaction of blades, azimuth angle, maximum and minimum torque values, changing of torque value with time, calculation of average torque, the effect of change of wind speed, the effect of turbulence, on the aerodynamics performance. Studies in the literature provide a detailed review of CFD modelling of Darrieus turbines, focusing especially on these issues to understand the performance of turbines, their aerodynamic properties, and how they behave under different operating conditions. These studies deepen our understanding of the design and efficiency of Darrieus turbines and provide an important basis for future improvements. A lot of contours can be obtained by CFD to understand the flow behaviour of the turbine.

1.6. PROBLEM STATEMENT

Recently, many academics have tried to modify or redesign wind turbine geometry to increase wind turbine performance. In this thesis, a new DVAWT design with dual blades and a different wind profile was selected for analysis using the software Fluent CFD. To address the issue of fluctuating wind speeds, researchers are exploring strategies to modify the flow of gusting winds and enhance their energy potential. One approach involves placing obstacles or structures firmly at the top of the turbine to create a more concentrated wind stream. This can lead to a noticeable increase in wind speed and, thus, power generation. However, studying and developing wind turbine designs specifically designed for low-wind speed environments is crucial to expanding the application of wind energy. [For example, double-bladed wind turbines have shown the potential to improve power production under low wind conditions, as the double blades help increase the efficiency of the Darrieus wind conditions turbine. It provides a larger surface area to capture the effects of wind].

1.7. OBJECTIVES OF THE PRESENT WORK

In this thesis, the effects of geometry change on Darrieus turbines on their power performance were investigated. For this purpose, blades were added to the Darrieus turbine, which has three blades, closer to the rotor center. The resulting three new Darrieus designs were analyzed in 2D using CFD. This CFD analysis was done unsteadily. It was revealed how the torque values of the turbines changed over time. The wind speed was taken as 10 m/s. and the two different cases of wind speed, uniform and nonuniform, were analyzed separately. Calculations were made at four different rotational speed values. The results obtained were evaluated with numerical values, graphics, and contours. Contours showing 8 different quantities were presented visually. Thus, progress was made in terms of the detailed analysis results of different designs that can be achieved with unsteady CFD.

1.8. THESIS LAYOUT

Part 1 describes the present condition of VAWT types and performance. The second Part provides an overview of VAWT and its performance and evaluation literature. The third Part introduces the design characteristics adopted from previous works and describes the new tasks performed in the quest for the optimal turbine. The preliminary CFD analysis and two-dimensional simulations of the turbine are presented in Part 4. Based on the results of two-dimensional CFD simulations, concentrate on the most important aspects and considerations associated with the turbine's new design and VAWT parameters. Part 5 contains the turbine design's conclusions, recommendations, and future work.

PART 2

LITERATURE REVIEW

2.1. BACKGROUND

The VAWT is a highly sought-after choice for the peri-urban landscape [21–24], boasting exceptional performance in turbulent and off-kilter airflows [25, 26]. Its low noise emissions make it a popular option for operation at low TSRs [27], while also being aesthetically pleasing [28]. As a result, there is a wide range of commercially available small-scale VAWT designs suitable for urban structures. Additionally, there has been a recent increase in interest in using VAWT in offshore floating environments [29], due to its simplicity and reliability. One of the main motivations for adopting VAWT technology is to increase reliability by minimizing unnecessary mechanical complexity and enhancing resilience for harsh environments [30–32]. VAWT systems can also be outfitted with untwisted blades of consistent cross-section, allowing for easy manufacturing [33–35].

The VAWT, through its unique design, presents an all-encompassing potential by being unaffected by wind direction, eliminating the need for a yaw mechanism [36–38]. This design trait holds particular significance for offshore implementation, where the yawing mechanism is a common cause of failure in HAWTs [39, 40]. Not only does the VAWT architecture eliminate the need for a blade pitch mechanism to control the angle of attack (AOA), but it also employs aerodynamic dynamic stall to efficiently and passively regulate and optimize power absorption [32, 33, 41, 42]. Most importantly, this feature provides an added layer of safety during turbulent and unpredictable wind gusts [30].

2.2. DARRIEUS VAWT AIMS AND LIMITATIONS

The ultimate objective of airfoil aerodynamic studies is to decipher the intricate mechanics of the WT rotor's aerodynamics, as well as to pinpoint the optimal pressure and velocity distribution along the surface of the airfoil. This includes studying the dynamic aspects, evolution of vorticity [43], and the impact of blade interaction in both steady and unsteady flow conditions [44, 45]. Furthermore, the primary focus of researching airfoil geometric parameters is to identify the ideal airfoil for efficient operation in the complex aerodynamic environment of the Darrieus rotor, ultimately maximizing the power coefficient.

Both of these research topics hold the overarching goal of guiding airfoil design. It is worth noting that the investigation of airfoil aerodynamics is the fundamental element of the inverse airfoil design methodology for the Darrieus rotor, an aspect that has been overlooked by previous researchers. On the other hand, studying airfoil geometric parameters is closely linked to the direct airfoil design approach for the Darrieus rotor. It should be kept in mind that DVAWTs have specific objectives and limitations that must be taken into account. Below, we outline some of the key goals and constraints of DVAWTs.

DVAWTs Aims:

- The major goal of DVAWTs is a vertical-axis configuration that allows them to catch wind energy from any direction [46], unlike horizontal-axis wind turbines (HAWTs), which utilise yaw mechanisms. Because of this design choice, DVAWTs may be able to collect wind energy more effectively in places where winds are strong and variable, such as in urban.
- DVAWTs are often constructed for urban and small-scale applications, where space limitations and wind direction variations render horizontal-axis turbines less practicable. The goal of these VAWTs is to offer a renewable energy option that is suitable for incorporation into urban environments and structures [47].

- Effective operation in low wind circumstances: Another goal of DVAWTs is to function well in low wind settings. In comparison to HAWTs, their design enables them to start and produce power at lower wind speeds, making them suited for locations with moderate wind resources.

DVAWTs Limitations:

- Low tip-speed ratio: Compared to HAWTs, DVAWTs usually have a smaller tip-speed ratio, which is the ratio of the speed of the blade tip to the speed of the wind. This makes them less efficient and less powerful overall, especially when the wind speed is high [48].
- Problems with torque and stability: DVAWTs often have problems with torque and stability. Because aerodynamic forces on the rotating blades aren't always the same, DVAWTs often have big changes in torque during each turn. This causes mechanical stress and reliability issues [49].
- Starting and self-starting: DVAWTs don't have the ability to start spinning on their own, so they often need an external power source or help from another individual. It can be hard to get past the initial static friction and make enough power to start turning, especially when the wind speed is low [50, 51].
- Less efficient overall: In general, DVAWTs are less efficient overall than HAWTs. Design weaknesses like the lower tip-speed ratio and the mechanical forces that act on the blades, make the turbine less powerful and less efficient [52].

It's important to note that research and development is still going on to fix some of the problems with DVAWTs and make them better in terms of their efficiency, ability to start, and security.

2.3. BLADE SHAPE OF DVAWT

Which blade shape is ideal for maximizing wind energy production? Flat blades, the traditional choice for mill blades for thousands of years, are losing popularity as other styles gain traction. The flat blades catch wind and resist its force, resulting in a gradual

rotation due to the redirection of power on the upstroke. These drag-based blades work against the wind, much like paddles attempting to row in reverse. Although flat blades offer benefits for do-it-yourselfers, such as low-cost and simple construction using plywood or metal, they are not nearly as efficient as alternative designs and present challenges in converting wind into electricity.

In contrast, bent blades resemble elongated airplane wings, also known as airfoils. As air passes around the curved blades, the air above moves faster than the air below, creating a low-pressure area on top and generating aerodynamic lift to drive the blades. This airfoil shape, also known as structural bending, provides an efficient design with minimal resistance. Due to their curved structure, they require more planning and expertise to construct, but the results are worth it in terms of energy production.

These lifting forces are always perpendicular to the top surface of the curved blade. This makes the blade move around the center hub. The blade spins faster because there is more lift on it when the wind blows faster [53].

2.3.1. H- Blade

Human writers often assess the efficacy of H-bladed turbines in contemporary literature due to their ability to address design parameter issues and provide a more streamlined manufacturing process. The use of 2D CFD evaluation and straight blades allows for simpler production. Various iterations of H-turbines have been introduced, including variable geometry versions that reduce swept area in high wind speeds and V-turbines that utilize acute angled struts instead of towers.

The development of H-Rotors in the UK occurred through research conducted in the 1970-1980s, which revealed that the complex mechanisms required to adjust the straight-bladed Darrieus VAWT blades were unnecessary. It was discovered that the drag and stall effects caused by a blade leaving the wind flow would impede the opposing blade's ability to propel the entire blade configuration forward. As a result, the H-Rotor became self-regulating in all wind speeds, reaching its optimal rotational speed shortly after its cut-in wind speed [54, 55].

VAWTs were also looked into in Europe, and some of the work was done at the same time as the Darrieus development in North America. However, the H-rotor idea got the most attention, and a number of large turbines were built to test it. Compared to the regular Darrieus turbine, the H-rotor has some benefits. It is typically put on a higher tower, which gives a better energy yield and lets the rotor stay above the lower surface-layer turbulence, which keeps it from getting tired. Also, the straight blades are easier and cheaper to make. They sweep a bigger, square-shaped area and don't need guy cables, so they take up less land. There are, of course, some problems with this design. The bent moments on the blades are bigger, and the need for struts makes it harder to optimize the aerodynamics and noise [55, 56]. Also, unlike the Σ -configuration Darrieus, the H-rotor has aerodynamic losses (drag) at the points where the blades are attached and tip losses at the free ends of the blades, both of which lower the power coefficient [55].

2.3.2. Twisted Blade

Wind turbines have been an important part of the renewable energy business for the past three decades. So, a lot of study and development goes into making them work better. Most wind generators have blades that are long. Since turbine blades are moving, they feel the speed of the wind in a similar way. There are two speeds for a wind turbine blade. Rotational speed is measured in Rad/s or RPM and stays the same as the length of the blade changes. Linear speed increases as the radius of the blade grows. Wind turbine blades have to be turned so that they face the wind at the best angle along their length [57-61]. The incorporation of a geometrical spanwise twist into the blades of a vertical axis wind turbine (VAWT) can greatly enhance its overall aerodynamic performance. This blade twist is essentially the distribution of preset blade pitch angle along the span of the blade. Research from 3D computational fluid dynamics (CFD) analysis shows that the downwash flow effect, caused by the vortex at the blade tip, reduces the effective angle of attack (AOA) towards the blade tip. To counteract this reduction, it has been proposed to use a larger preset pitch angle at the blade tip compared to the blade mid-span, thereby increasing the aerodynamic efficiency [62].

2.3.2. Helical Blade

Other than the above ways, the helical blade design was suggested because it has low changes in aerodynamic torque and is easy to start on its own [63]. Some ideas for spiral VAWTs, like VertiWind [64], SeaTwirl [65], The use of V-shaped blades for vertical axis wind turbines (VAWT), such as the ones proposed by Falkowski and Gwind [66], has gained significant attention. In addition, a series of investigations [67-69] have been conducted to analyze the aerodynamic performance of VAWTs equipped with spiral blades. The helical twist angle, which represents the phase shift between the upper and lower cross-sections of a helical blade, plays a crucial role in determining the torque behavior. Castelli and Benini [70] examined the effectiveness of different spiral twist angles (0, 30, 60, 90, and 120 degrees), while Marsh et al. [71] utilized CFD models to assess turbines with overlap angles ranging from 0 to 120 degrees and section inclination angles between 15 and 45 degrees. In their parameter study of VAWTs, Guo et al. [72] concluded that the optimal helical twist angle falls within the range of 70° to 110° , aimed at minimizing torque fluctuations.

2.4. VERTICAL AXIS WIND TURBINE PERFORMANCE

There are a number of design parameters that influence the aerodynamic efficiency of a VAWT. In this section, the design parameters depicted in Figure (2.1).

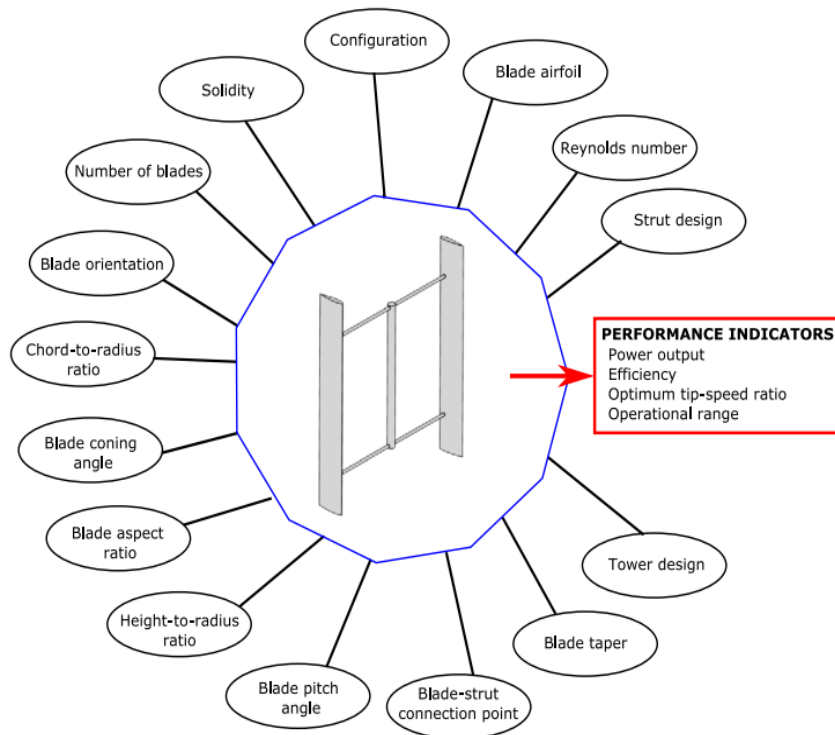


Figure 2.1. Displaying the aerodynamic efficiency of a Vertical Axis Wind Turbine (VAWT) is crucial in assessing its performance [73].

To achieve this, it is necessary to determine the appropriate design parameters. Figure (2.2) illustrates the characteristic performance curve of a VAWT, represented by the C_p and TSR curve, which serves as a benchmark for its efficiency.

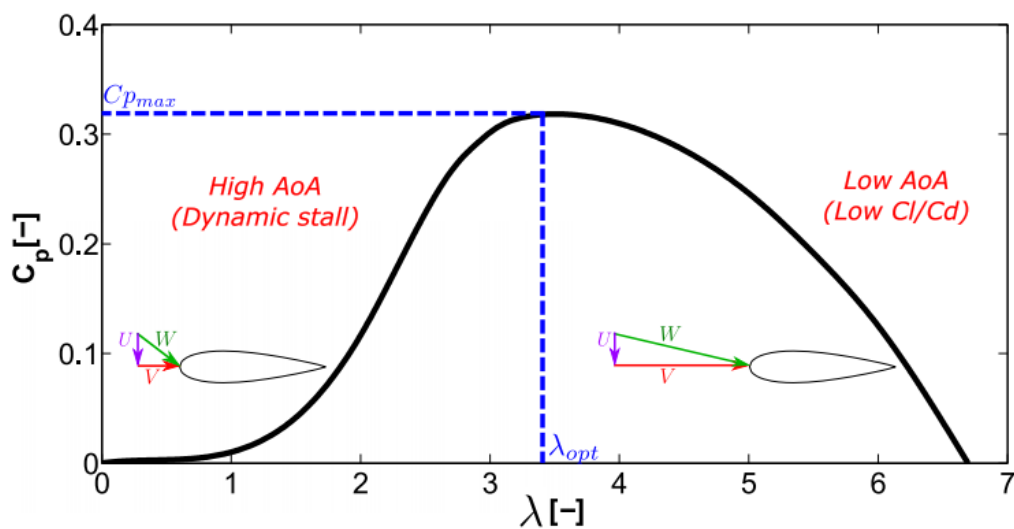


Figure 2.2. The trajectory of efficiency for a Vertical Axis Wind Turbine (VAWT).

The visual representation showcases pivotal statistics, including the peak power coefficient, C_p max, and the matching optimal TSR, opt . At this particular configuration, the VAWT blades operate under ideal flow circumstances, efficiently harvesting energy from the current. Deviating from this setting and decreasing the TSR below opt , leads to a decrease in efficiency. This stems from the interference of an obstruction, hindering the flow from passing through the VAWT. Alternatively, the flow tends to circumvent the turbine [73].

Bellow discussed the popular parameters of DAWT design.

2.4.1. The Significance of Blade Number

The usage of a specific quantity of blades plays a pivotal role in the development process, as it necessitates balancing blade stiffness, aerodynamic efficiency, and cost considerations [74]. As a convention, the number of blades directly influences the solidity of the turbine, as depicted in Figure (2.3). In their study, Blackwell et al. [75] investigated the effects of varying blade numbers ($N = [2, 3]$) on the performance of the SNL 2-m turbine. To maintain parity in the chordal Reynolds numbers for both turbines, the three-bladed turbine was evaluated at a rotational speed approximately 1.5 times higher than that of the two-bladed turbine, incorporating leading edge serrations through the implementation of Taguchi's methodology.

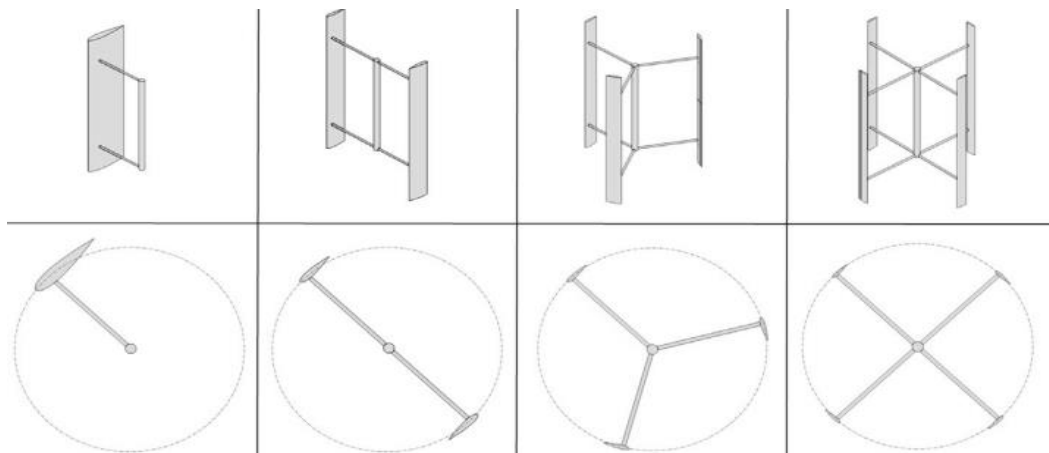


Figure 2.3. Pictorial Depiction of a Steady and Robust Vertical Axis Wind Turbine (VAWT) with Varied Blade Count.

It was revealed that the twofold spindle performance overshadowed the threefold spindle, and the quadruple spindle displayed inferior performance in comparison to the latter. In a qualitative examination conducted by Sun et al. [76], there is a direct correlation between blade count and the frequency of blade vortex shedding. This effect is more pronounced at lower tip-speed ratios (TSRs). In a similar vein, Bedon and his team [77] utilized the DMS model to investigate how blade count affects the efficiency of the DeepWind turbine. Additionally, Figure 2.3 illustrates the momentary power coefficient throughout one full revolution of the turbine, with varying blade counts ($N = [1, 4]$) for both individual blades and the entire turbine.

The total torque of a turbine is greatly influenced by the number of blades, with a higher number resulting in less variation in shaft torque. However, a turbine with only one blade is not feasible due to balance issues and the need for a counterweight, which also increases parasitic drag [78]. As observed by Li et al. [79], using a low number of blades (two or three) is the most practical solution. While adding a third blade reduces torque ripple, it also significantly increases the overall cost of the turbine. Furthermore, utilizing fewer blades enhances efficiency but leads to greater fluctuation in instantaneous power. From a structural design standpoint, it is more advantageous to have a few blades with a larger chord rather than more blades with a smaller chord. This is due to the exponential increase in blade bending stiffness with chord size, while aerodynamic loads only increase proportionally [70]. Additionally, increase in the number of blades also improves the VAWT's self-starting capability [79, 80]. Studies conducted by Dominy et al. [81] and Hill et al. [82] have shown that a three-bladed turbine is capable of self-starting, while a two-bladed turbine can only self-start at specific azimuthal positions. Table (2.1) compares the design features of a VAWT with two or three blades [83].

Table 2.1. Comparing Design Features of a Two-Blade vs. Three-Blade Turbine [83].

Characteristic	Two blades	Three blades
Complexity of Blade Reynolds Number	H	L
Production Expenditure	L	H
Overall Assembly Expenses	L	H
Ratio of Blade Durability to Weight	H	L
Rotational Inertia	L	H
Amplitude of Engine Shaft Torque Variations	H	L
Easily Commencing Capability	L	H
Intensity of Blade Vortex Shedding	L	H
Quantity of Support Struts Needed	L	H

Where : (L : lower and H : Higher)

2.4.2. Tip Speed Ratio

Given its tip speed ratio (TSR), a vertical axis wind turbine (VAWT) will exhibit various flow dynamics and unsteadiness while in operation. Therefore, selecting an appropriate computational domain, turbulence model, and defining other numerical settings that minimize discrepancies across all TSR ranges can be a time-consuming and challenging task. In general, analyzing the flow behavior around VAWTs can be divided into three TSR ranges: low TSRs, medium TSRs (where the optimum TSR is typically achieved), and high TSRs. Out of these ranges, predicting the performance and flow behavior of VAWTs in the low TSR range proves to be the most challenging. This is mainly due to the fact that the VAWT blades experience local angles of attack (AoA) that exceed the stall AoA for most azimuthal angles.

Consequently, the blade is capable of generating a minuscule or even negative torque [84]. It is a well-known fact that VAWTs are subjected to significant levels of unsteadiness, some of which are originated from the incoming background flows. According to Malael et al., low TSRs exhibit the second level of unsteadiness, attributed to the dynamic stall phenomenon with drag reduction[85].

In practical terms, VAWT blades operating in this TSRs range are susceptible to two types of dynamic stall. These stalls are linked to the presence of two peaks in the lift coefficient curve of a non-rotating aerofoil in low TSRs. The first type is known as lift dynamic stall, influenced by the Reynolds number (Re), as well as a combination effect

of the boundary layer separation and the unsteady (rotating) motion of the aerofoil [86].

The subsequent enclosure, known as the drag dynamic stall, remains unaffected by the Reynolds number. This stall solely manifests when the blades are in operation within a confined flow field. As a force machine, the VAWT blades direct a section of separated air towards the radial direction of the blade. This term is also employed to portray the postponement of the drop in second static lift coefficient when a rotating blade passes through the downwind phase of an upstream blade (i.e. azimuthal angle 180) [86]. Drag dynamic stall generates a marginal lift component, yet greatly reduces drag over a brief period of time in the low TSRs range. This proves to be a crucial factor in ensuring the continuity of torque production and directly impacts the self-starting capability of VAWTs. Therefore, performing CFD modelling that accurately predicts the performance of VAWTs, particularly in low TSRs range, is of utmost importance.

The velocity of VAWTs' rotation is often denoted in a non-dimensional manner by the Tip Speed Ratio (TSR), which can be calculated using the formula $TSR = \Omega R / U_{\infty}$, where Ω refers to the turbine's angular velocity, R is its radius, and U_{∞} is the speed of the free-stream. Numerous experimental studies have delved into the impact of TSR, or more broadly, the turbine's dynamic solidity, on the characteristics of the wake. For instance, research conducted by Brochier et al. [87], Simao Ferreira et al. [88], Araya and Dabiri [89], Li et al. [90], Parker and Leftwich [91], Ryan et al. [92], Parker et al. [93], Battisti et al. [94], Buchner et al. [95], and Hohman et al. [96] all agree that as TSR increases, the wake of VAWTs experiences a greater deficit in momentum. This can be attributed to the heightened dynamic solidity of the turbine.

Additionally, investigations have revealed increased occurrences of dynamic stall and more prominent coherent structures within the wake when TSRs are smaller. Levels of turbulent stresses exhibit a bimodal distribution pattern, with peaks observed at both the advancing and retreating edges of the wake. Some computational analyses have also delved into how TSR affects wake characteristics, such as those conducted by Zanforlin and Nishino [97], Nazari et al. [98], and Rezaeiha et al. [99, 100]. These

findings align with the experimental studies mentioned above regarding the impact on momentum deficiency in the wake, which appears to be more substantial for higher TSR values, but with a quicker wake recovery process as well. However, although these studies have contributed significantly to enhancing our knowledge of how wake properties are sensitive to working conditions, they primarily rely on solving the Reynolds-averaged Navier-Stokes (RANS) equations. The unresolved nature of turbulence presents a challenge in computational studies, with the time-averaging of equations and turbulent modeling impacting the accuracy and wealth of information that can be extracted from them. This provides limitations in the second-order statistical results, such as velocity and pressure fluctuations, which are crucial in accurately characterizing the wake signature of VAWTs. The use of RANS, due to time-averaging, diminishes the effectiveness in replicating the usual coherence of VAWT wakes, particularly at low TSRs and high angles of attack. As a result, significant dynamic stall phenomena occur and further complicate the situation.

2.4.3. Aspect Ratio

The proportion between the measurement of height and that of radius, denoted as H/R , serves as a pivotal element in the construction of a straight-bladed VAWT. It can be determined by multiplying two variables: blade aspect ratio, H/c , and chord-to-radius ratio, c/R .

While expanding the swept area of the VAWT, it may seem appealing to decrease the H/R ratio in order to maximize the blade's chordal Reynolds number. However, it is essential to note that a larger VAWT radius allows for a greater length of blade chord, resulting in an increase in the chordal Reynolds number [101].

As with any endeavor, there are both positive and negative aspects to consider. In the case of utilizing low aspect ratio blades, the inevitable consequence is an increase in blade tip losses. A thorough study conducted by Zanforlin and Deluca [102] discovered that the impact of blade tip loss outweighs that of Reynolds number effects. As such, it is imperative to prioritize adopting a turbine with a large H/R ratio and

longer blades. According to the theory of finite wings, blade tip vortices arise from the pressure disparity between the opposing sides of a finite wing [103].

Upon examination of the position of the local maximum power coefficient, one can observe its emergence occurring later in the revolution as the blade nears the tip. This phenomenon can be attributed to the decrease in instantaneous angle of attack, brought about by the spanwise vertical flow component, commonly known as downwash [102, 104, 106]. As the H/R ratio is increased, the blade-induced drag component decreases. Li et al. [106] conducted a comprehensive analysis using a 3D panel model to study the impact of the H/R ratio. Their findings reveal that a higher H/R ratio leads to a subsequent increase in peak efficiency, with a corresponding increase in the optimum TSR value. Furthermore, Li et al. [107] discovered a positive correlation between the H/R ratio and both blade failure probability and efficiency. However, the specific turbine under study displayed a practical limit at a H/R ratio of 3, as the blades had reached their structural threshold. It is evident that while an increased H/R ratio has significant aerodynamic benefits, there remains a practical restriction due to considerations of blade flapwise strength. These aforementioned findings align with the analyses conducted by Paraschivoiu [78], who advocates for an optimum H/R ratio falling within the range of 2.6 to 3.

2.5. ENVIRONMENTAL IMPACT

In contrast to fossil fuels and nuclear power, wind turbines do not emit greenhouse gases and do not produce radioactive waste, making them an environmentally friendly source of energy. However, it is important to note that wind energy still has some impact on human existence, albeit minor. The long-term effects of wind turbines cannot be overlooked and must be thoroughly understood and addressed in order to achieve a truly sustainable society.

Unfortunately, the impact of wind turbines on the environment is still being debated and needs further investigation. To ensure a sustainable future, it is imperative that we carefully examine and mitigate any potential environmental effects of wind energy.

While there have been previous discussions and studies on this topic, a review of the existing research will be presented here.

2.5.1. Sound and Visual Influence

The environmental consequences of wind turbines are restricted to their immediate surroundings. The auditory and visual impact of onshore wind turbines in operation can prove to be quite bothersome for humans[108] .

There are two main methods by which wind turbines generate sound: mechanical noise and aerodynamic noise. Even without concrete evidence, the latter is considered a significant issue. Some experts [109] assert that its low frequency could cause disruption in the daily lives of individuals. However, other researchers believe this is of particular concern for residents in close proximity to wind farms, and have conducted studies and surveys on the topic. In his investigation, Pedersen [110] found that individuals who were disturbed by the presence of wind turbines displayed symptoms of stress, such as migraines. Summarizing recent research in this field, Punch et al. [111] discovered that the low-frequency aerodynamic noise of wind turbines can cause sleep disturbances, hearing loss, and vestibular damage. Potential solutions have also been proposed by researchers. For instance, some suggest that wind turbines should be built at least 2 km away from homes, or that the structure of the house be optimized to minimize noise [92]. Son et al. [112] conducted an experiment using a combined numerical method based on Ray theory and concluded that placing obstacles in the path of propagation can substantially reduce wind turbine noise. Similarly, Oerlemans et al. [113] found that implementing an optimized or serrated blade can decrease noise levels by an average of 0.5 and 3.2 dB, respectively.

It is evident that individuals tend to subjectively assess the visual impact of objects [114]. While some may find wind turbines to be visually appealing and impressive, others may hold a different perspective. According to recent surveys, a significant majority of the British population (over 70%) do not view wind turbines negatively [115]. However, certain officials involved in the tourism industry believe that these structures could potentially harm local tourism [114]. When considering the various

environmental effects of wind turbines, the visual impact proves to be the most challenging to gauge [116]. To address this challenge, several evaluation methods have been developed, including the Quechee Test, Multicriteria Analysis, and the Spanish Method [117].

The Quechee Test is a theoretical evaluation aimed at determining the potential negative aesthetic impact of wind turbines on surrounding landscapes. It utilizes analytical factors closely tied to both wind turbines and landscapes. Meanwhile, the widely employed multicriteria analysis technique produces a score between 0 and 100 by examining physical attributes (PA) such as water, land form, and snow, as well as aesthetic attributes such as color and texture. On the other hand, the Spanish method utilizes CAD software and a Geographical Information System to generate a topographical solid surface for simulating the placement of wind turbines. The level of visual impact is then evaluated using the PA value. It has been discovered that the use of the Spanish method can increase public acceptance of an innovation by quantifying potential visual impact [117,118]. In conclusion, employing the Spanish method can aid in determining the level of visual impact and promoting public acceptance [119].

2.5.2. Impact on Animals and Birds

Concerns have been raised by animal enthusiasts regarding the potential harm wind turbines may cause to birds, particularly as wind farms are often built in their natural habitats. However, studies have shown that local birds are adaptable and can quickly learn to avoid obstacles, making wind turbines a minimal concern for them [116].

Despite the continued use of wind energy, it's worth noting that the impact of wind turbines on bird mortality is vastly overshadowed by that of deforestation and urbanization [114]. Furthermore, precautionary measures can be implemented to protect birds from wind turbines. For instance, in a wind project in Texas, avian radars are utilized to detect the presence of birds; if any potential threats are identified, the system will automatically shut down the wind turbines [120]. Additionally, conducting professional wildlife surveys before constructing wind farms can provide valuable

insight into the nesting and feeding patterns of local birds, helping to reduce their risk [121].

Although the offshore wind industry is relatively new, its effects on coastal marine life have been thoroughly examined by numerous researchers. Certain delicate sea creatures, including dab and salmon, possess the ability to detect pile-driving pulses from a considerable distance during the building and usage of offshore wind turbines. As a result, their behavior may be influenced by these turbines [122]. However, the knowledge in this realm remains limited, and further investigation is imperative due to the growing number of offshore wind constructions.

2.5.3. Climate Change

As the stature of wind farms continues to grow, apprehensions arise about their potential impact on nearby weather systems. Two notable incidents have sparked widespread unease. According to precipitation data provided by the Water Statistics Bureau, there has been a severe drought in Xilingo League, Inner Mongolia since 2005, with the drought emerging at a faster rate in areas with wind turbines. Additionally, in the San Gorgonio wind fields of the United States, Roy and Justin [124] discovered a significant correlation between temperature records and wind turbine placement – colossal wind turbines can cause fluctuations in local temperatures, warming them during the night and cooling them during the day. Although this study implies that these towering structures do have an influence on the environment, it is not yet certain whether this impact is beneficial or detrimental. Keith et al. [125] utilized two distinct general circulation models to simulate the effects of wind turbines on climate by modifying surface drag coefficients, demonstrating that wind power can bring about climate change on a continental scale, but has a minimal effect on the global average surface temperature. Furthermore, some environmental engineers suggest that the turbulence in the vicinity of wind turbines may alter local climate by disrupting air flow in both an upward and downward direction, which can be detected from considerable distances. This turbulence in the wake of the turbines can also reorient high-velocity wind at the surface, intensifying the evaporation of moisture in the surrounding area [126].

Although we cannot definitively ascribe this aberrant incidence to wind turbines currently, it is imperative to persist in scrutinizing these implications, given the projected surge in wind farms over the next few decades. In conclusion, the environmental impact of wind turbines remains a contentious topic.

It is indisputable that all human endeavors have repercussions on the environment. However, as wind energy gains prominence as a primary source of power in the near future, the potential consequences of seemingly inconsequential environmental effects today could be catastrophic and must not be disregarded. Thus, there is a pressing need for further investigation and strategic optimization to transform wind power into a sustainable and eco-friendly method for generating electricity.

2.6. SUMMARY OF PREVIOUS STUDIES

There are many previous studies according to different cases, such as airfoil type of the blade as shown in table (2.2).

Table 2.2. Summary of VAWT airfoil development.

Ref.	Airfoil type	Main objective
[127]	DU 06-W-200	VAWT airfoil optimization
[128]	NACA 0012, NACA 0021, NACA 5522, LS0421	Effect of airfoil thickness and camber
[129]	DU 12-W-262	Genetic optimization of airfoil design with focus on lift-to-drag ratio
[130]	DU 06-W-200 J	shaped airfoil to improve VAWT starting torque
[131]	NACA 0018	Improvement if leading edge serrations using Taguchi's method.
[132]	NACA 0021	Enhancing Airfoil Design through Gurney Flap Implementation
[133]	NACA0018	This article presents a hybrid approach, combining both numerical modeling and experimental analysis, to delve into the complex physical behaviors exhibited by a Darrieus VAWT in turbulent flows.
[134]	NACA 0021	Augmentation devices increase wind velocity at inlet due to venturi effect. Self-starting ability improved for both lift and drag type VAWTs.
[135]	NACA 0021	Delve into uncharted depths of understanding surrounding the impact of deflectors on the aerodynamic properties of VAWT blades.

2.7. ORIGINAL POINTS OF PRESENT WORK

This chapter presents a Computational Fluid Dynamics (CFD) numerical analysis to investigate the impact of numerous parameters on the functionality of Double Vertical Axis Wind Turbine (DDVAWT), particularly regarding its double blade configuration. Additionally, it delves into the examination and assessment of various factors that dictate the power generation capabilities of DDVAWT. The study also sheds light on the influence of actual wind profiles on the performance of double-bladed vertical axis wind turbines, while further enhancing the understanding of the forces exerted on the blades. Notably, the research showcases the significant improvements in power and efficiency achieved by implementing the DU06W200 airfoil, developed by the Delft University of Technology in 2006.

PART 3

WIND TURBINE MODELING

3.1. INTRODUCTION

The design parameters of VAWTs are defined in the present chapter, along with the models utilized for calculating their aerodynamic performance.

Approaches of the WTM are separated into three classifications, comprising experimental, analytical, and numerical approaches. Every technique possesses its own benefits and limitations. The analytical approaches are enclosed in the preceding chapters. Also, in the current chapter, the numerical approaches are being regarded. Additionally, in the whole analytic model, an estimated solution is determined for the problem by making the fluid flow's governing equations. To obtain more exact outcomes, Navier-Stokes equations have to be solved in the domain of computation. This theory is dependent upon the supposition that the rate of the momentum variation of the air that passes across the wind turbine is equivalent to the force upon the turbine blades. And the theory details can be obtained from [137, 138].

3.2. ANALYSIS PARAMETERS OF A WIND TURBINE

The parameters considered in the design process of wind turbines are shown in Figure 3.1:



Figure 3.1. Flow chart of Wind Turbine Design Parameters.

3.2.1. Power Coefficient (C_P)

The obtainable power in the wind for a vertical-axis wind turbine is written by:

$$P_A = \frac{1}{2} \rho A_s u^3 \quad (3.1)$$

Where:

- ρ : The density of air.
- A_s : The blades' swept area.
- u : wind velocity.

The power output of wind is proportionate to the cubic power of the average velocity of wind, and this means every simple change in the velocity of wind can be caused by a big variation in the power of wind [3]. The coefficient of power (C_P) is the energy rate that can be absorbed via the turbine from the wind. The wind turbine efficacy possesses a theoretical limit; such a value is named the Lanchester-Betz limit. Also, it designates the ultimate power that can be extracted from wind, autonomous of a wind turbine design into the open flow. In accordance with the limit of Betz, no wind turbine can attain higher than the value of 16/27 (59.3%) for the HAWT and 16/25 (64%) for the VAWT, as well as this being recognized as the coefficient of Betz [37, 38]. The coefficient of power, or efficiency, of the turbine is stated via:

$$\begin{aligned}
C_P &= \frac{\text{Captured mechanical power by blades}}{\text{Available power in wind}} \\
C_P &= \frac{P_e}{P_A} = \frac{P_e}{\frac{1}{2}\rho A_s u^3}
\end{aligned}
\quad \left. \vphantom{\begin{aligned} C_P &= \frac{\text{Captured mechanical power by blades}}{\text{Available power in wind}} \\ C_P &= \frac{P_e}{P_A} = \frac{P_e}{\frac{1}{2}\rho A_s u^3} \right\} \quad (3.2)$$

Where P_e represents the real power that can be extracted from the wind.

3.2.2. Tip Speed Ratio (TSR)

TSR is the relationship between the rotor's tip speed and the speed of wind. The speed of wind is a changing parameter, the rotation's accelerating speed of the wind turbine relies on the TSR. For generating electricity, there's a requirement for augmented rotational speed. In comparing the ultimate speed of the tip, the ratios of drag kind cause around (1), whereas the lift style wind turbines cause around (10). For comparing the two, the lift-type wind turbine is the supreme choice for this, as it needs a high rotational speed.

How well the wind turbine is capable of achieving is only reliant upon the rotor, as well as how many blades are utilized for constructing it, as well as the total area that's being enclosed. It's important for the wind to be capable of smoothly flowing above the blades for the wind turbine to be capable of conducting as it's anticipated to. The detailed specifics around the space between blades are significant for keeping in mind, as it's significant to guarantee that no difficulties like turbulence take place during the procedure. To avoid any difficulties in functioning, it's significant to guarantee that the wind turbines comprise merely (2) or (3) blades.

$$\begin{aligned}
\text{TSR} &= \frac{\text{rotational speed at the blade tip}}{\text{Wind velocity}} \\
\text{TSR} &= \frac{\omega R}{u}
\end{aligned}
\quad \left. \vphantom{\begin{aligned} \text{TSR} &= \frac{\text{rotational speed at the blade tip}}{\text{Wind velocity}} \\ \text{TSR} &= \frac{\omega R}{u} \right\} \quad (3.3)$$

Where:

ω : The angular speed in rad/s

R: The radius of a rotor in m.

3.2.3. The Swept Area (A_s)

A_s the section of air surrounding the turbine is flowing, its shape relies upon the configuration of the rotor and possesses a rectangular form. It is computed by:

$$A_s = 2RH = DH \quad (3.4)$$

Where, (R) and (D) represents the radius of the rotor and the diameter in (m), respectively, and (H) represents the blade height in (m). The power output from the wind turbine is connected to A_s . Thus, if the diameter of the rotor or the blade height rises, this power rises.

3.2.4. Number of Blades (N_b)

The working of the rotor is affected by the blade number of a wind turbine. And the coefficients of power reduce with the blades' rise. Also, the initial feature of such a wind turbine gets better with the blade rise [139]. The working of the rotor is affected by the blade number of a wind turbine. And the coefficients of power reduce with the blades' rise. Also, the initial feature of such a wind turbine gets better with the blade rise [139].

3.2.5. Chord Length of The Blade (c)

The chord length of the blade is the fictional straight line that joins the blade's front edge to the blade's back edge. The chord length is the length of the blade cross-section. And, the thickness of the blade is obtained via the utilized airfoil; in the present investigation, the employed airfoil is (DU06W200), where the curvature of the blade and the ultimate thickness are described as a chord percentage.

The ultimate thickness of the airfoil is 19.8% at (31.1%) chord, and the ultimate camber is 0.5% at (84.6%) chord. The airfoil data file is provided in Appendix (A-1). Figure 3.2 depicts the airfoil (DU06W200) cross-section.

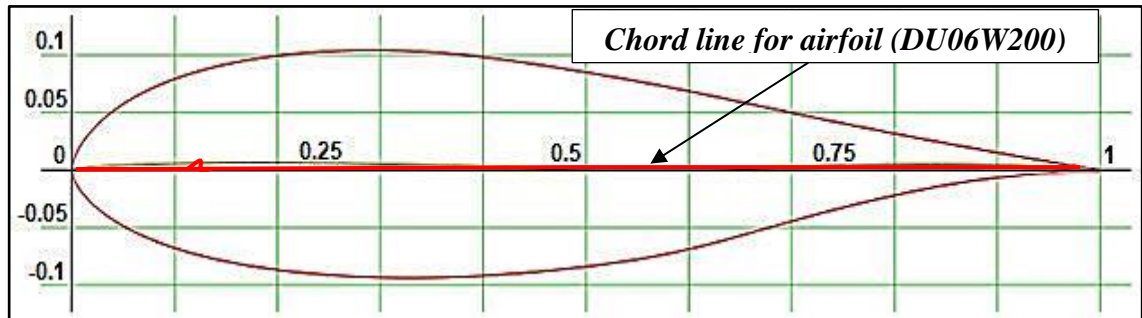


Figure 3.2. Airfoil (DU06W200) cross-section [136].

3.2.6. Solidity (σ)

The solidity of the blade cannot be confused with the solidity of the rotor, which is the ratio of the rotor blade's total area to the area of the rotor. It's a non-dimensional factor that influences the competencies of self-starting. Reducing the solidity enhances the wind turbine's self-starting as well as raises the TSR range with the creation of energy, but induces an increasing ineffectiveness. The solidity is dependent on the chord of the blade, the blade number, and the radius of the rotor. It's written by:

$$\sigma = \frac{N_b c h}{2R h} = \frac{N_b c}{2R} \quad (3.5)$$

Where:

N_b : The blades no.

c : The chord length of the blade

h : The height of the rotor height

R : The radius of is rotor [40, 42].

3.2.7. Initial Attack Angle (α)

It's the angle between the comparative velocity of wind (u) and the line of the chord, as revealed in Figure 3.3.

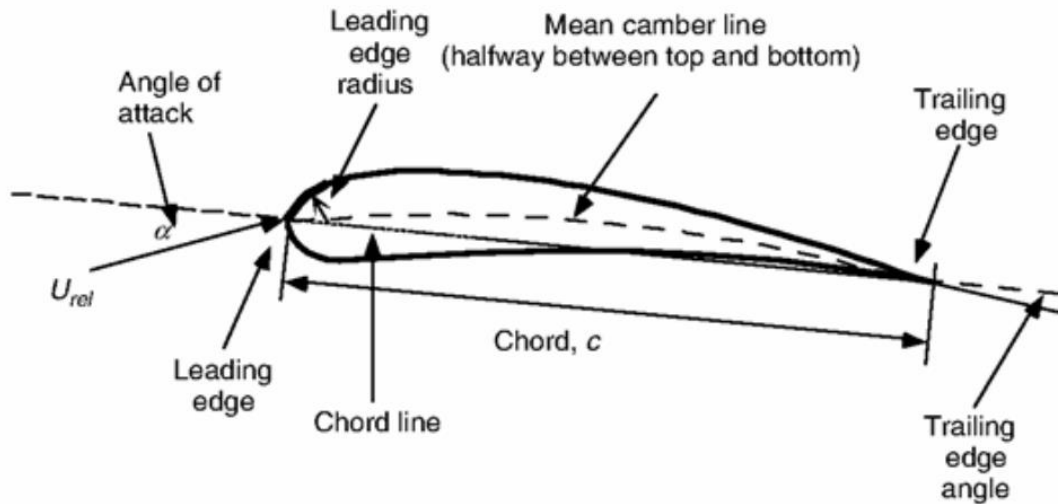


Figure 3.3. Nomenclature of airfoil [140].

The attack angle distribution throughout the whole cycle possesses a significant influence on the VAWT's overall power coefficient (C_p). The value of the circulation attack angle should have the appropriate value, which guarantees that the flow smoothly leaves the trailing edge. Also, the positive value for the initial attack angle enlarges the angular speed working range, but the negative value reduces it. Additionally, the torque is influenced in a similar manner if the negative attack angles cause a lower torque and ultimate (C_p). Furthermore, the angle of attack for (DVAWT) in the present investigation was taken to be 10° , depending upon the airfoil kind (DU06W200) database as well as the numerical simulation [136].

3.3. DVAWT ANALYSIS

The rotor of the Darrieus WT rotor can be analyzed by either a single stream-tube technique or a multiple stream-tube technique. And, in a single stream-tube analysis, the ultimate C_p is 0.5926(Betz limit). Figure (3.4) displays the DWT's forces and blades' velocities.

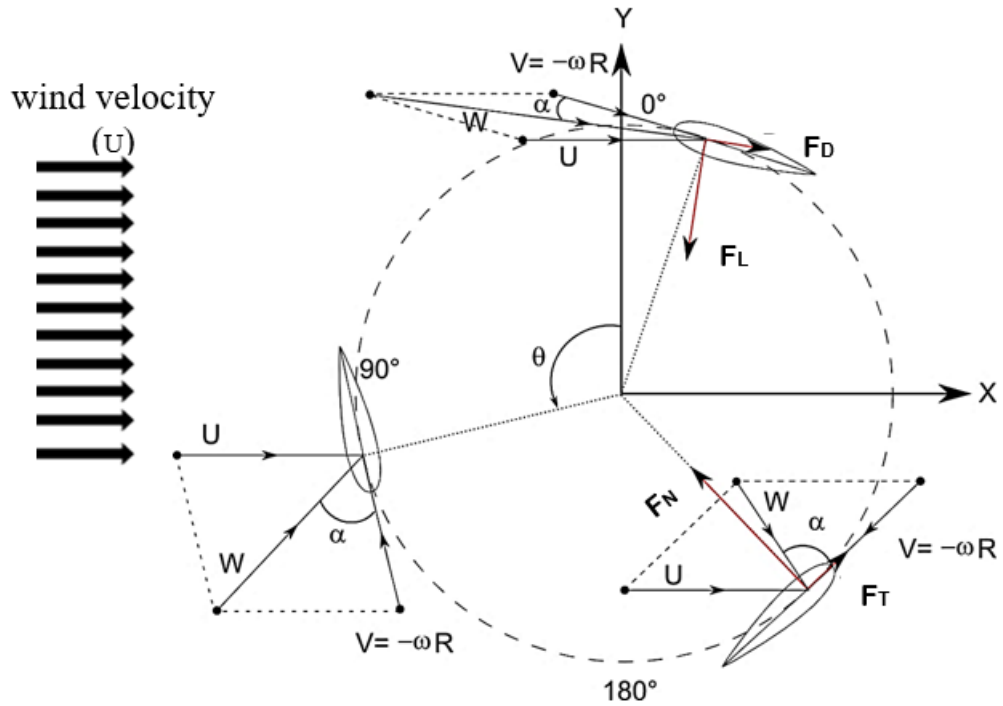


Figure 3.4. Forces and velocities of the blades of DWT [141].

The equations for lift force (F_L) and drag force (F_D) are among the most important equations of aerodynamics. It determines the amount of force acting on objects moving in the air.

$$F_L = \frac{1}{2} C_\rho V^2 C_c \quad (3.6)$$

$$F_D = \frac{1}{2} C_\rho V^2 C_D \quad (3.7)$$

$$V = -\omega R \quad (3.8)$$

The operating principle of the whole wind turbine is based on the aerodynamics of the applied forces on the particularly designed blades. The overall analysis of a section of the blade (the airfoil) was already conducted in the preceding section. Also, the form as well as the dimension of such profiles possesses a higher influence on machine efficiency and expense and, thus, on their economic feasibility. Then, it's essential to evaluate the features of a specific design before appropriately adapting it to achieve its ultimate efficacy. There are numerous approaches for evaluating the applied forces

upon the rotors and the resulting power provided, as well as their efficacy. Now, their concise depiction will be given because thorough evolutions can be obtained in the literature, as shown in Figure 3.5.

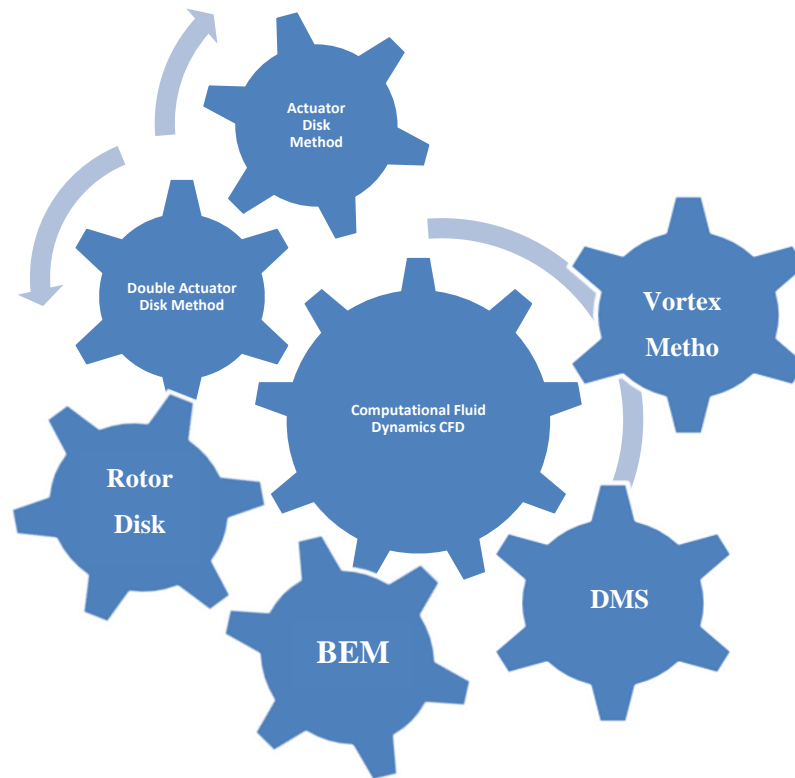


Figure 3.5. Flowchart of wind turbine analysis.

3.3.1. Actuator Disk Method

The analysis, depending upon the actuator disk model, espouses the subsequent suppositions:

- The flow of fluid is perfect across the control volume; that means it's steady, inviscid, uniform, not compressible and non-rotational.
- There's an unlimited blade number, therefore fitting the depiction of the actuator disk.
- The flow as well as the thrust is homogenous across the area of the disk.
- The undisturbed ambient static pressure is supposed for the static pressure remote downstream and upstream of the disk of the rotor.

In such a technique, a perfect rotor is supposed to. It's assumed that there's a pressure discrepancy across the rotor, causing the creation of a thrust which conducts the operation upon the turbine, as illustrated in Figure 3.6.

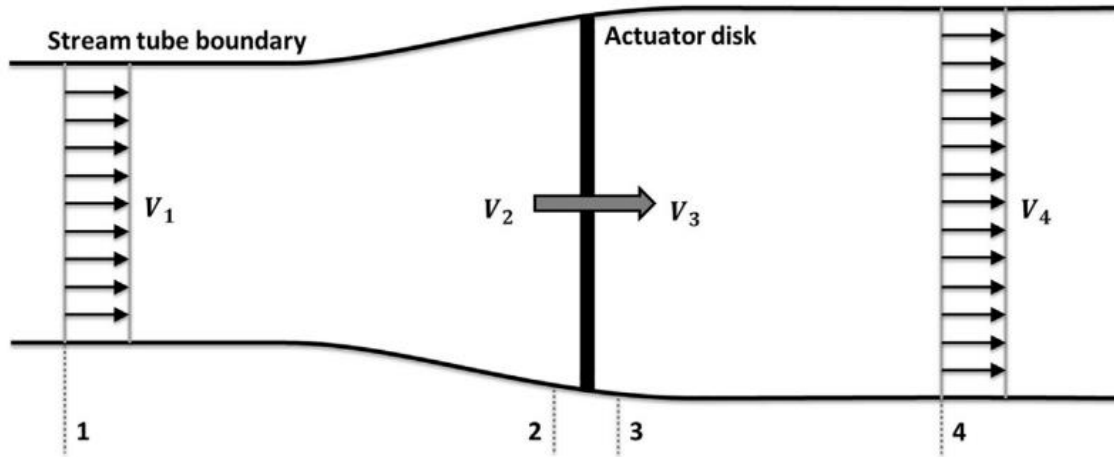


Figure 3.6. The control volume for the model.

$$V_1 = V_2 + u \quad (3.9)$$

V_1 : wind speed at the blade edge

V_2 : wind speed at the rotation axis

And, in exchange, the disk of the actuator decreases the free speed of the stream as energy is conveyed to it. Such a model is utilized for describing the Lanchester-Betz or the Lanchester-Betz-Joukowsky limit, which is a theoretical limit on the energy quantity that can be removed via a rotor-based wind turbine. And, the ultimate efficacy for the disk of the actuator is obtained to be 59.3% [142].

The control volume for the model of the wind turbine's actuator disk, Figure 36, where V represents the velocity of air; 1, 2, 3, and 4 specify the sites [142].

3.3.2. Double Actuator Disk Procedure

According to Paraschivoiu [143], it was manifested that the obtained theoretical limit for a single-actuator disk would be negative if implemented for the VAWT.

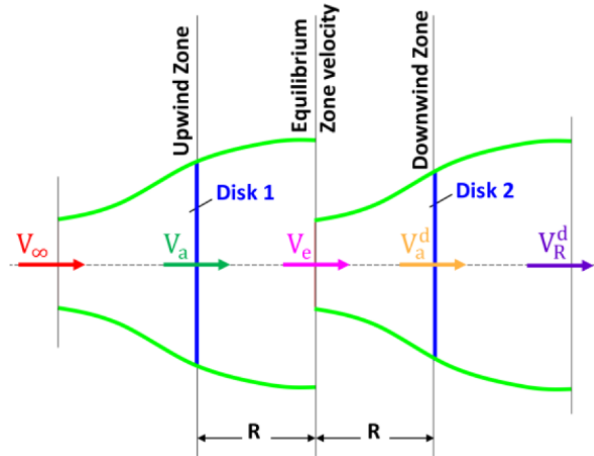


Figure 3.7. Schematic of two-actuator disk [143].

$$P = \frac{1}{2} \rho (V_a - V_d)^3 (\pi R^2) C_p \quad (3.10)$$

P is power generated by the wind turbine.

V_a is wind speed in the front region

V_d is the wind speed in the rear region

R is the radius of the rotor

That is mostly due to the fact that the fluid intersects the rotor two times in one rotation: in the downstream and upstream turn parts. Thus, when the methodology utilized in the preceding state is implemented for both disks of the actuator in sequence, the ultimate efficacy is obtained to be 64%, as defined by Newman [144], as shown in Figure 3.7.

3.3.3. The Rotor Disk Procedure

In such a situation, instead of suggesting a thrust as in the preceding situation, a torque was utilized [137]. Thus, it travels away from an abstract turbine to a further turbine

rotor that has also been modelled extra believably, integrating the wake rotation. This means that as a portion of energy is moved to the wake, the general amount of energy removed will decrease. Nevertheless, it has to be taken into consideration that such theory presumes an unlimited blade number and, extra significantly, has evolved regarding the pattern of wake created via a HAWT.

3.3.4. Theory of Blade-Element/Momentum (BEM)

It is also recognized as a strip theory; it's an amalgamation of two theories. The theory of momentum is applied to a blade's control volume for analyzing the forces upon it depending upon the linear and angular momentum conservation in a streamtube. Also, in the theory of blade-element, the forces are scrutinized at the blade's section and rely upon the geometry of the blade. Theory BEM is highly hard and can be utilized for obtaining the wind turbines' theoretical performance curves, their axial forces, and their torque. The blades are separated into sections that are individually investigated in a stream moving in the reverse sense of the rotor rotation. Also, the forces in every section are determined from the examinations conducted in the wind tunnel for various airfoils, and thus, the viscosity is considered indirectly. Additionally, as the interaction between every blade and the other wake isn't regarded, such a technique isn't appropriate for the VAWTs' design and analysis, as it has mainly been implemented in the HAWTs.

3.3.5. Method of Double Multiple Streamtube (DMS)

Such a model is an amalgamation of a derivation of the theory of momentum employing many streamtubes and the technique of double actuator disk, Paraschivoiu [143], as shown in Figure (3.8).

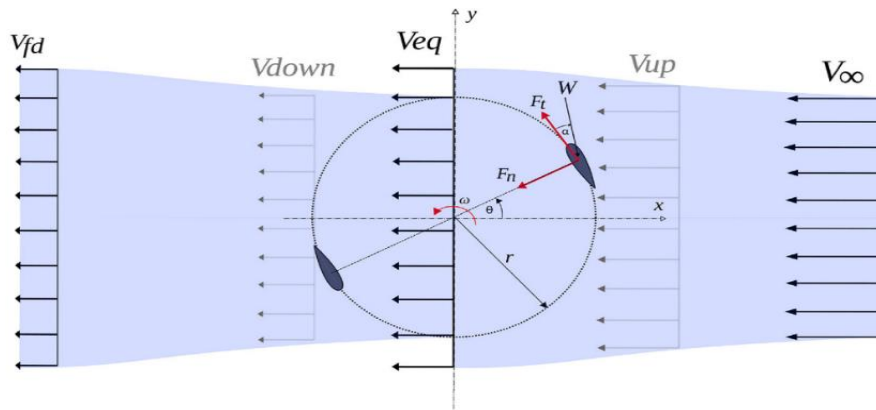


Figure 3.8. Illustration of the velocity field for the actuator disk theory in the DMS approach [145].

And it possesses the drawback that the (2) disks influence is similar for the whole streamtubes as well as cannot be adapted for anyone. Also, its use is restricted to the low ratios' values of tip speed and with some restrictions to the dimensions of blades for staying within the validity range of the theory of momentum. The modifications to the technique comprise the integration of dynamic stall models that can also be semiempirical or theoretical, as presented and modified for use in VAWTs as presented by Brahim et al. [146].

3.3.6. The Vortex Method

In such a technique, blades as well as vorticity downstream and upstream are modelled by lifting lines, as clarified via Milne-Thomson [147]. The strength of the vortex is determined by considering the circulation of the blades and the lift created via the flow above them. Also, there's a trailing wake created via the circulation's span-wise change in addition to the shed wake created via the circulation's temporal change. Then, it's likely to determine the generated velocity at each point from the vortices' position and strength. Later, such a technique was substituted by introducing the free vortices idea that is shed from the revolving blades. Such vortices describe a slipstream as well as create the generated velocities. Nevertheless, it's likely to utilize a separate application of the vortex technique for computing the VAWT's aerodynamic sound, as it was depicted that the intricate structure of the wake can be caught [148].

3.3.7. Computational Fluid Dynamics (CFD)

Such a technique includes the numerical solution of the fluid dynamics governing equations. The continua are separated or discretized into small volumes, resulting in what is recognized as a grid or mesh, where the intricate, incomplete differential formulas are solved. Today, owing to the rise in computational power, it's highly normal to utilize the CFD for wind turbine investigation as well as scrutiny. Also, in such a manner, when sufficient hypotheses and models are being applied, it's likely to employ the simulations of CFD as a means for testing and comparing qualitatively a broad range of shapes and operating circumstances prior to defining a set of encouraging designs for proceeding with the prototype building and investigational testing. The functions evolved as a part of the present thesis will be dependent mainly on CFD calculations, with suitable analytical and theoretical confirmations when likely. Also, in the project's highly progressive steps, a group of investigational tests will be conducted, giving respected outcomes for validating the computations achieved at this time.

3.4. NUMERICAL MODELING

For obtaining a fruitful design and appropriate VAWT rotor geometry, different styles of modelling have to be implemented. The ansys-fluent program was utilized in the present investigation for simulating and validating. Transient conditions are considered for this modelling. Figures (3.9) and (3.10) display a 2D computational domain for the model of DVAWT. Two parts are divided via a sliding interface into the domain. The wind tunnel testing region is stationary; that's the domain's initial part. Also, the wind experimental (stationary domain) dimensions are 80 m x 50 m. Figure (3.11) evinces the mesh in the CFD domains, the mesh upon the rotor, and the mesh around the rotor; it also shows the mesh close to the blade, depicting the boundary layers. Additionally, the flow around the rotor is turbulent; therefore, the CFD simulation around the rotor is intricate. The CFD simulations were implemented for solving the equations of the states depending upon the 2D unsteady finite volume incompressible Reynolds Averaged Navier-Stokes (URANS). Furthermore,

controlling the turbulence flow equations are the equations of continuity and Navier-Stokes, and such equations in the conservative shapes include [149–151]:

$$\text{Continuity eq.: } \frac{\partial \rho}{\partial t} + \sum_{i=1}^3 \frac{\partial}{\partial x_i} (\rho u_i) = 0 \quad (3.11)$$

$$\text{Momentum eq.: } \frac{\partial (\rho u_i)}{\partial t} + \sum_{j=1}^3 \frac{\partial}{\partial x_j} (\rho \overline{u_j u_i}) = -\frac{\partial P}{\partial x_i} + \sum_{j=1}^3 \frac{\partial}{\partial x_j} (\overline{\tau_{ij}} - \rho \overline{u_j u_i}) + S_{ui} \quad (3.12)$$

Where:

$$S_{ui} = -\rho [2 \vec{\Omega} \times \vec{u} + \vec{\Omega} \times (\vec{\Omega} \times \vec{r})] \quad (3.13)$$

$$\overline{\tau_{ij}} = -\mu \left(\frac{\partial \overline{u_i}}{\partial x_j} + \frac{\partial \overline{u_j}}{\partial x_i} \right) \quad (3.14)$$

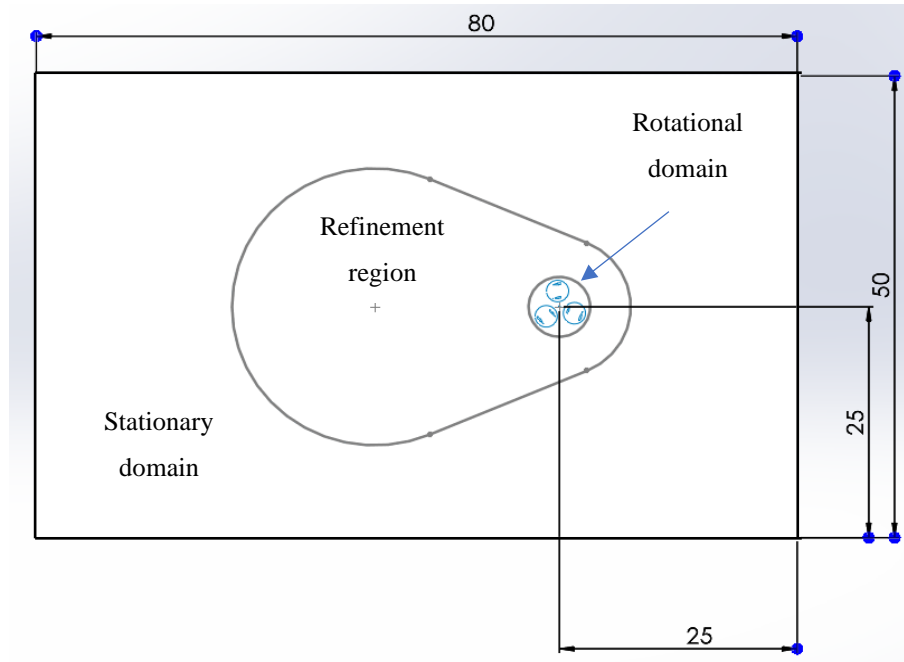
S_{ui} : Centrifugal and Coriolis force $\vec{\Omega}$: Rotational speed (rpm) \vec{r} : Position vector
 $\overline{\tau_{ij}}$: Average shear stress \vec{u} : Relative velocity of fluid ρ : Air density
 μ : Dynamic viscosity

For numerically solving the state of the field of flow around the rotor, the models of turbulence were supplemented with the URANS, CFD solvers.

3.4.1. The Boundary Conditions

Simulation boundary conditions for such an investigation include:

Numerical simulation using the SST k- ω turbulence model. The wind speed is 10 m/s, and the Rotor diameter is 6.5 m, the distance from the rotating domain axis is 25 m at the stationary domain entrance, as shown in Figure 3.9.



Dimensions in meter

Figure 3.9. The 2D computational domain for the DVAWT model.

The pressure on the exterior surface is the same as that on outside air. the rotor blade is designed as a nonslip flat wall. In the present investigation, a prismatic mesh was implemented on the rotor blades' sides to acquire accurate boundary layers and study the flow in the boundary layers of rotor blades with greater precision. Consequently, the lattice density was greater near the rotor blades' wall than in other areas. The stationary domain's walls (sides and top) are configured to be permeable to atmospheric pressure. Also, A nonslip, smooth wall serves as the foundation of the stationary domain. Numerical simulation using the SST $k\omega$ - turbulence model.

3.4.2. Turbulence Models

One of the key issues with turbulence modelling is the precise prediction of flow separation from a smooth surface. Under unfavorable pressure gradient conditions, typical two-equation turbulence models frequently fail to predict the beginning and the amount of flow separation. For this purpose, a number of cutting-edge turbulence models have been developed by aerodynamics researchers .

The 2D SST $k-\omega$ turbulence model was utilized in previous research, and it is consistent with the results of experiments [152]. This model is used to examine the transient forces that affect wind turbines with vertical axes, as shown in Figure 3.10.

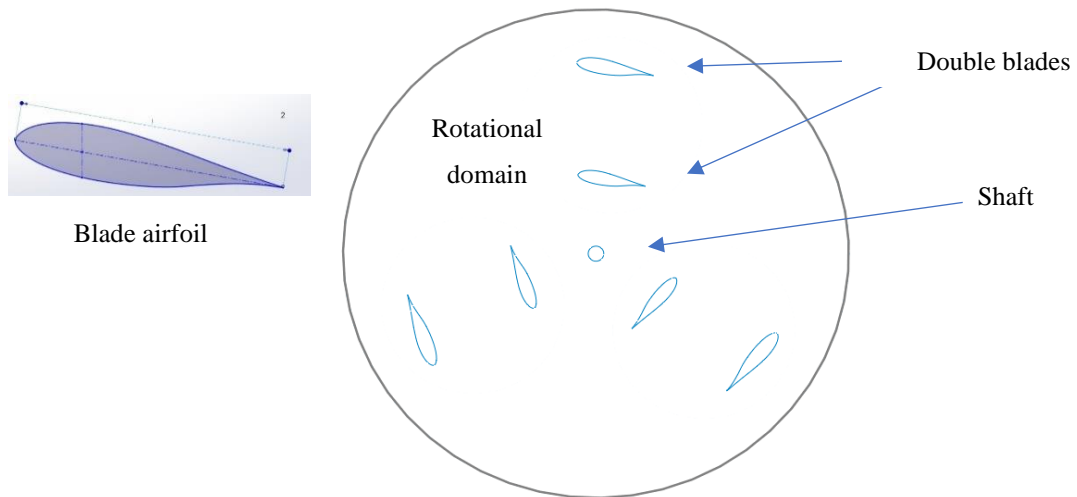


Figure 3.10. Rotational domain for the DVAWT model.

To achieve decent results, Y^+ must have a low value (Y^{+1}) [153]. A reliable two-equation eddy-viscosity turbulence model used in computational fluid dynamics is called shear stress transport (SST). In order to apply the model of k -turbulence into the boundary layer's internal zone and transition to the k -turbulence model in the free shear flow, the SST model combines the k - and k -turbulence models. Without any additional damping factors, the shear stress transport SST $k-\omega$ turbulence model can be utilized as a model of low Re turbulence [154]. So, in this study, numerical simulation was used to apply the SST $k-\omega$ turbulence model.

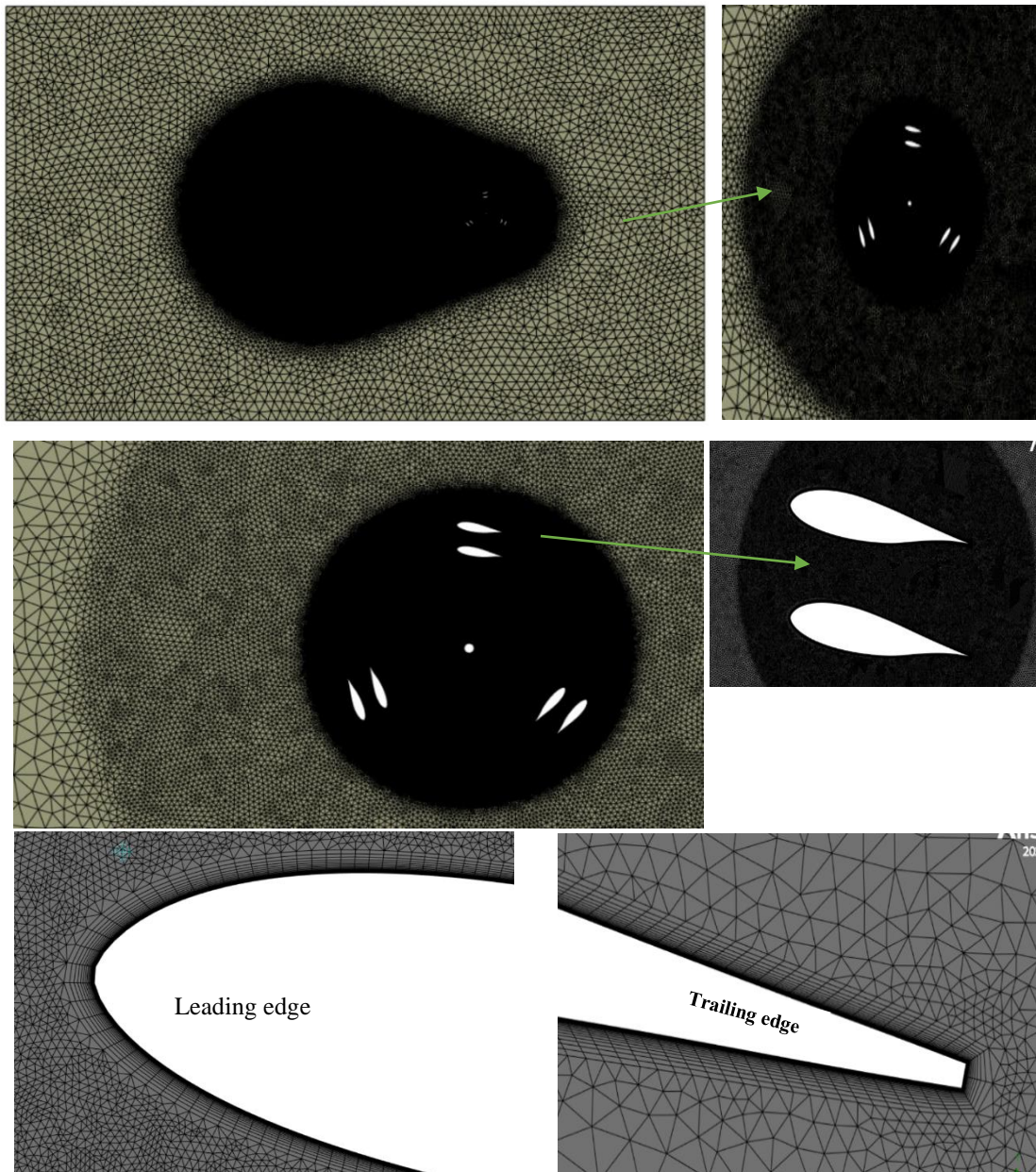


Figure 3.11. Mesh generation for CFD domains with different views.

3.4.3. Mesh Dependency

Before beginning a simulation process, a mesh sensitivity analysis was performed to ensure minimal numerical simulation error and to shorten the duration of the process. Design 3 demonstrates the testing of five different meshes for the fresh models of design by varying sizes of the element, as revealed in Table (3.1), like TSR (3.25), and a (10 m/s) speed of wind and $Y^+ = 0.0008$ to 3.4, Courant number from 0.241 to 32.

The experiments were included in order to compute power. The relationship between the power coefficient and grid size is depicted in Figure 3.11.

Table 3.1. Grid optimization (Design 3, TSR=3.25)

No.	Total no. of cell (Millions of cells)	Cp
1	0.937	0.1978
2	1.180	0.2201
3	1.364	0.2155
4	1.780	0.2134
5	2.016	0.2140

3.4.4. Orthogonal Mesh Quality

Mesh quality histograms are graphical representations of the distribution of mesh quality values in a computational mesh. Mesh quality is a measure of how well the elements in a mesh conform to certain criteria, such as shape, size, and aspect ratio, in the context of finite element analysis or computational simulations.

To create a histogram of mesh quality, you'll need simulation software or mesh generation tools that provide information about the quality of each element in the mesh. The frequency, or count, of elements falling within different quality ranges will then be displayed on the histogram.

- Aspect ratio, skewness, and other measures that assess the geometric properties of individual mesh elements are examples of mesh quality metrics. Analyzing a mesh quality histogram can assist engineers and researchers in identifying areas of a simulation where the mesh may require refinement or improvement

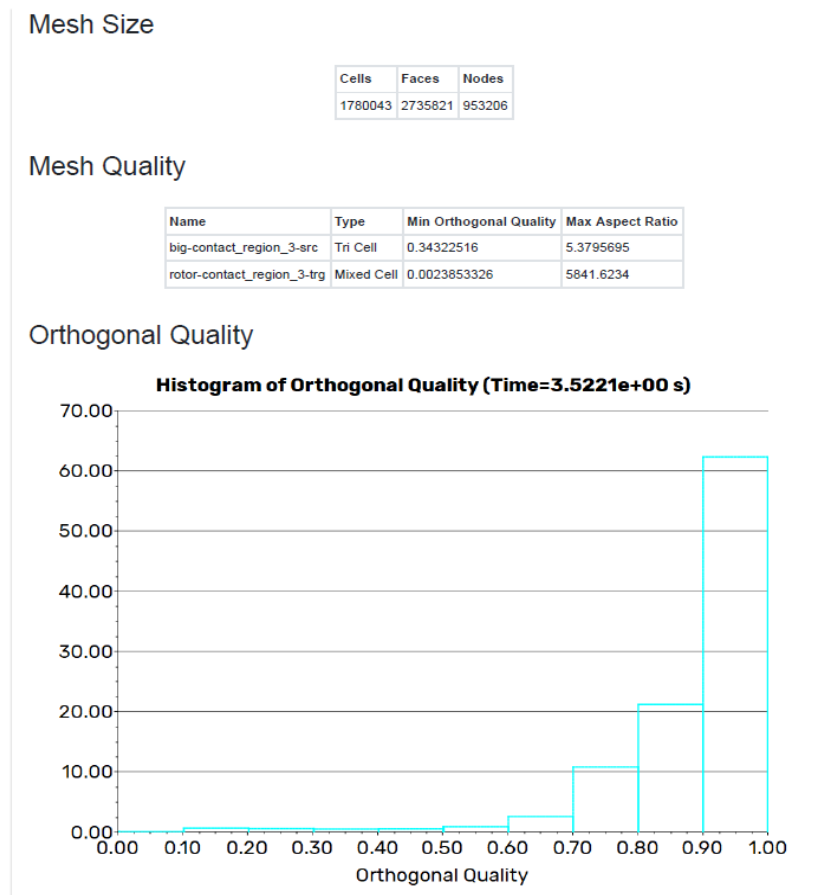


Figure 3.12. Mesh Orthogonal Quality Generation for CFD.

Figure 3.12 shows The numbers on the vertical axis represent the mesh quality value. These values range from 0 to 1, where a value of 0 indicates a mesh with low quality and a value of 1 indicates a mesh with high quality.

- The mesh quality stops improving significantly at about the height of 60.00 on the element. In general, it is recommended to use a mesh with a quality of at least 0.9. However, the same applications may require higher-quality meshes.
- More information about mesh properties can be found in Figure 3.13.

Scope	
Scoping Method	Geometry Selection
Geometry	1 Face
Definition	
Suppressed	No
Boundary Scoping Method	Named Selections
Boundary	BLADES
Inflation Option	Smooth Transition
<input type="checkbox"/> Transition Ratio	Default (0.272)
<input type="checkbox"/> Maximum Layers	40
<input type="checkbox"/> Growth Rate	1.2
Inflation Algorithm	Pre

Scope	
Scoping Method	Geometry Selection
Geometry	1 Body
Definition	
Suppressed	No
Type	Body of Influence
Bodies of Influence	3 Bodies
<input type="checkbox"/> Element Size	5.e-003 m
Advanced	
<input type="checkbox"/> Growth Rate	Default (1.2)

Defaults	
Sizing	
Quality	
Inflation	
Use Automatic Inflation	None
Inflation Option	Smooth Transition
<input type="checkbox"/> Transition Ratio	0.272
<input type="checkbox"/> Maximum Layers	40
<input type="checkbox"/> Growth Rate	1.2
Inflation Algorithm	Pre
View Advanced Options	No
Batch Connections	
Advanced	
Number of CPUs for Parallel...	24
Straight Sided Elements	No
Rigid Body Behavior	Dimensionally Reduced
Triangle Surface Mesher	Program Controlled
Topology Checking	Yes
Use Sheet Thickness for Pin...	No
Pinch Tolerance	Default (9.e-003 m)
Generate Pinch on Refresh	No
Sheet Loop Removal	No
Statistics	
<input type="checkbox"/> Nodes	744198
<input type="checkbox"/> Elements	1362019
Show Detailed Statistics	No

Figure 3.13. Mesh generation technique in the present study.

3.5. VALIDATION CASE STUDY

Elaborate CFD analysis was conducted on the two-dimensional unsteady Darrieus turbine with 3 blades as outlined in Reference [155]. This particular turbine, boasting a diameter of 5 meters, employed the Naca 0018 airfoil for its blade cross-section ,as shown in table 3.2. geometry. The flow areas where both the flow field and the rotational motions of the blades were defined are visually depicted in the figure 3.14. and 3.15, The wind speed was maintained at a consistent 8 meters per second throughout the study.

Adopting the identical Darrieus turbine geometry used in Reference [155], our study focused on arranging analyses according to the unsteady CFD flow field and mesh creation strategy to be employed. Similar to the methodology chosen in Reference [155], we also opted for the SST k-e turbulence model. These analyses were carried out across various tip speed ratio values, with wind speeds set at 8 m/s and 15° angle of attack, yielding torque and power values. Additionally, a torque-time graph was generated, displaying the variations in torque over a single revolution. Contours for that the value of Tip Speed Ratio (TSR) is 3 are presented in the figures.

Figures 3.14 and 3.15. In the domain, a sliding interface separates two segments. The wind experimental testing zone represents the first portion of the domain, which is stationary. The CFD wind (stationary domain) measures 85 meters by 50 meters. Figure 3.16 depicts the mesh in CFD domains: the mesh upon the rotor and the mesh surrounding the rotor, as well as the mesh close to the blade displaying the boundary layers. Since the flow around the rotor is experimental, the simulation of CFD around the rotor is intricate. The cases founded upon the equations of 2D unsteady Reynolds finite volume incompressible URANS, were solved using CFD simulations.

Table 3.2. Validation case study details.

Number of blades	3
Rotor diameter	5 m
Chord length	1 m
Rotation speed	8 rad/s
Velocity inlet	8 m/s
Blade type	NACA0018 symmetry

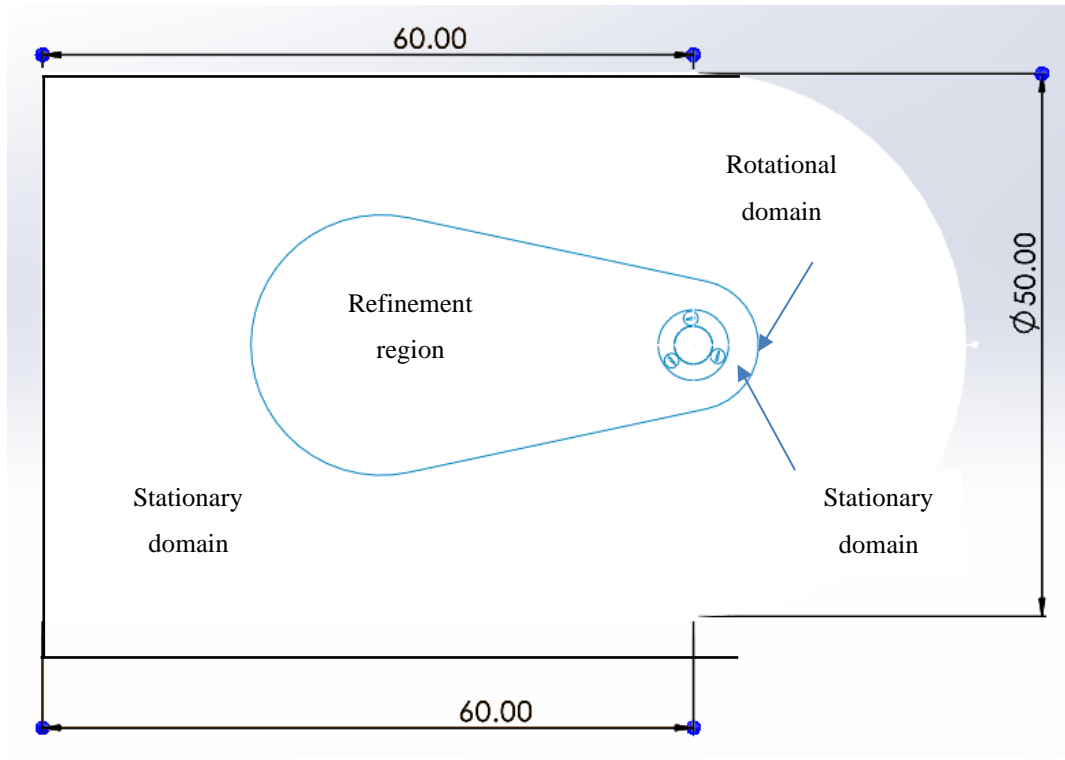


Figure 3.14. The 2D computational domain for DVAWT model according to [155].

The rotor diameter is 6.5 m and all dimensions are in meters in Figure 3.14.

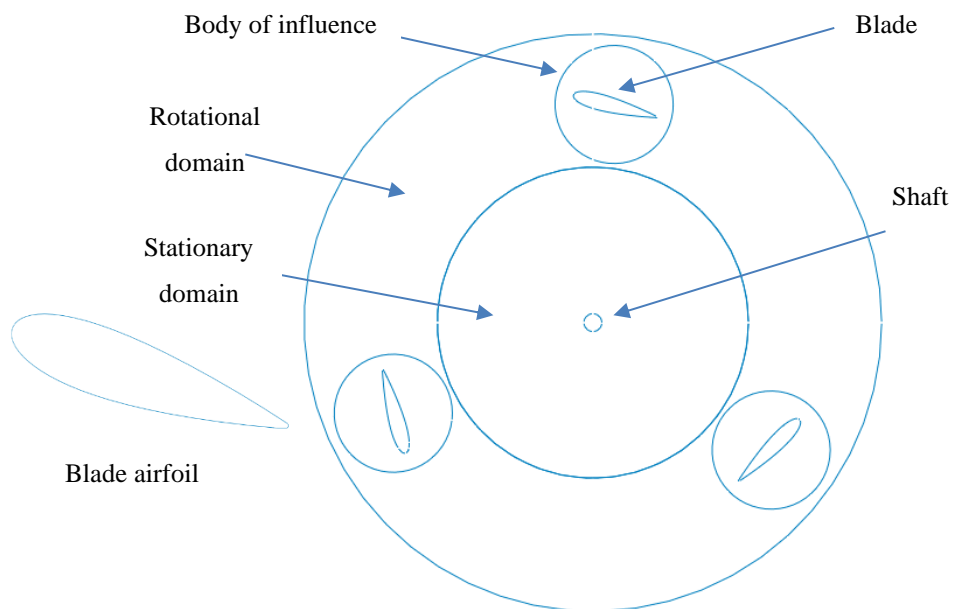


Figure 3.15. Rotational domain for the DVAWT model.

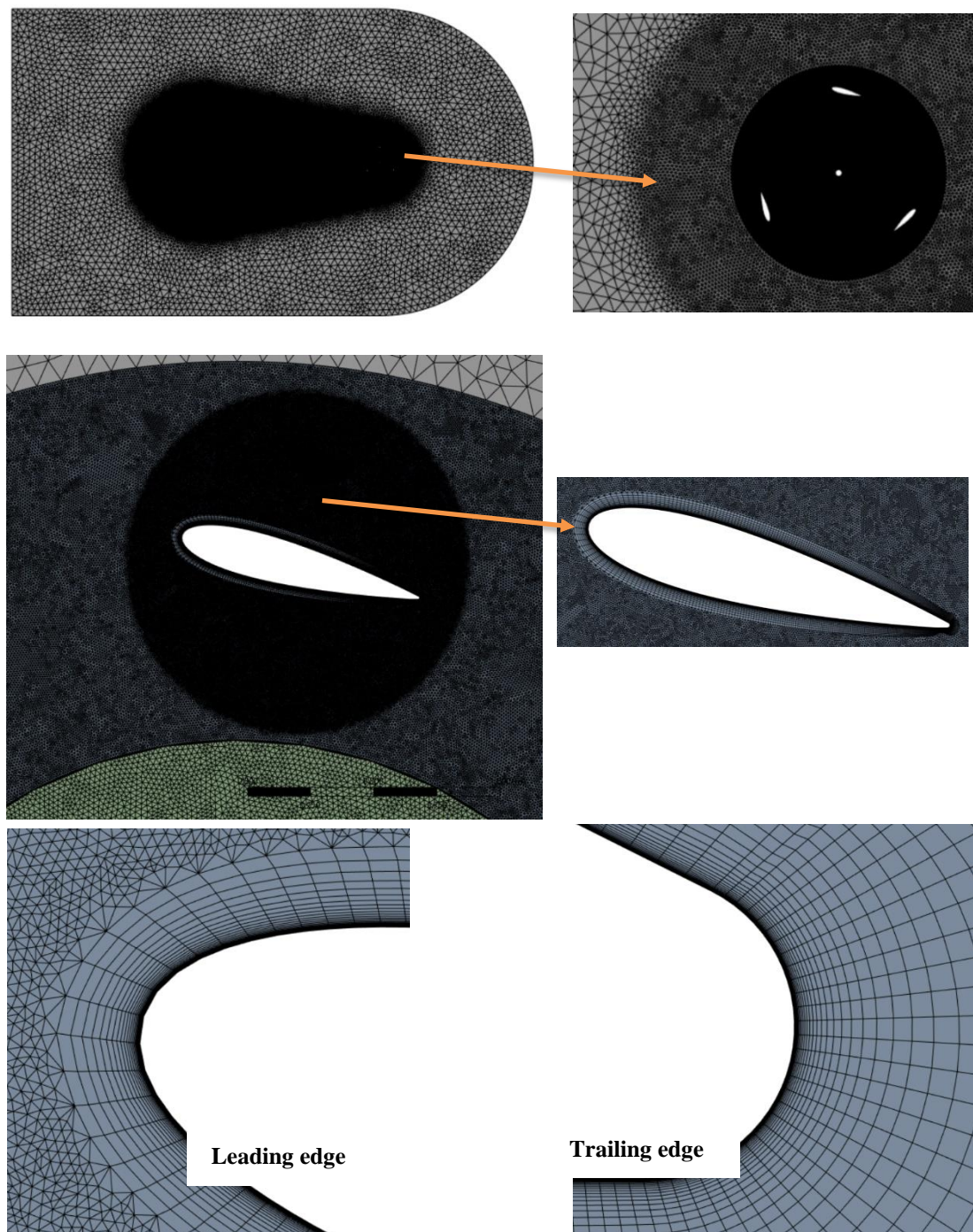


Figure 3.16. Mesh generation for CFD domains with different views.

According to the validation results, the numerical results from this study and the data from [155] are in good agreement, as shown in Figure 3.17. The Darrieusturbine geometry used in this study and the geometry used in the reference have the same characteristics. Both studies were performed with two-dimensional unsteady CFD analysis. For comparison purposes, the C_p -TSR values obtained in our study was

compared with the one derived from Reference [155], showcasing a notable alignment between the findings. The coherence observed between the torque graph and the obtained contours further bolstered the reliability of our CFD study. Following this validation process, four distinct two-dimensional Darrieus turbine designs were developed. The CFD analyses of these unique designs were conducted in adherence to our previously validated CFD analysis strategy. In the present study, DU06W200 airfoil is used for Design1, Design 2, Design 3 and Design4.

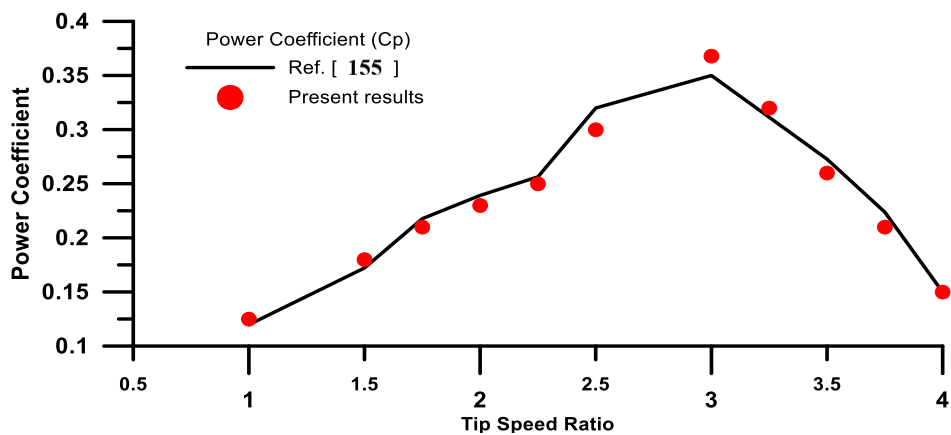


Figure 3.17. Power Coefficient (C_p) versus Tip Speed Ratio.

Torque variation results from our unsteady CFD analysis are similar to the results of Reference 155. The torque variation results after four cycles at TSR=3 is shown in Figure 3.18.

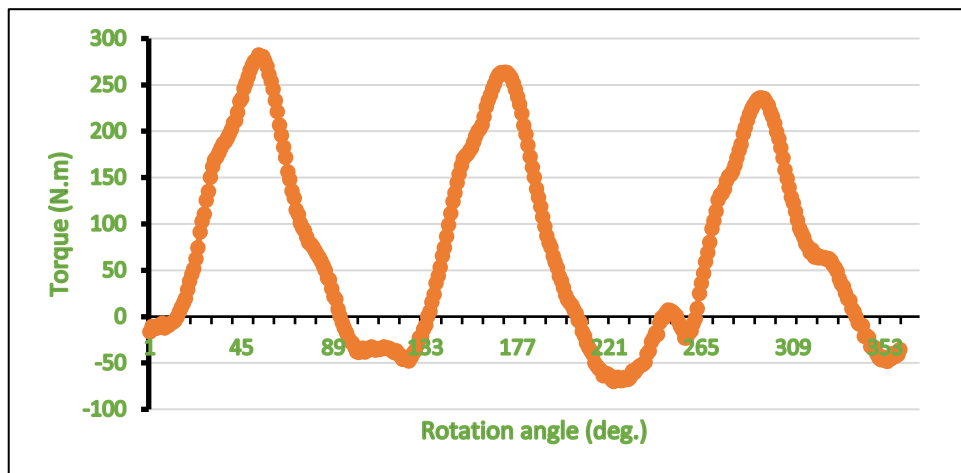


Figure 3.18. Torque variation of Darrieus for the present CFD study.

The geometry was simplified in the numerical simulation, especially by leaving out the connecting rods, which may be the cause of the little disparity between the current results and experiments. Additionally, some counter-findings at TSR value 3 are shown below.

Figures 3.19 to 3.26 show the contours for cases of validation at TSR =3.

Figure 3.19 shows the movement of the three rotor blades and the vortexes around them resulting from the highest velocity field at which they rotate.

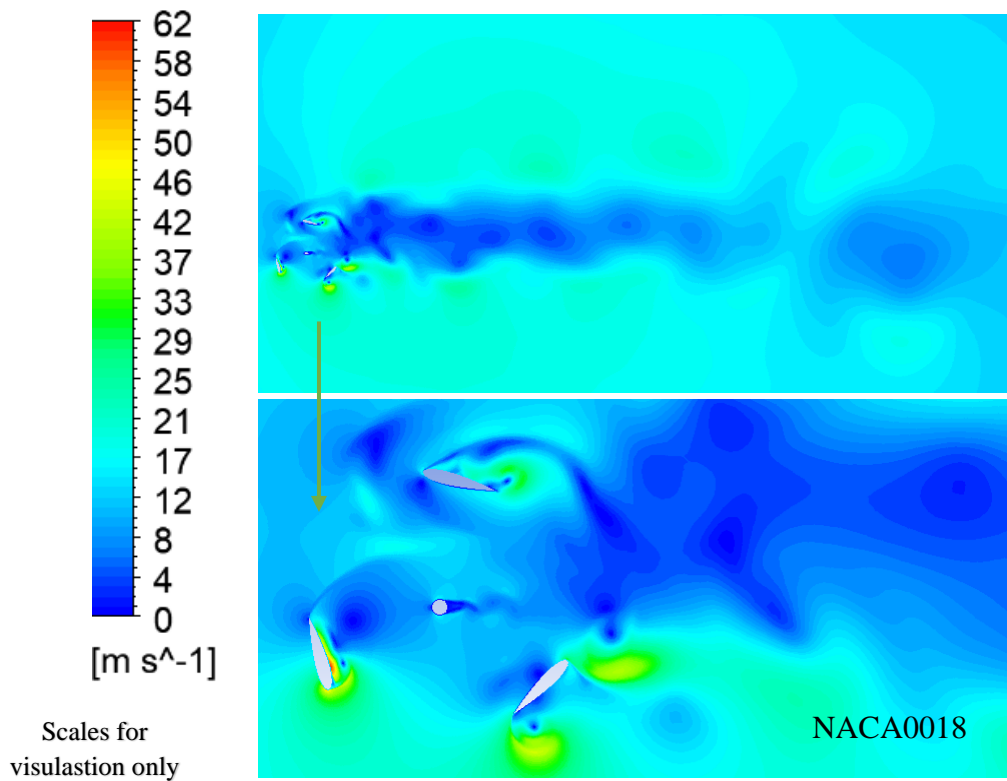


Figure 3.19. Velocity field contour.

In the validation case, when the velocity field contour, the maximum value is 62 m/s, after four cycles.

Figure 3.20 shows the extended velocity, and vortex force contour, which is greatest near the edge of the blade.

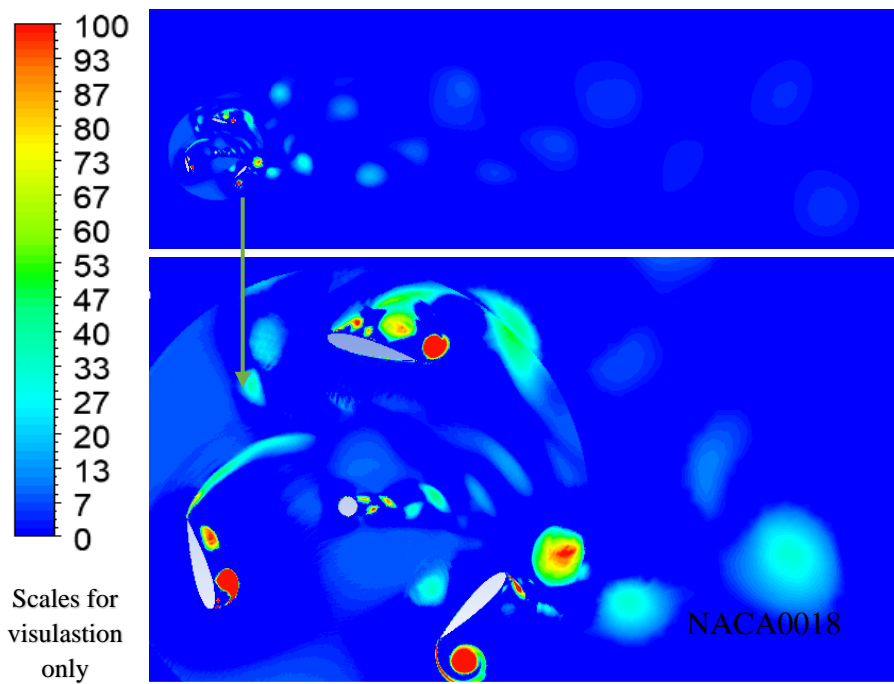


Figure 3.20. Velocity stretched swirling strength contour.

In the validation case, velocity stretched swirling strength contour, the maximum value is 37.122 after four cycles.

The expansion of the area and the effect of vortices around the blades show the contour of turbulent kinetic energy (Figure 3.21).

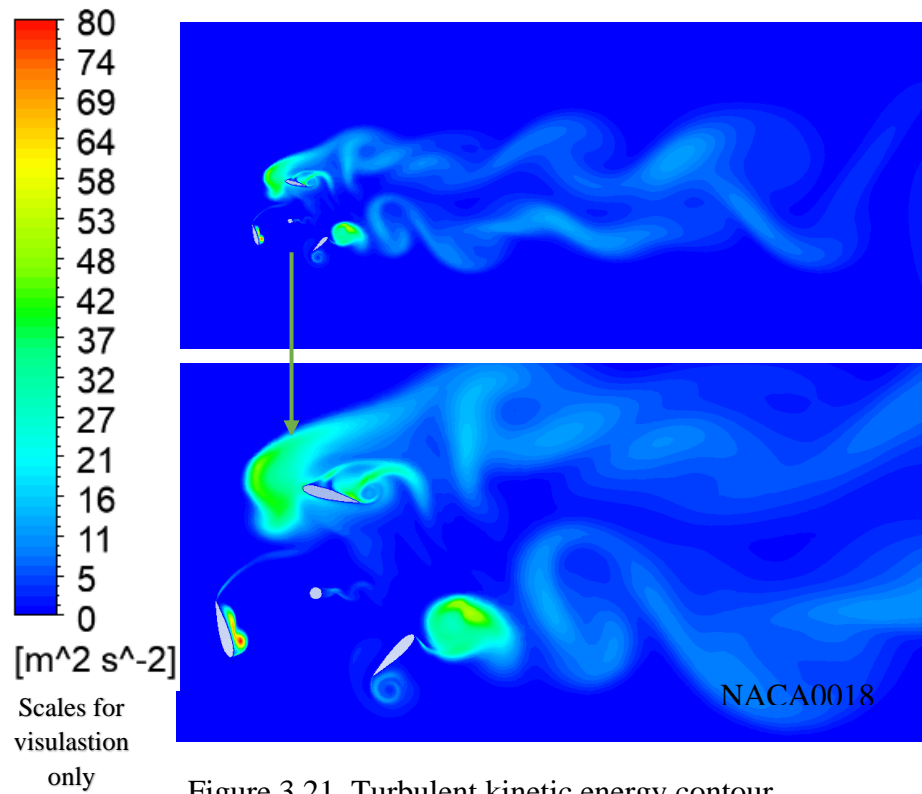


Figure 3.21. Turbulent kinetic energy contour.

In The validation case, the Turbulent kinetic energy contour and, the maximum value is $80 \text{ m}^2/\text{s}^2$, after four cycles.

Figure 3.21. shows the effect of vortexes around the blades, which may cause turbulence and vibration of the blade due to increased turbulence intensity

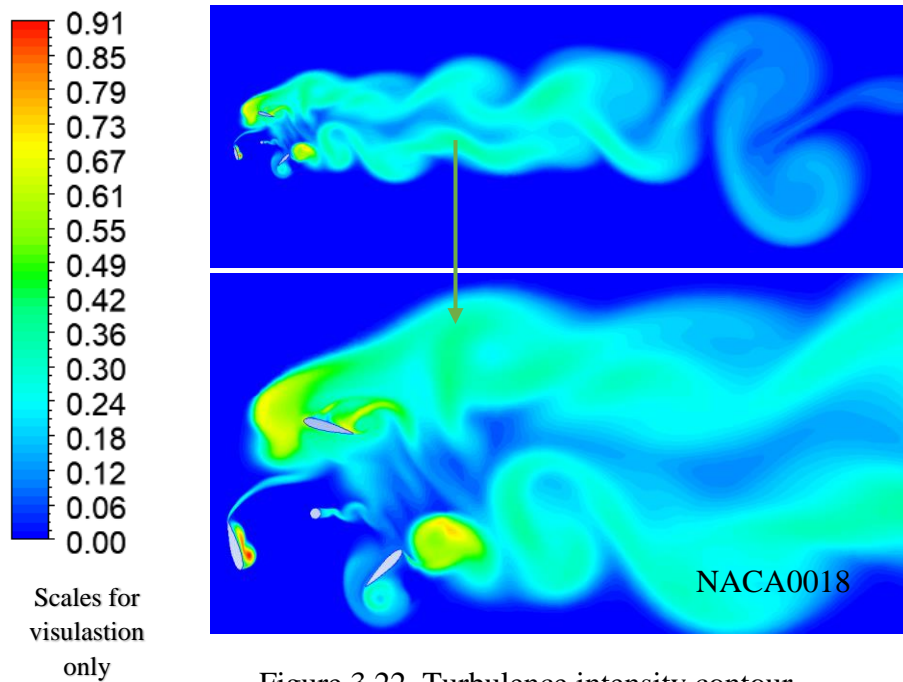


Figure 3.22. Turbulence intensity contour.

In The validation case, when the turbulent intensity contour and the maximum value is 0.91 after four cycles.

Figure 3.23 shows the effect of total pressure on the surfaces and ends of the blade.

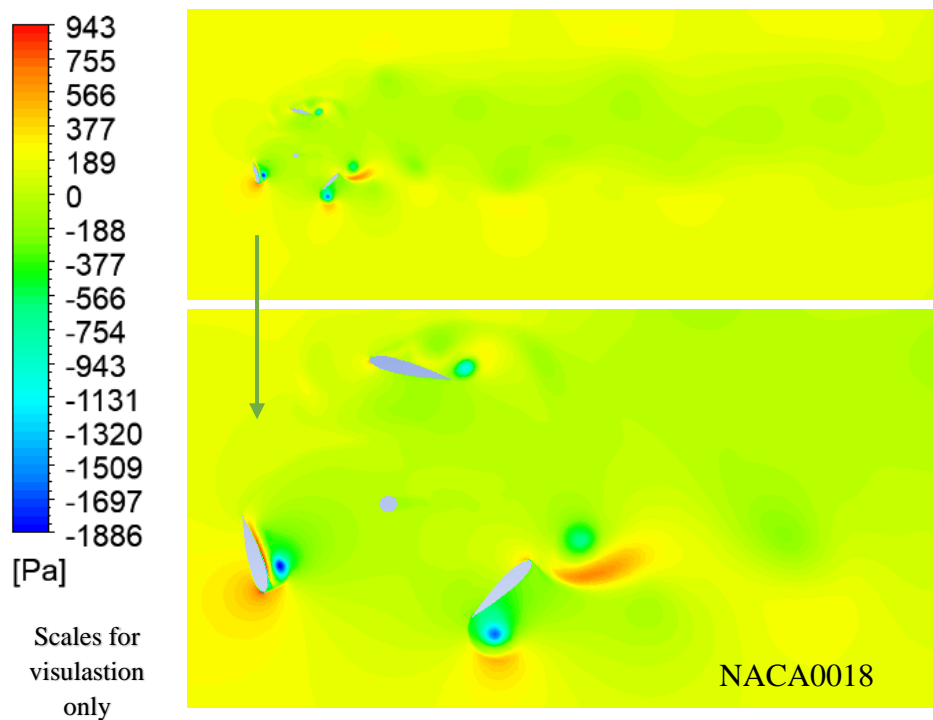


Figure 3.23. Total pressure contour.

In the validation case, when the total pressure contour and the maximum value is 943 Pa, while the minimum value is -1886 Pa m/s after four cycles.

Figure 3.24 shows the maximum value of vortex turbulence around the three blades and its significant effect.

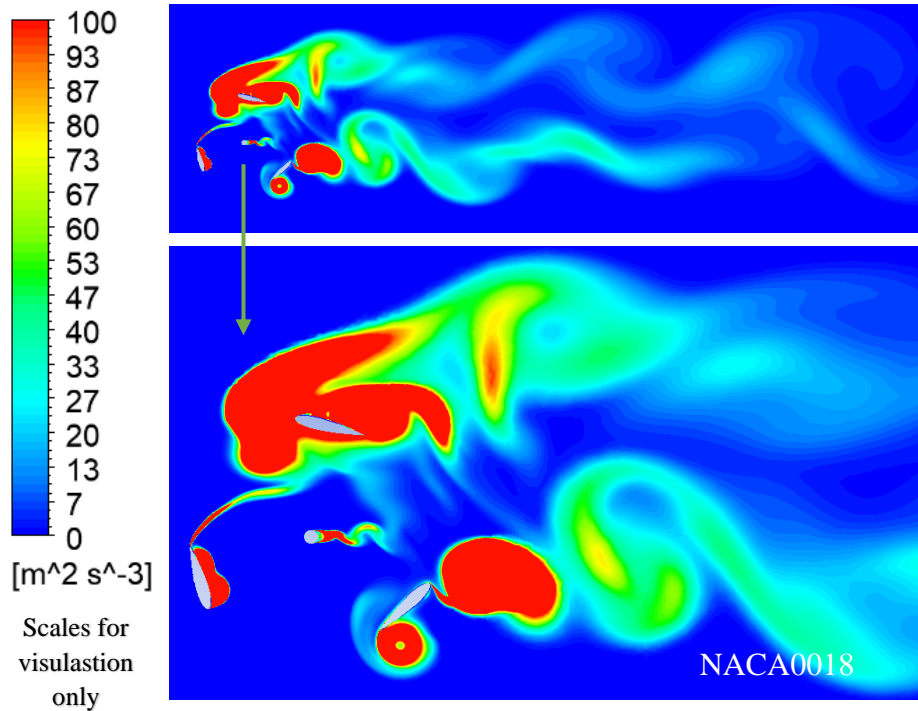


Figure 3.24. Turbulence eddy dissipation contour.

After four cycles, in the validation case, when the turbulent eddy dissipation contour and the maximum value is $716422 \text{ m}^2/\text{s}^3$.

Vortex turbulence can have a significant impact on the performance of vertical wind turbines. It can lead to increased drag, which reduces efficiency. They can also cause wind turbines to vibrate, potentially damaging them. In this image, the vortex turbulence lines indicate that the vortex turbulence is concentrated in an area in front of the wind turbine. This is where the airflow meets the rotor of the air turbine.

Figure 3.25 shows the vortices that are formed due to the effect of the velocity-invariant Q environment, which is evident near the surfaces of the blades and edges

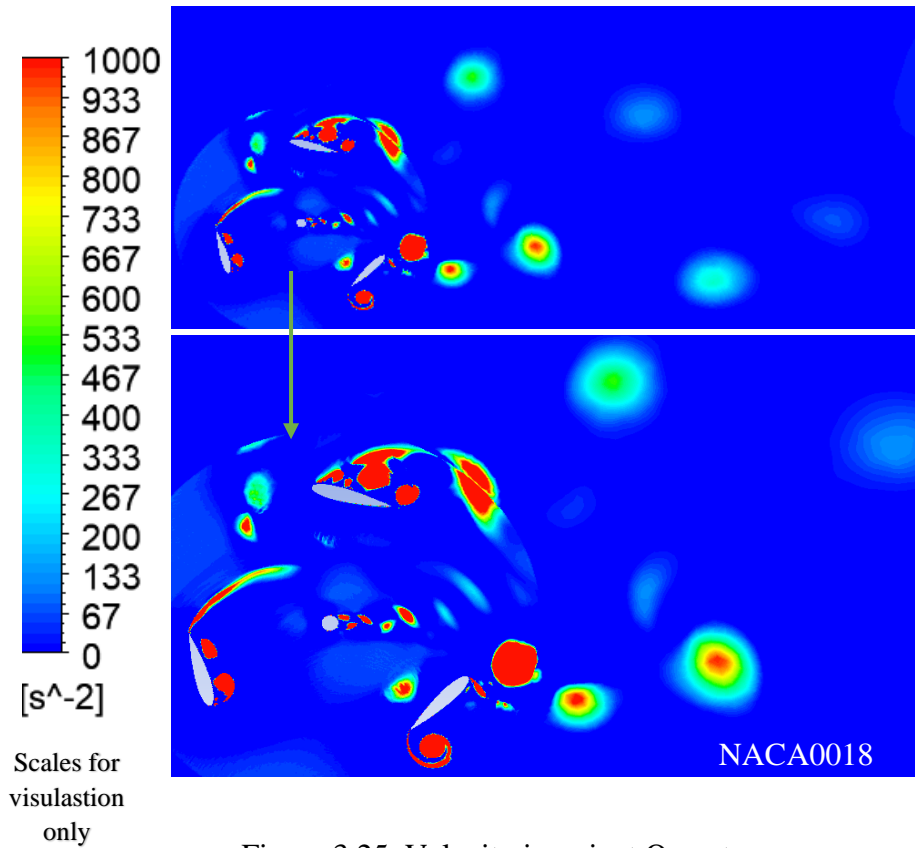


Figure 3.25. Velocity invariant Q contour.

In After four cycles, in the validation case, when the velocity invariant Q contour and the maximum value is $1.3 \cdot 10^9 \text{ s}^{-2}$, while the minimum value is $-3.5 \cdot 10^9 \text{ s}^{-2}$.

Figure 3.26 shows the vortices that are formed due to the effect of the constant Velocity swirling strength, which is evident near the surfaces of the blades and edges.

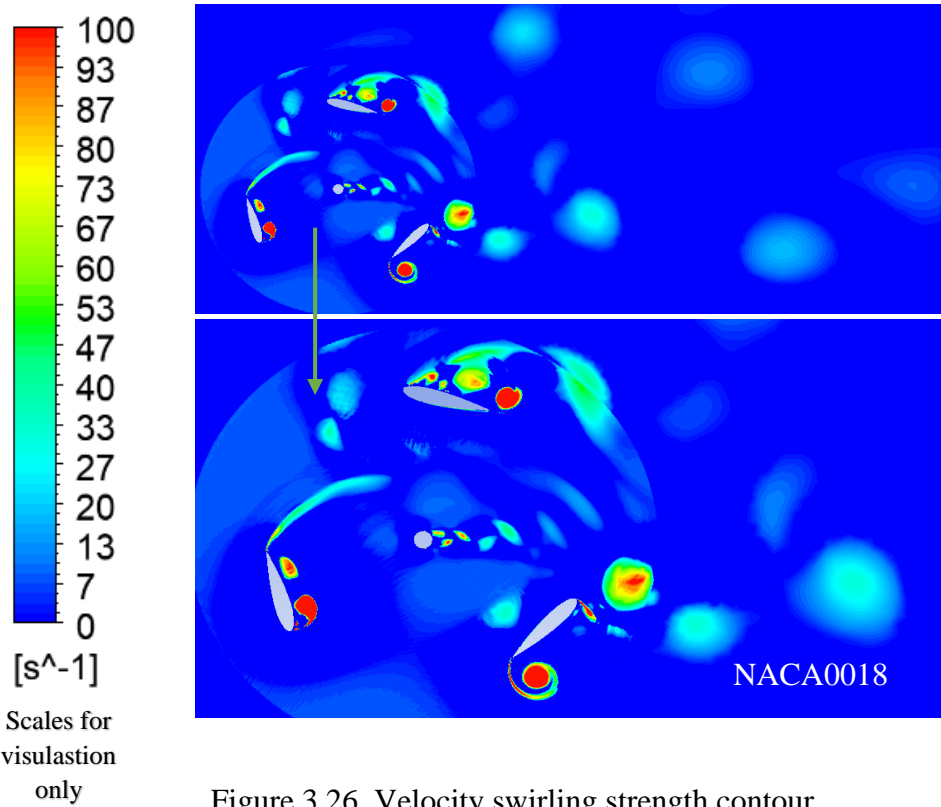


Figure 3.26. Velocity swirling strength contour.

Velocity swirling strength contour after four cycles, after four cycles , the maximum value is 37122 s^{-1} .

PART4

RESULTS AND DISCUSSION

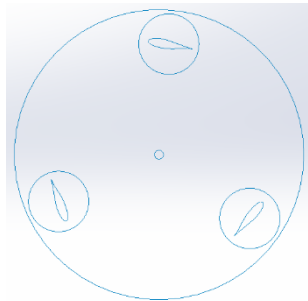
4.1. INTRODUCTION

The design parameters of DWTs are presented in the current chapter, in addition to the different cases of study that are used to calculate their aerodynamic performance. The aerodynamics of DWT, particularly the interaction between the blades and the wind, are a significant focus of research. Discussions might revolve around issues like generated power and measures to mitigate these effects to enhance overall performance and efficiency. Four models have been studied to choose the supreme DWT model that has to be operated with high efficiency. The airfoil type (DU06W200) has been utilized at the blades of Darrieus WT. Also, the first angle of attack (AoA) for the blades of Darrieus WT has been established at (8°), depending upon the airfoil kind database, as shown in Appendix B.

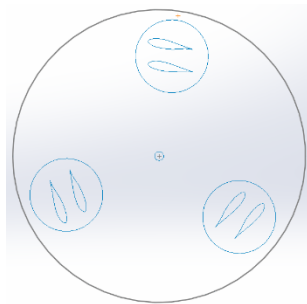
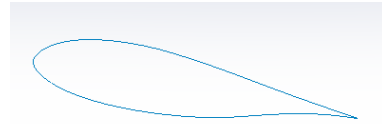
4.2. PRESENT CASE STUDIES

Figure 4.1 presents the case studies applied in the current study. Design 1 included the results of a single blade as a reference for other modified models. Design 2 was applied to the DWT of double blades, with the distance between each double blade being about 1 m. The distance between each double-blade blade was increased to 3 m to decrease the negative interaction effects between the couple blades, as shown in Design 3. Another blade distribution can be found in Design 4, with a staggered profile for the blade's location in the rotor. Also, the effect of velocity profiles at the inlet was studied according to uniform or non-uniform profiles, as shown in Figures (4.2) and (4.3).

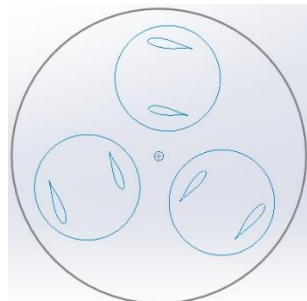
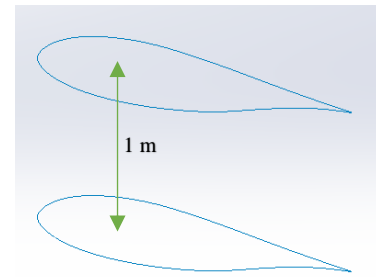
When you mention the first case, the second case, the third case, or the fourth case, it leads to the same meaning as the first design, the second design, the third design, or the fourth design.



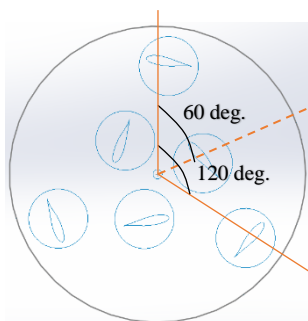
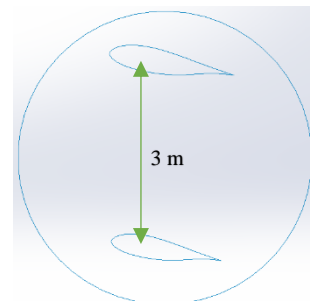
Design 1 Single Blade



Design 2 Double Blade



Design 3 Double Blade



Design 4 Double Blade Staggered

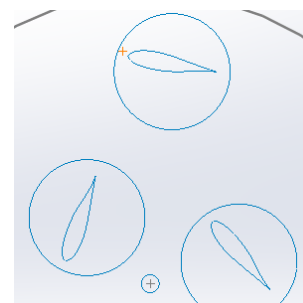


Figure 4.1. Design studies of present research.

Where the non-uniform wind profile represents real wind speed in the environment, A non-uniform wind profile refers to a situation where the wind speed and direction vary with height above the ground. In many designs, the wind speed increases with altitude, which is known as wind shear. Studying uniform and non-uniform flow is considered to enhance efficiency by reducing forces caused by aerodynamic turbulence. The results of studying non-uniform flow can be used to enhance the design of VAWTs by determining ideal blade angles for different flow conditions and increasing safety by reducing the chance of turbine failure or damage.

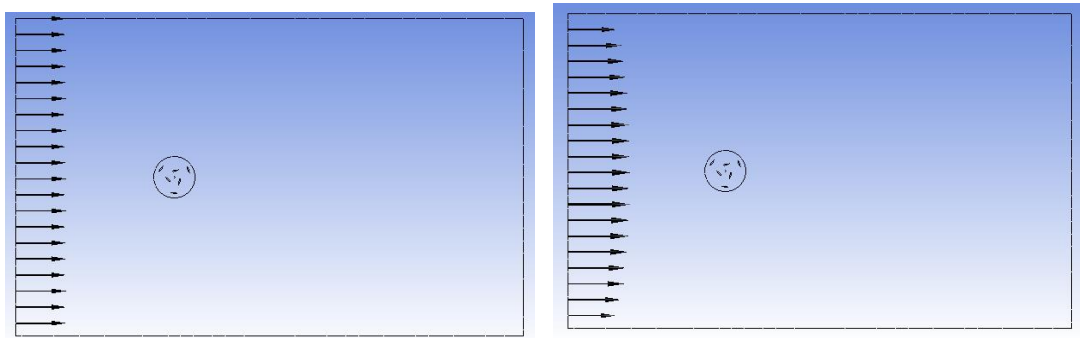


Figure 4.2. Boundary condition of velocity vector profile at the inlet.

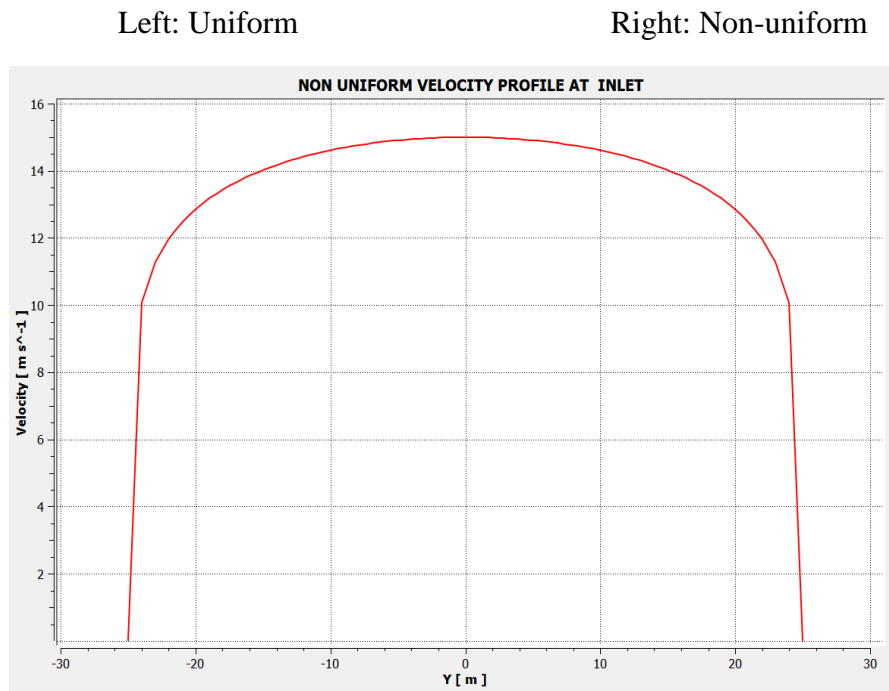


Figure 4.3. Boundary condition of the non-uniform velocity profile at the inlet.

4.3. NUMERICAL RESULTS

This thesis aims to study the numerical results of Darius-type vertical wind turbines. CFD software will be used to simulate turbine performance under a variety of conditions. The results will be used to find new designs aimed at improving efficiency.

4.3.1. Wind Turbine Torque History

Assessment of the torque generated by the shaft via the WT is essential for calculating the mechanical power and understanding the initial conduct. Also, it aids in choosing an appropriate effective generator whose torque-rpm features match the rotor of the turbine that produced a negative torque coefficient for high TSR, as shown in the present results.

The average torque value can be calculated during transient simulation from the below equation

$$T_{ave} = \frac{1}{t_2 - t_1} \int_{t_1}^{t_2} T(t) dt \quad (4.1)$$

Where the torque value at the beginning of the wind turbine starts fluctuating and is random. During this period, the torque value was not correct so we waited for more cycles of wind turbine rotation to react to the stable rotation of the turbine and at this point, we calculated the torque value according to numerical integration.

Figures 4.4 to 4.8 illustrate the instantaneous torque distribution from the DWT for design 1 due to rotating different cycles during different periods of time depending on the tip speed ratio. The torque value was too high at the starting time and then gradually began to have a fluctuation behaviour for the rotational cycle depending on the number of blades, as shown in Figure 4.4, where at TSR = 0.5, the angular velocity was equal to 1.53 rad/s and at a constant wind speed of 10 m/s.

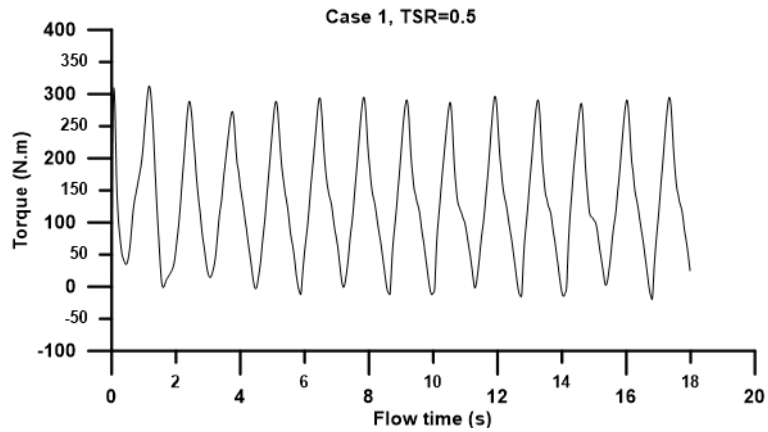


Figure 4.4. Wind turbine torque history for Design 1, TSR=0.5.

From the results, it is noticed that with every rotation, a cycle of the blades is fixed for three torque fluctuations according to the number of blades in the rotor WT. Where the maximum and minimum torque values in each cycle are about 285 Nm and -15 Nm, respectively. Increasing the angular velocity leads to an increase in the tip speed ratio of the turbine and, moreover, to almost regular cycles of torque distribution, as shown in Figures 4.5 to 4.8.

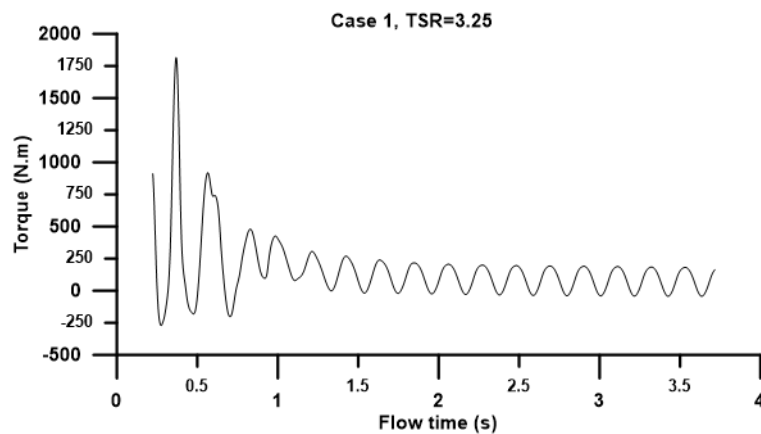


Figure 4.5. Wind turbine torque history for Design 1, TSR=1.

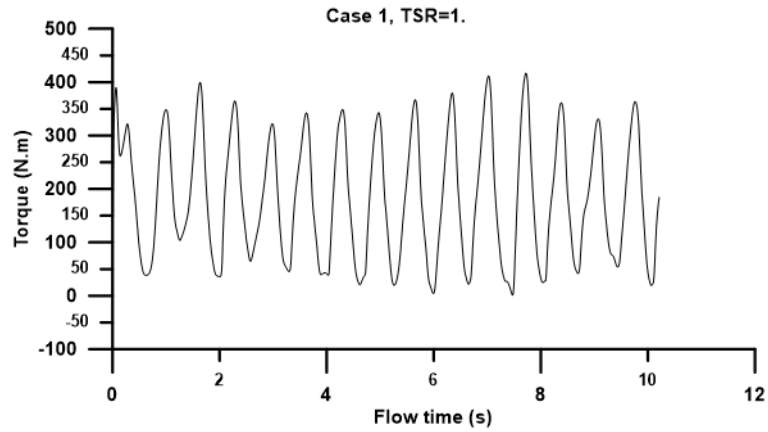


Figure 4.6. Wind turbine torque history for Design 1, TSR=3.25.

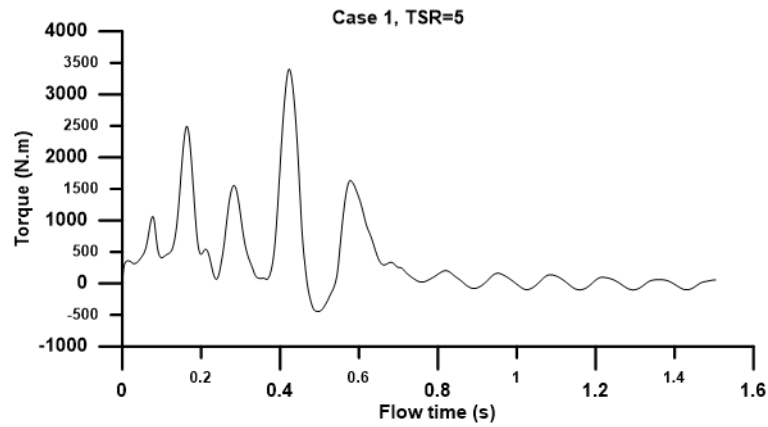


Figure 4.7. Wind Turbine torque history for design 1, TSR=5

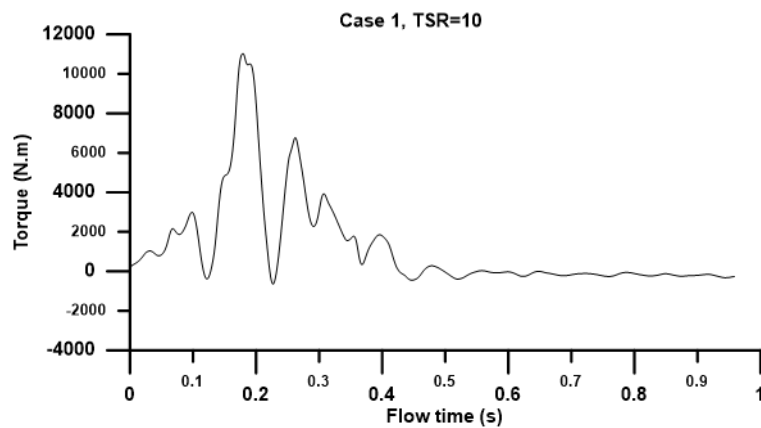


Figure 4.8. Wind turbine torque history for Design 1, TSR=10.

The predicted torque coefficient gets steady as it espouses the boundary condition and displays the converged solution. Beyond the first rotations, the dynamic torque gets sinusoidal, having an even episodic rotation as well as a realistic one. And, the

computation of time-averaged torque was calibrated from the converged data regarding the previous (4) rotation cycles, ignoring the transient conduct in the first cycles.

The variations in the power coefficient with the azimuth angle are owing to the attack angle change of blades with the WT rotation. And, the initial peak of plots occurs at the 90° azimuth angle, where the wind is vertical to Blade 1, as well as big aerodynamic forces being generated. Because there are (3) blades at intervals of 120°, at 120° azimuth angle, blade 3 attains the first blade (1) location, and the whole thing recurs. Also, the 2nd and 3rd peaks match the high attack angle of the blade (3) and blade (2), respectively. Such peaks occur at 210° and 330° azimuth angles. As well, the whole instant coefficient of torque is the summation of the torque generated via its blades as well as its backing structure. Additionally, the backing structure creates a negative or resistant torque, whereas its blades chiefly create a positive torque, as can be noted in the figures. The negative torque created via the backing structure decreases the power coefficient of the turbine.

In the torque history in design 2 for double blades with a distance between them of about 1 m, the results were negative, and the DWT had no performance enhancement due to the interaction effect between the double blades, as depicted in Figure 4.9 at TSR = 3.25. Whereas the torque cycles were nearly regular, with maximum and minimum torque values in each cycle of about 125 Nm and -100 Nm, respectively.

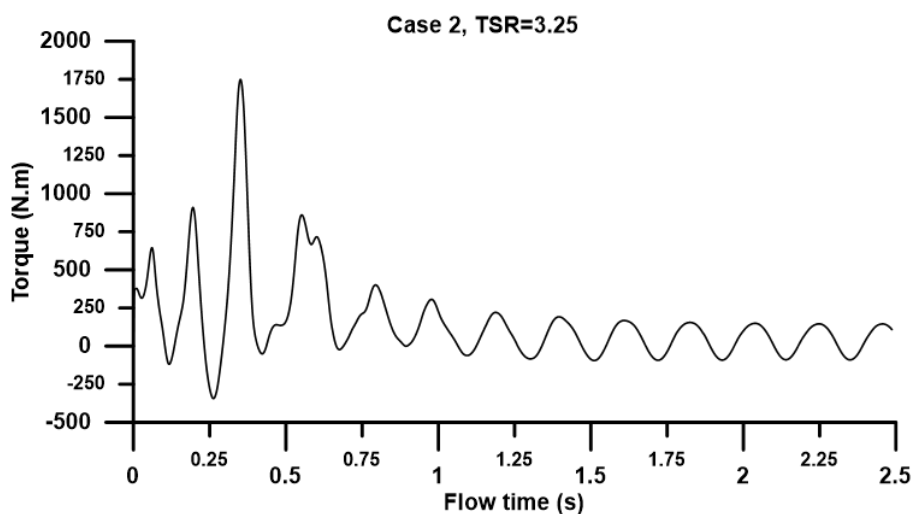


Figure 4.9. Wind turbine torque history for Design 2, TSR=3.25.

Although the torque cycles are regular during the operation conditions, these values are not suitable for a wide range of wind turbine operations. Where the double-blade interaction leads to a reduction in the blade's torque values compared with case 1.

To modify this design, the distance between the blades was increased to 3 m, as shown in design (3). Figures 4.10 to 4.14 display the blade torque distribution with flow time during the wind turbine rotation cycles. Where the torque distribution was unregular and fluctuating at low TSR, as shown in Figure 4.10.

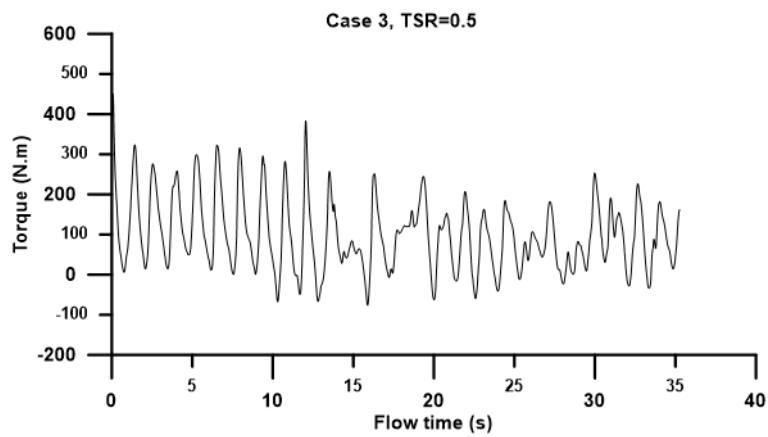


Figure 4.10. Wind turbine torque history for Design 3, TSR=0.5.

but when the TSR increased, the torque profiles changed and had more stable behaviour with good power generation, as revealed in figures 4.11 to 4.13.

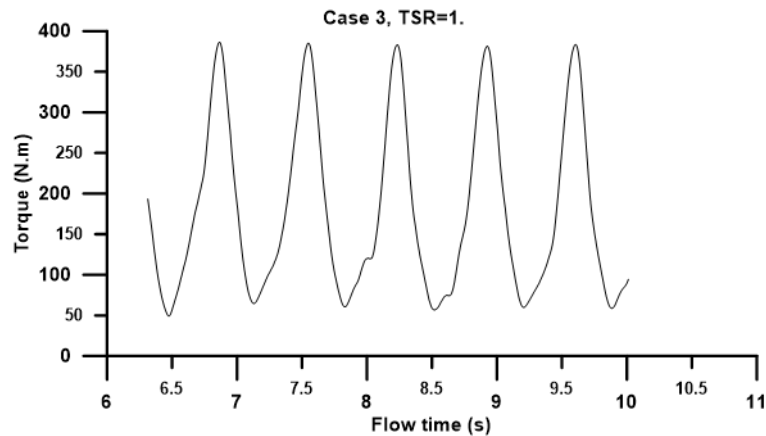


Figure 4.11. Wind turbine torque history for Design 3, TSR=1.

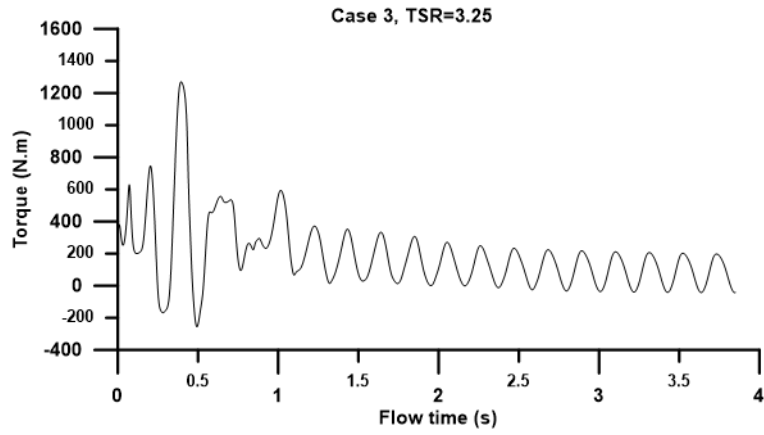


Figure 4.12. Wind turbine torque history for Design 3, TSR=3.25.

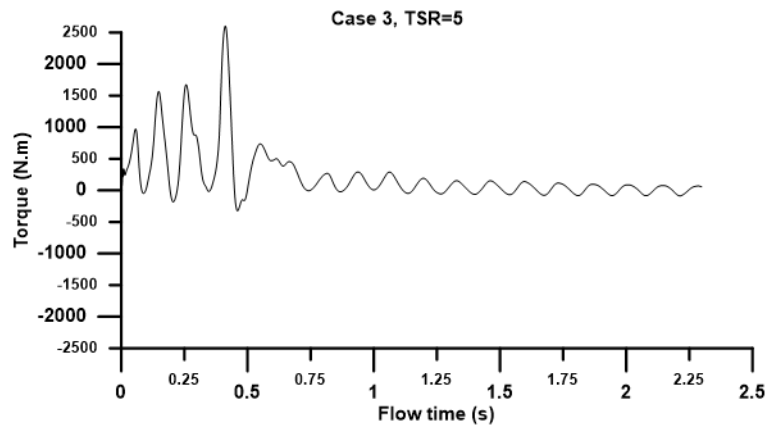


Figure 4.13. Wind turbine torque history for Design 3, TSR=5.

The blade stall, which can be found in all designs at TSR=10 due to the turbulence effect, is shown in Figure 4.14.

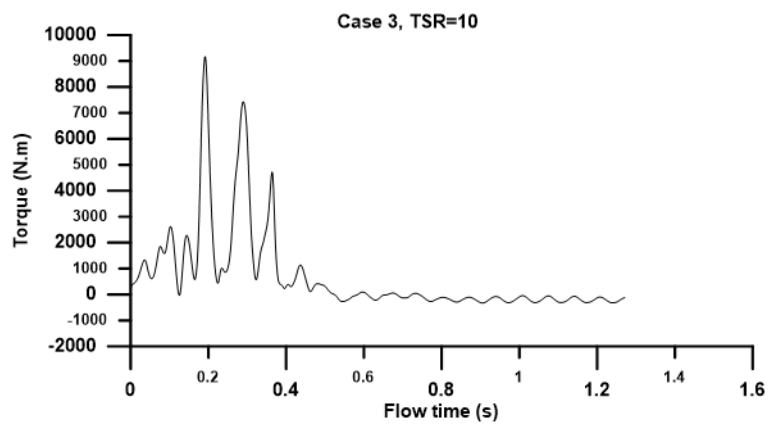


Figure 4.14. Wind turbine torque history for Design 3, TSR=10.

The influence of the turbulence of fluid flow around DWT underneath the working is too intricate, owing to the pairing of these phenomena occurring at the same time:

- The dynamic stall
- The separation of the boundary layer and the shedding of the vortex
- The flow above the airfoil with unceasingly varying attack angle
- The flow around the wall with dynamically varying curvature (from the fluid viewpoint).

Such phenomena directly affect the working of the turbine as well as its performance; thus, the simulation of such a procedure is exciting. The highly significant phenomenon of flow around the rotor of the turbine is introduced into the results.

The reduction in torque values due to this reason will not enable the wind turbine to work with the correct design case study. The same behaviour can be found in Design 4 but with high wind turbine efficiency. Where the double blades are distributed with staggered profiles, this shape will change the blade angle of the attachment outer and inner blades, as shown in Figures 4.15 to 4.19.

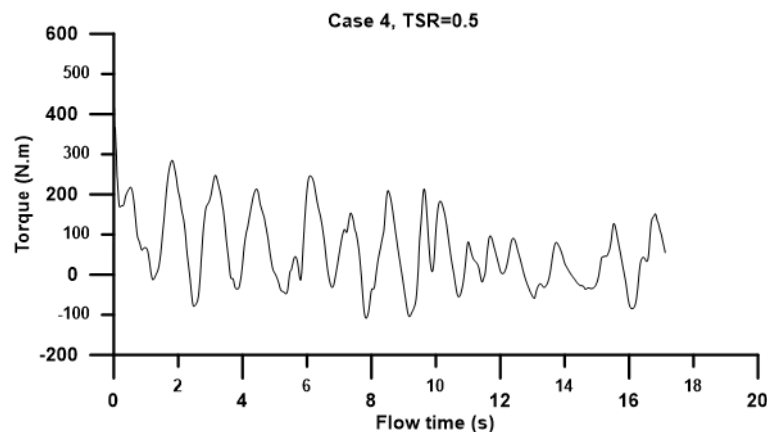


Figure 4.15. Wind turbine torque history for Design 4, TSR=0.5.

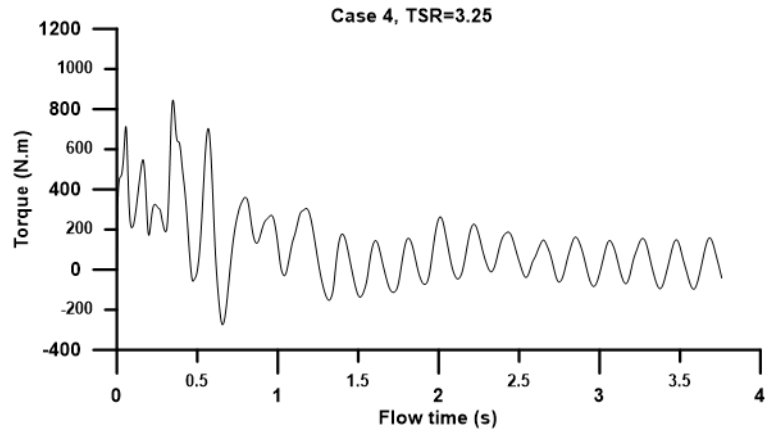


Figure 4.16. Wind turbine torque history for Design 4, TSR=1.

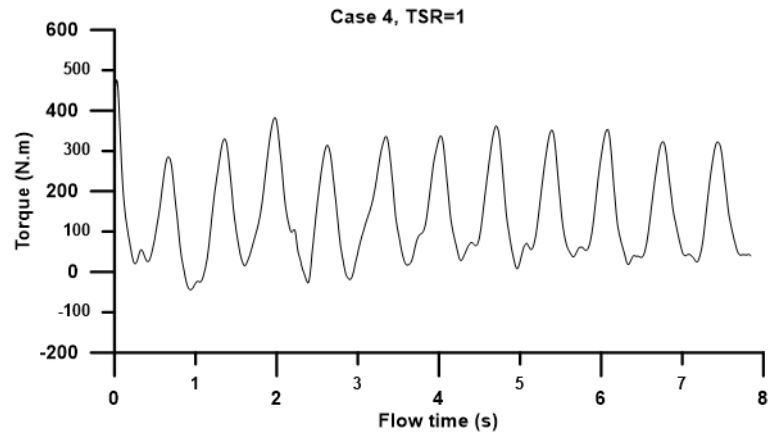


Figure 4.17. Wind turbine torque history for Design 4, TSR=3.25.

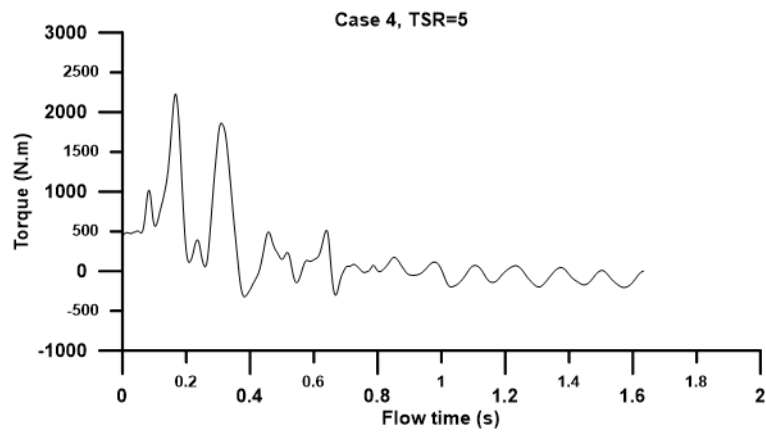


Figure 4.18. Wind turbine torque history for Design 4, TSR=5.

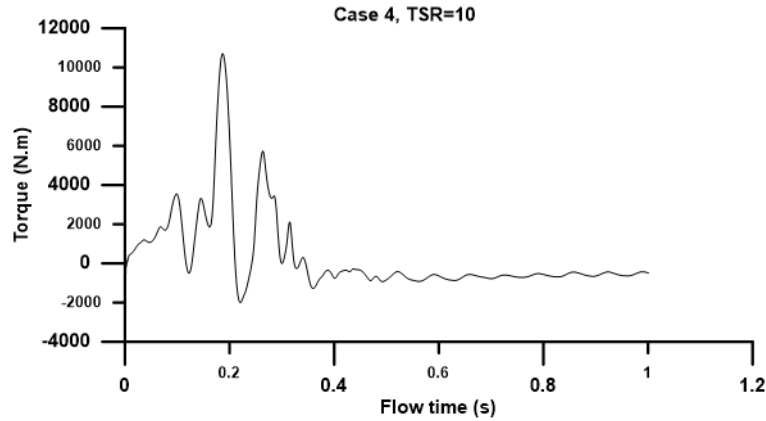


Figure 4.19. Wind turbine torque history for Design 4, TSR=10.

Tables 4.1 to 4.3 present the wind turbine parameters and power coefficient for different cases and TSR. With operation conditions of wind speed 10 m/s and rotor diameter 6.5 m Circumference is equal to $(\pi * D)$.

Table 4.1. The wind turbine parameters and power coefficient for design 1.

TSR	0.5	1	3.25	5	10
ω (rad/s)	1.53	3.07	10	15.38	30.7
Tangential Velocity (m/s)	5	10	32.5	50	100
Circumference (m)	20.42	20.42	20.42	20.42	20.42
Time to complete one revolution (s for one cycle)	4.084	2.042	0.628	0.408	0.204
Time step for one deg. (s)	0.011	0.005	0.001	0.0011	0.0005
P_{air} (W)	3981	3981	3981	3981	3981
Torque (N.m)	126	183	81.38	70.4	-196.5
P_{actual} (W)	194	563	813	1084	-6049
C_p	0.04	0.141	0.20	0.272	-1.5

Table 4.2. The wind turbine parameters and power coefficient for design 3.

TSR	0.5	1	3.25	5	10
ω (rad/s).	1.53	3.07	10	15.38	30.76
Tangential Velocity (m/s).	5	10	32.5	50	100
Circumference (m)	20.42	20.42	20.42	20.42	20.42
Time to complete one revolution (s for one cycle).	4.08	2.04	0.628	0.408	0.204
The time step for one. deg. (s)	0.0113	0.0056	0.0017	0.0011	0.0005
P_{air} (W)	3981.25	3981.25	3981.25	3981.25	3981.25
Torque (N.m)	87.4	179.9	84.9	27	-203.3
P_{actual} (W)	134.4	553.6	849.6	415.3	-6258.0
C_p	0.033	0.139	0.213	0.104	-1.571

Table 4.3. The wind turbine parameters and power the coefficient for design 4

TSR	0.5	1	3.25	5	10
ω (rad/s)	1.53	3.07	10	15.38	30.76
Tangential Velocity (m/s)	5	10	32.5	50	100
Circumference (m)	20.42	20.42	20.42	20.42	20.42
Time to complete one revolution (s for one cycle)	4.08	2.04	0.62	0.40	0.20
The time step for one deg. (s)	0.011	0.005	0.0017	0.0011	0.0005
P_{air} (W)	3981.25	3981.25	3981.25	3981.25	3981.25
Torque (N.m)	20.59	143.27	31	-82.6	-560
P_{actual} (W)	31.68	440.83	310	-1270	-17231
C_p	0.0079	0.110	0.077	-0.319	-4.32

The applied non-uniform velocity profile is shown below, from which we obtain the maximum energy for each section below:

- Design 1 at TSR=5 (Figure 4.20)
- Design 3 at TSR=3.25 (Figure 4.21)
- Design 4 at TSR=1 (Figure 4.22)

The power equation used to describe the non-uniform velocity profile at the inlet according to wind speed remained with the same average wind speed as in the uniform velocity case. The results of the current case are presented below with important findings. The difference between the torque values for a uniform wind profile and a non-uniform wind profile can be calculated as below:

$$\text{Increase or decrease torque value} = \frac{T_{non\ uniform} - T_{uniform}}{T_{non\ uniform}}$$

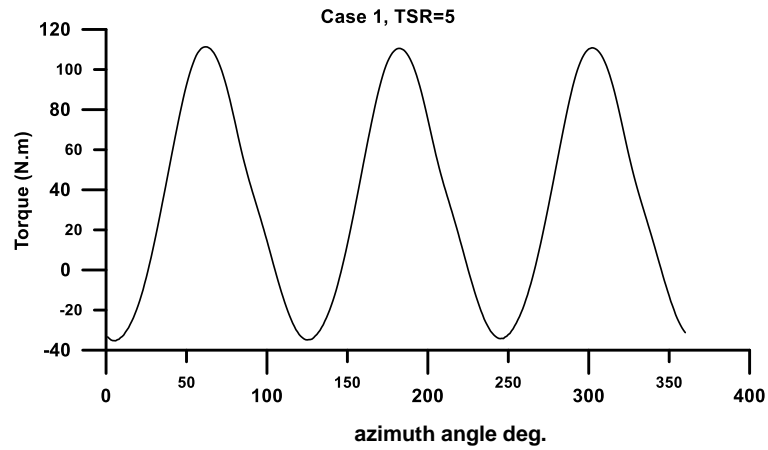


Figure 4.20. Torque history for Design 1, TSR=5 for nonuniform velocity profile at inlet.

Where the average torque value equals about 34 N.m. with a reduction of about 52% from the uniform wind profile test.

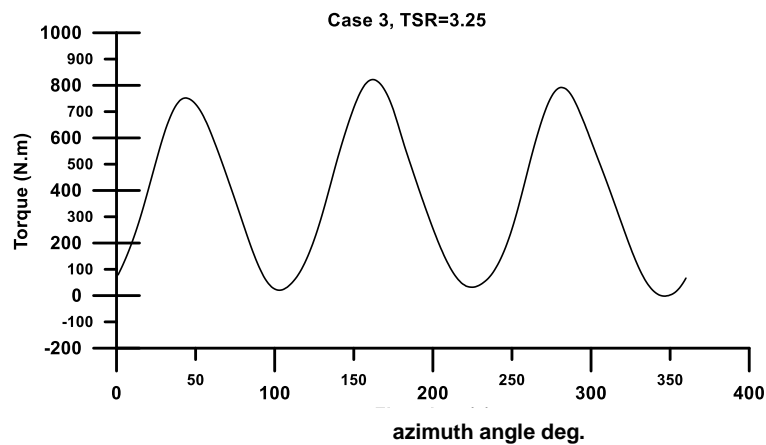


Figure 4.21. Torque history for Design 3, TSR=3.25 for nonuniform velocity profile at inlet.

Where the average torque value equals about 375 N.m., with an increase of about 77% from the uniform wind profile test.

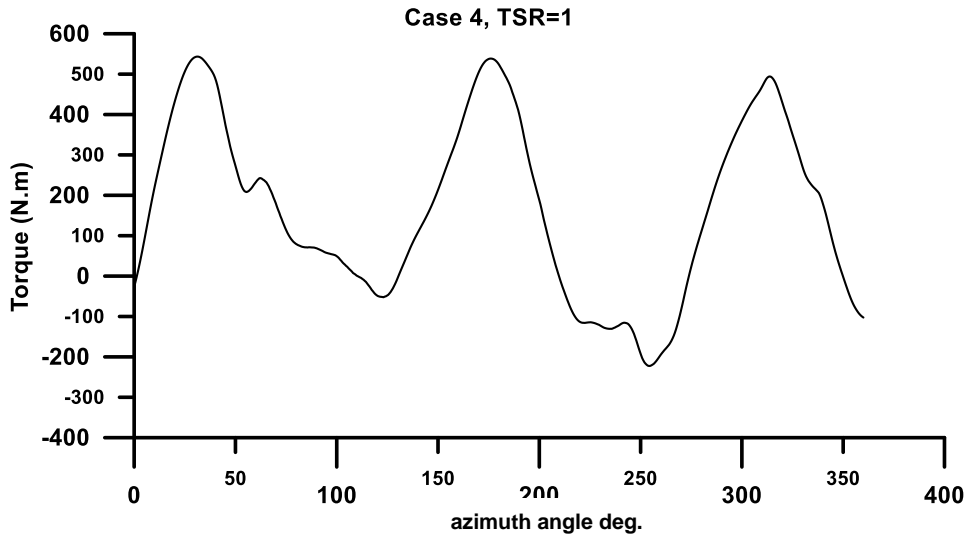


Figure 4.22. Torque history for Design 4, TSR=1 for nonuniform velocity profile at inlet.

Where the average torque value equals about 166 N.m., with an increase of about 13% from the uniform wind profile test.

4.3.2. Power Coefficient

The wind turbine power coefficient is a crucial parameter that describes the efficiency of a wind turbine in converting the kinetic energy of the wind into mechanical power. It is denoted by the symbol " C_p " and is calculated using the following formula:

$$C_p = (\text{Power Extracted by the Turbine}) / (\text{Power Available in the Wind})$$

In more technical terms, it's the ratio of the actual power extracted by the wind turbine to the theoretical maximum power that could be extracted from the wind passing through the rotor area. A higher C_p value indicates a more efficient wind turbine. The theoretical maximum efficiency (Betz limit) is around 59.3%, which implies a C_p value of 0.593. Various factors influence the C_p value, including the design of the wind turbine, the shape of the rotor blades, the wind speed, and the pitch angle of the blades. Researchers and engineers work to optimize the C_p value to improve the overall performance and energy production of wind turbines. Figures 4.23 to 4.25 manifest

the power coefficient with TSR for designs 1, 2, and 3. The figures are divided into two regions: the positive region to work wind turbines and the negative region.

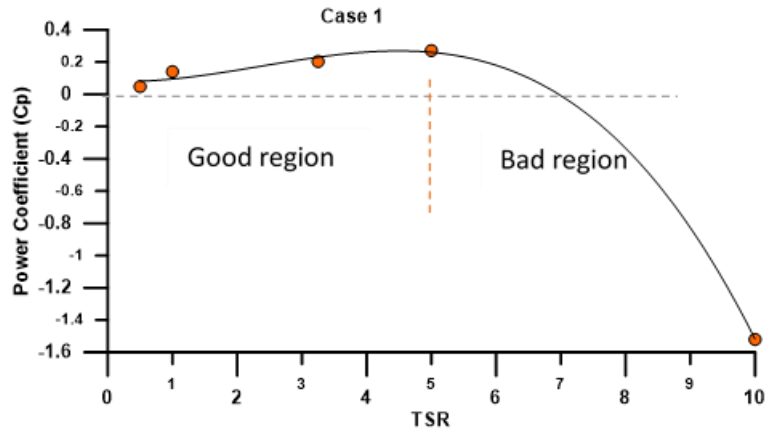


Figure 4.23. Power coefficient vs. TSR for Design 1.

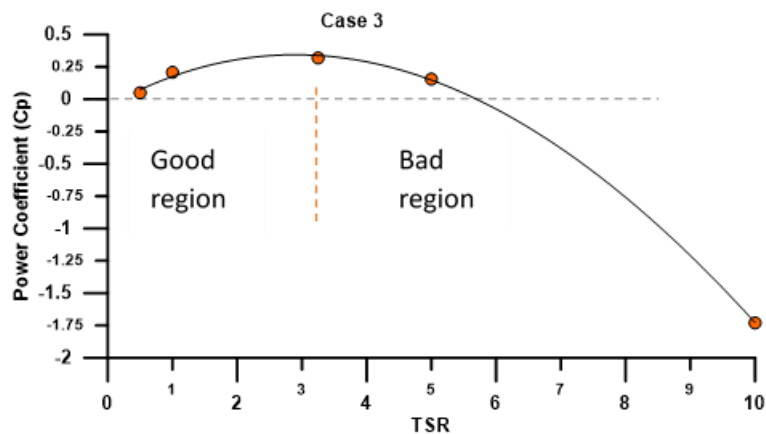


Figure 4.24. Power coefficient vs. TSR for Design 3.

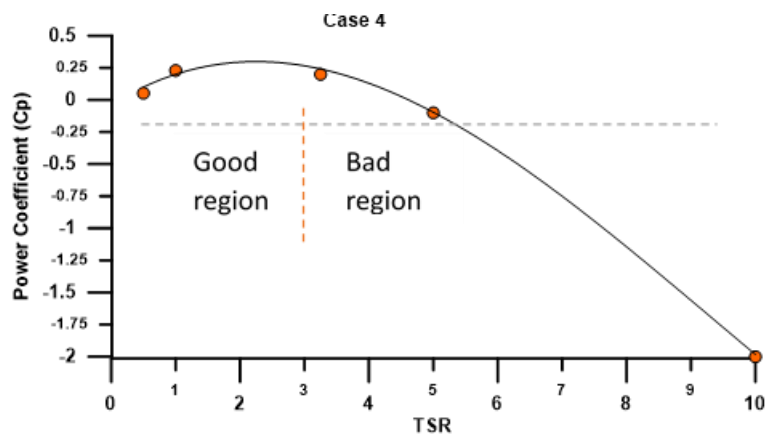


Figure 4.25. Power coefficient vs. TSR for Design 4.

The maximum value of the power factor for all current designs is. when the TSR value is equal to 5 In the first design, the C_p value is equal to 0.272, and in the third design, where the speed value decreases to 3.25, the C_p value also decreases, equal to 0.213, and in the fourth design, the speed TSR is equal to 1. The C_p for this design is 0.110. The graph shown in Figure 4.23 shows the relationship between power factor and tip speed ratio. The power factor is defined as the ratio of the power generated by a wind turbine to the power it reaches from the wind. The tip speed ratio is the ratio of the blade rotation speed to the wind speed.

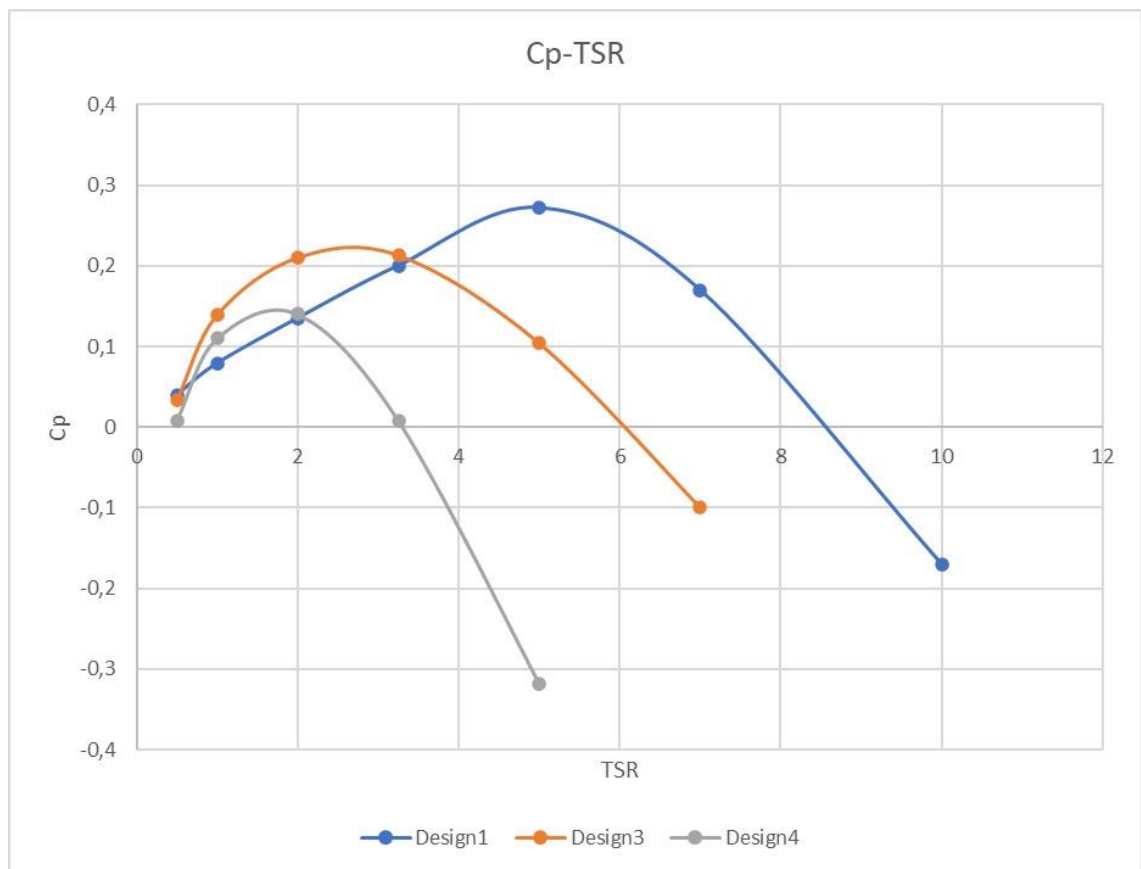


Figure 4.26. Power coefficient vs. TSR for different Designs.

As a result of the CFD analysis, the values at which the four designs work were determined. For Design 1, when the TSR value was equal to 5, the highest C_p value was 0.272, and for Design 3, when the TSR value was equal to 3.25, the highest value was obtained C_p , which is 0.213, and for design 4, when the TSR value was 1, the highest C_p value was 0.110. At a TSR value of 10, a negative torque value is obtained in all designs.

4.3.3. Velocity Field

The velocity field in vertical-axis wind turbines (VAWTs) is the distribution of wind speed around the turbine.

Figures 4.27 to 4.30 elucidate the velocity contours for designs 1, 2, 3, and 4, respectively, for uniform WSP and non-uniform WSP.

In addition, a special drawing scale was used for each figure that differs from the maximum and minimum values of the results to suit the clarity of the figures.

Figure 4.27 reveals the comparative velocity contours for design 1 and TSR 5. The 2D CFD model's virtuous ability for predicting the stall and the wake influences is obvious. It shows the vortex development alongside the wake as well as the various locations of flow in the DWT for each blade. Also, the stagnation point and reverse flow are very clear.

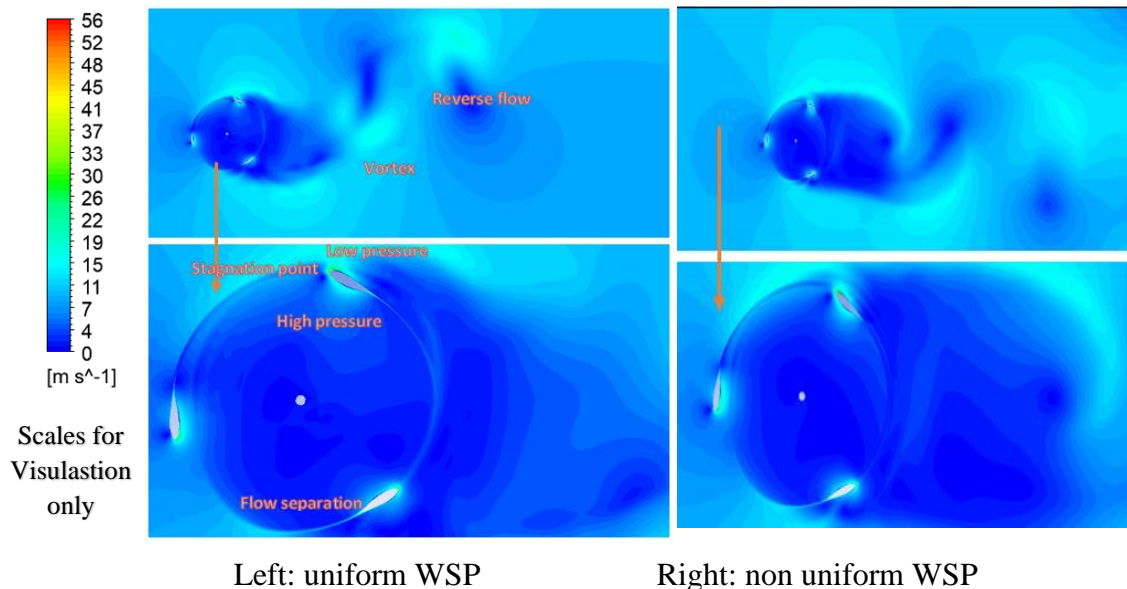


Figure 4.27. Velocity contour in stn frame after four cycles for Design 1.

In Design 1, when the velocity field and TSR are both 5, the maximum value for a uniform wind speed profile is 56 m/s.

This figure also illustrates a solid dispute as a function of speeding up the flow in the tip zone of the blade and flowing in the direction of the blade's suction spot. The speeded-up flow creates a vigorous tip vortex, tending to rotate the turbine in the direction of flow, reinforces the pressure of suction upon the progressing blade, and finally dispels. Where the strong speeded-up flow, which in turn generates huge low- and high-pressure differences around the blades, rotates the wind turbine.

This phenomenon is reduced in Figure 4.28, with the maximum value of velocity in Design 2 being about a maximum of 36 m/s at TSR = 3.25. The maximum influence in this design is the interaction effect between each double blade. Where the double blade interaction leads to a reduction in the generated blade's torque values compared with Design 1.

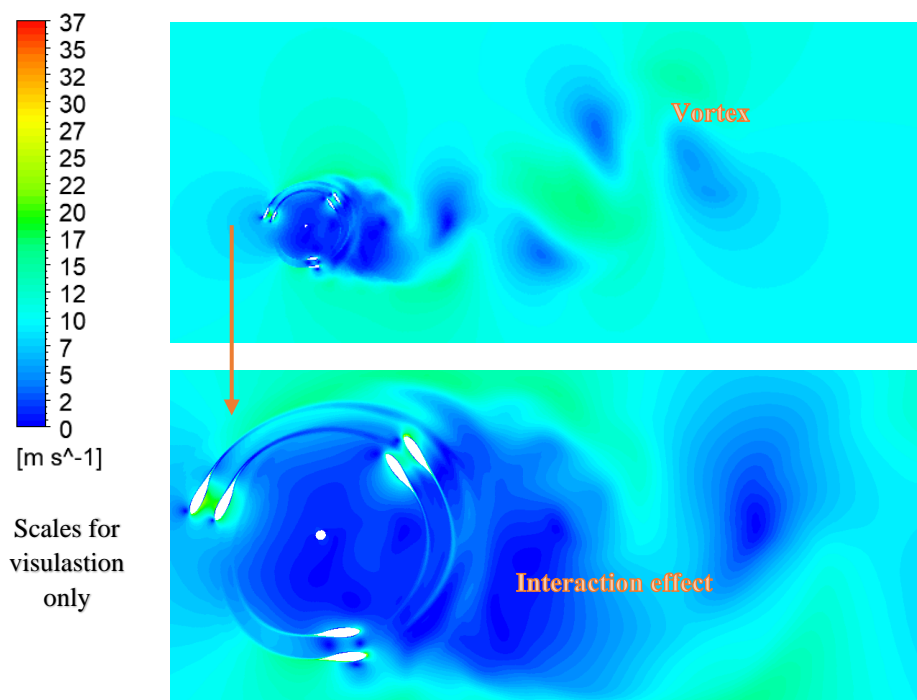


Figure 4.28. Velocity contour in stn frame after four cycles for Design 2.

In Design 2, when the velocity field and TSR are both 3.25, the maximum value for a uniform wind speed profile is 37 m/s.

This effect was reduced in Design 3, as shown in Figure 4.29, due to the increased distance between the double blades from 1 m to 3m.

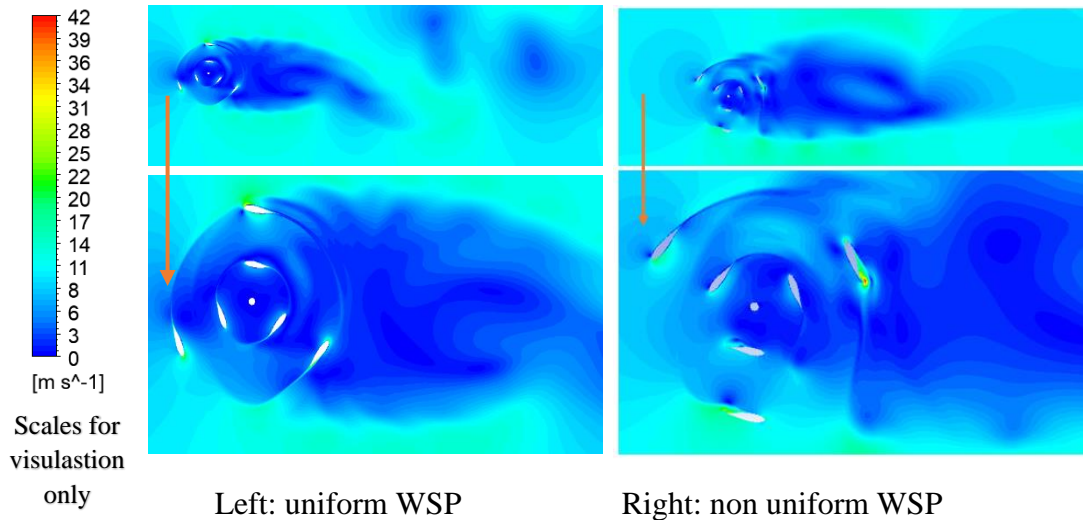


Figure 4.29. Velocity contour in stn frame after four cycles for Design 3.

In Design 3, when the velocity field and TSR is equal to 3.25, the maximum value for a wind speed profile is 42 m/s.

However, in design 4, the maximum value of velocity in this Design is 32 m/s at TSR is equal to 1, due to the high turbulence effect from the blade's distribution in the rotor, as shown in Figure 4.30.

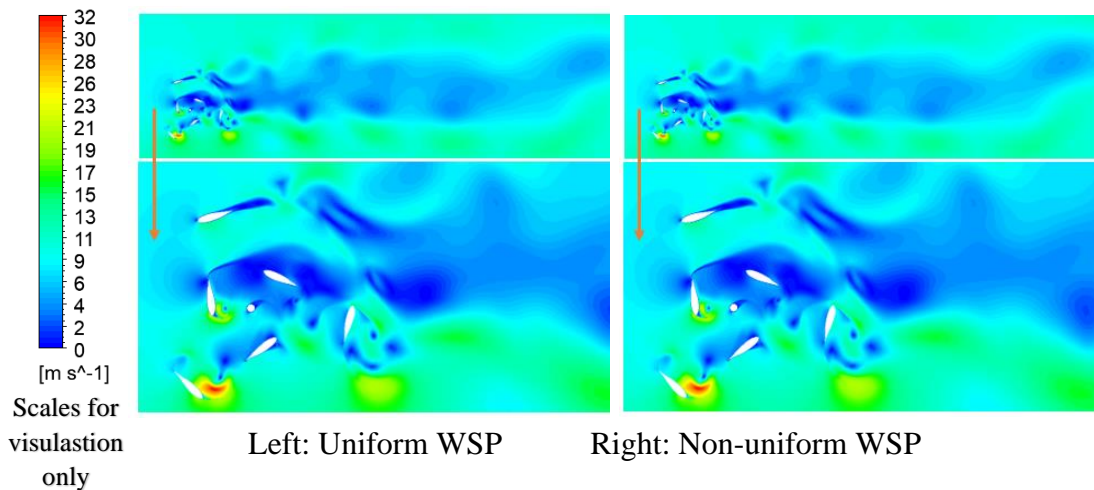


Figure 4.30. Velocity contour in stn frame after four cycles for Design 4.

When the contours of figs. 4.27, 4.28, 4.29, and 4.30 are examined, while the maximum flow velocity reached in the flow area for Design 1 is 56 m/s, this value is 37 m/s for Design 2, 42 m/s for Design 3, and 32 m/s for Design 4. It can be said that

in Design 2, when the airfoils are too close to each other, it causes a decrease in the torque value and ultimately the power value to be produced as a result of the interaction of the two airfoils. We see that when the distance between the two airfoils is increased for the Design, this negative interaction disappears.

4.3.4. Velocity Stretched Swirling Strength

Velocity stretched swirling strength, Indicates the intensity of rotational motion at speed. High swirling strength shows how the speed around the turbine changes with a rotating tendency. Rotation can positively affect the turbine's performance by providing a more even distribution of speed to the turbine blades.

Velocity Stretched Swirling Strength (VSSS) is a parameter used in Ansys Fluent to quantify the swirling motion of a fluid flow. It is calculated using the velocity vector field and represents the strength of the swirling motion in a particular region of the flow, as shown in Figs. 4.30 to 4.33 for uniform WSP and non-uniform WSP. Velocity Stretched Swirling Strength (VSSS) makes it difficult to describe a vortex core numerically founded upon the calculated field of flow. The vorticity magnitude appears to be the most appropriate factor to apply. Nevertheless, the vorticity being the rotational nature measure of, or shearing inside, the field of the flow that will be well-known, this may or may not match a revolving fluid structure or a vortex.

In Figure 4.31, Design 1, the movement of three blades and the effect of wind on the blades are shown.

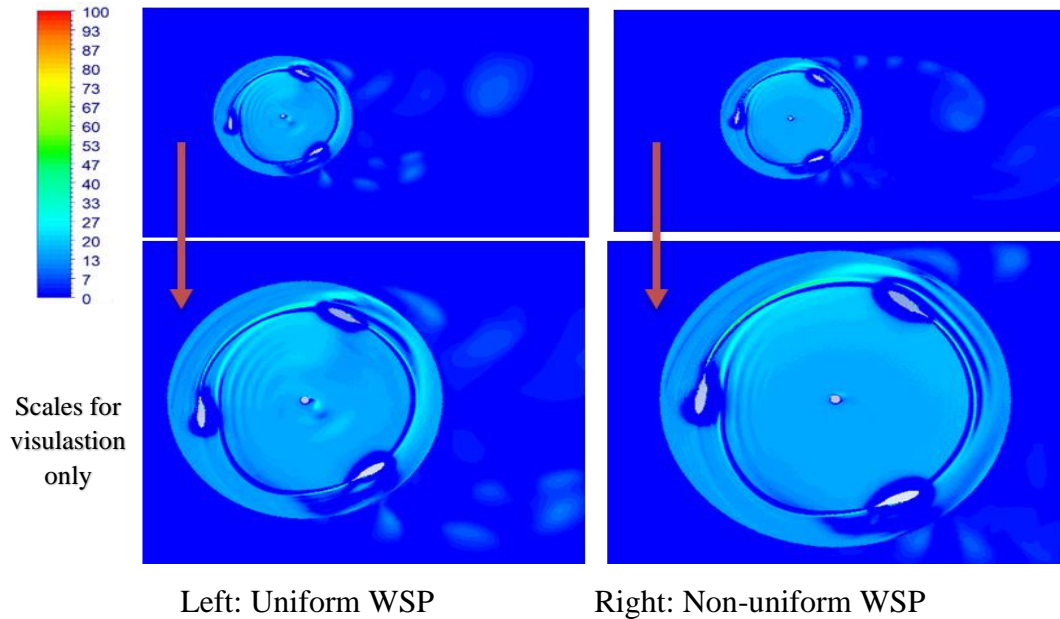


Figure 4.31. Velocity stretched swirling strength contour after four cycles for Design 1.

There is an extremely powerful vortex at the third end of the blade when the velocity stretched swirling strength value is maximum =102892, at the tip speed ratio (TSR= 5)

In Figure 4.32, Design 2, the distance between the double blades is 1 meter, and the location of the two blades is parallel to each other.

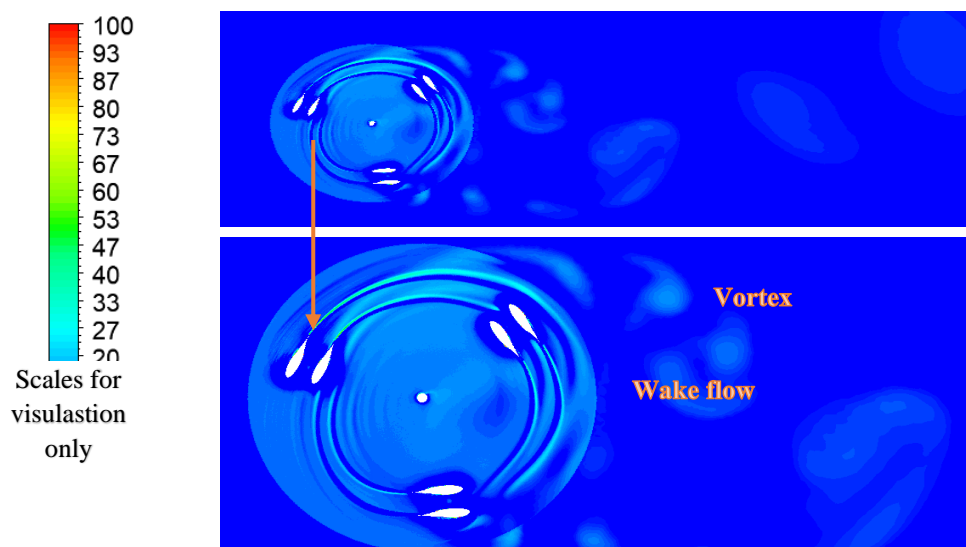


Figure 4.32. Velocity stretched swirling strength contour after four cycles for Design 2.

In Design 2, the velocity stretched swirling strength value is maximum =89498 and the tip speed ratio (TSR = 3.25). There is a powerful vortex at the third end of the blade.

In Figure 4.33, Design 3, the distance between the double blades is 3 meters, and the location of the two blades is parallel to each other.

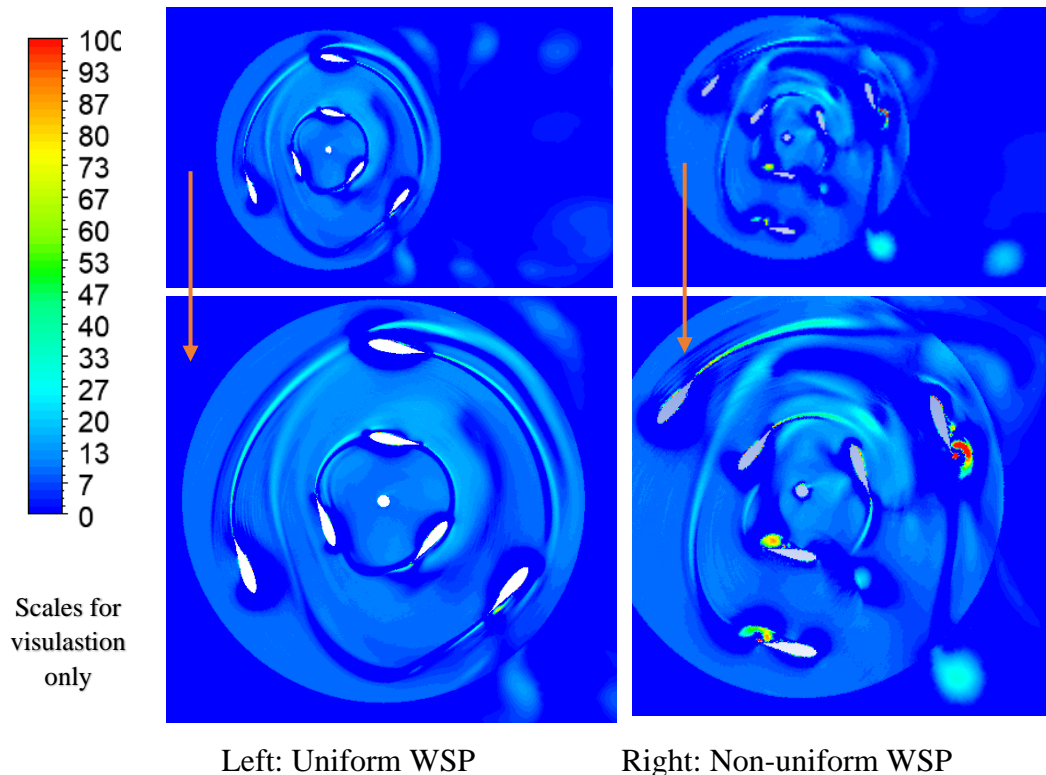


Figure 4.33. Velocity stretched swirling strength contour after four cycles for Design 3.

In Design 3, the velocity stretched swirling strength value is maximum =97344 for the same uniform and non-uniform, and the tip speed ratio (TSR = 3.25), there is an incredibly powerful vortex at the third end of the blade.

In Figure 4.34, Design 4, the distance between the double blades is 3 meters, and the location of the two blades is not parallel to each other, but rather there is a deviation from the centre line located between every two blades.

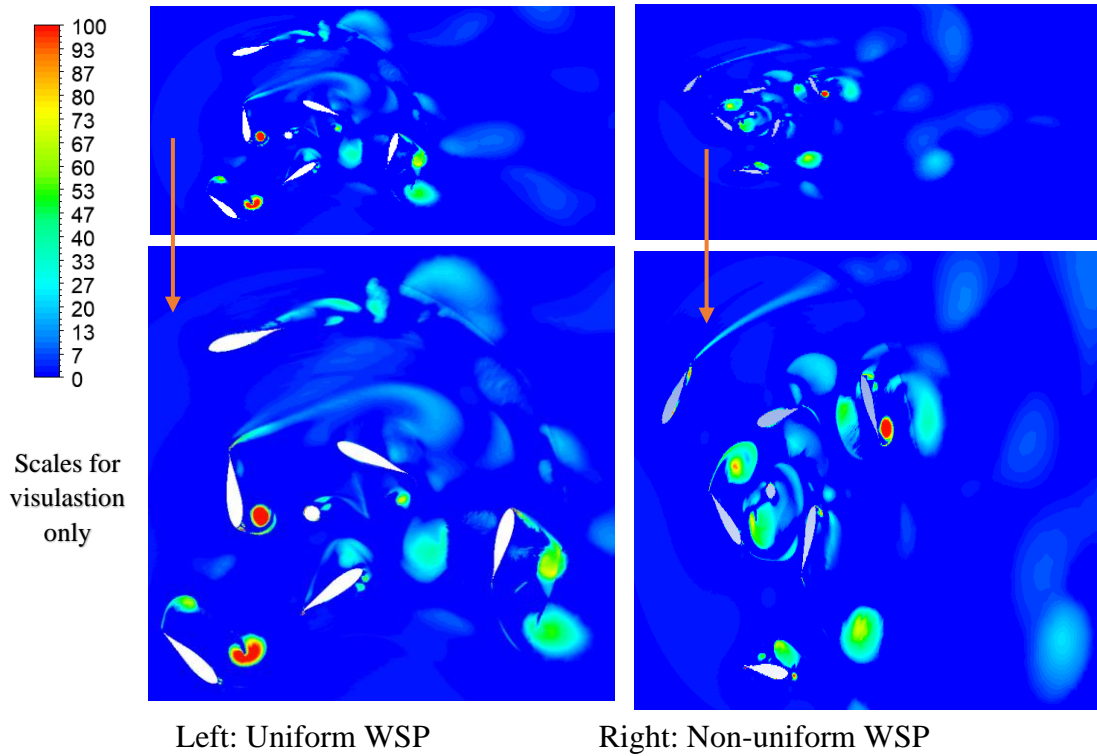


Figure 4.34. Velocity Stretched Swirling Strength contour after four cycles Design 4.

When the rotational force extends to the speed at Design 4, at the speed ratio $TSR = 5$, the maximum value is 28078 for the uniform and 116077 for the non-uniform, which means a very powerful, strong vortex is formed at the third end of the blade. Whereas, the maximum value of VSSS accumulates in Design 1 due to high TSR and then decreases in another design. A high value of VSSS leads to increased drag on the blade, which reduces the efficiency of the blade. The vortex can also cause the blade to become unstable, leading to vibrations and noise.

When the contours of Figs. 4.31, 4.32, 4.33, and 4.34 are examined, and it is seen that the maximum value of velocity stretched swirling strength' is 102892, 89498, 97344, and 28078 for design 1, Design 2, Design 3, and Design 4, respectively. It can be said that these values are directly proportional to power efficiency. For example, design 1 has the highest power efficiency, and this contour value is the largest in this design.

4.3.5. Turbulent Kinetic Energy

Turbulent Kinetic Energy, shows the level of turbulence in the kinetic energy within the flow around the turbine. Higher kinetic energy levels can be associated with greater energy production and higher turbine performance.

The intricate interplay between the atmospheric boundary layer and the wind turbines is one of the important topics in recognizing and forecasting the wind farm's performance. One of the chief factors to be regarded in such a context is the turbulence approaching a wind turbine. The turbulence features, motivated via atmospheric steadiness as well as wind shear, sturdily rely upon the location, season, and synoptic state. The turbulence created via mesoscale atmospheric procedures, like facades, or micro-scale phenomena, such as convection and resident wind shear, does not merely influence the generation of power but structural factors, such as peak loads and fatigue. Also, this directly influences the wind turbines and indirectly the entire wind farm, since the structure as well as the dynamics of wind turbine wakes also vary with the atmospheric circumstances. Selecting the suitable turbulence class is thus a critical location evaluation verdict for the whole park's effectiveness.

Turbulent kinetic energy is the main factor that determines the efficiency of vertical wind turbines. The greater the striking kinetic energy, the greater the efficiency of the turbine. The striking kinetic energy can be increased by increasing the wind speed or the diameter of the turbine blades.

For transient simulations, using the model of RANS, the wind characteristics retrieval in the turbine wakes can influence the precise performance forecast of a downstream turbine.

Basically, turbulent kinetic energy (TKE) is a concept used in fluid dynamics to quantify the energy associated with a turbulent motion in a fluid flow. Where, turbulence refers to the chaotic, irregular, and unpredictable movement of a fluid, characterized by the formation of vortices and fluctuations in velocity and pressure. In a turbulent flow, the energy is transferred from large-scale eddies to smaller ones

through a process called the "energy cascade." This transfer of energy continues until it reaches the smallest scales, where it is eventually dissipated into heat through viscosity.

The TKE represents the intensity of turbulent motion in the fluid and is often used in the study of various engineering, atmospheric, and oceanic phenomena, as well as in the design of structures and systems subject to turbulent forces. In turbulent flows, the TKE can vary significantly throughout the flow field and is affected by factors such as the flow velocity, geometry of the flow domain, boundary conditions, and the presence of obstacles or eddies. Understanding TKE is crucial in many fields, such as aerodynamics, meteorology, oceanography, and engineering, where the behaviour of turbulent flows plays a vital role in predicting and optimizing various processes and designs. Figure 4.35 to 4.38 for all cases at uniform WSP and non-uniform WSP.

Figure 4.35 portrays the turbulent kinetic energy contour after four cycles for design 1. The reverse flow and turbulent eddies are very clear, and a high value of TKE occurred around the blade geometry.

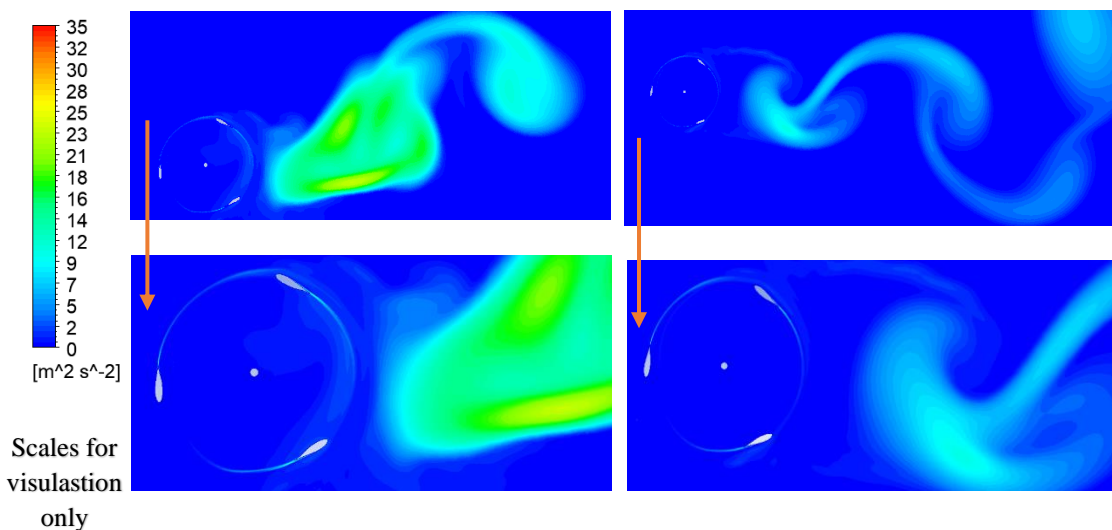


Figure 4.35. Turbulent kinetic energy contour after four cycles for Design 1.

At $TSR = 5$, the turbulent kinetic energy in Darius wind turbine Design 1, with uniform W_{sp} , has a maximum value of $35 \text{ m}^2/\text{s}^2$, and non-uniform W_{sp} has a maximum value of $31 \text{ m}^2/\text{s}^2$.

While Figure 4.36 shows the van Karmen vortex in the wake region with max in design 2.

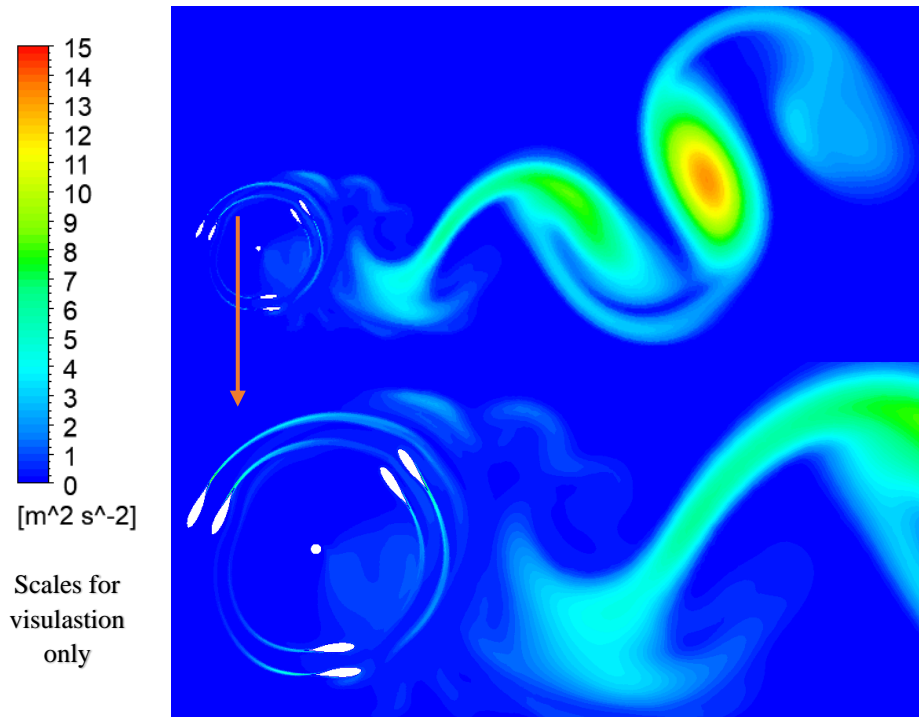
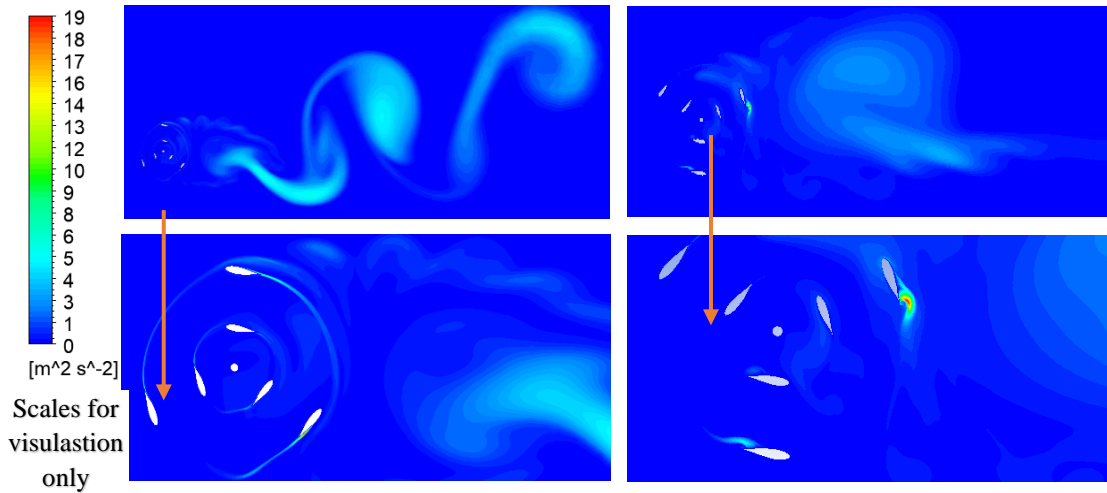


Figure 4.36. Turbulent kinetic energy contour after four cycles for Design 2.

When TSR (Tip Speed Ratio) is equal to 3.25, the turbulent kinetic energy in Design 2 with a uniform Wind Speed Profile (WSP) has a maximum value of $15 \text{ m}^2/\text{s}^2$.

Figure 3.37 also illustrates the same behaviour for Design 3.



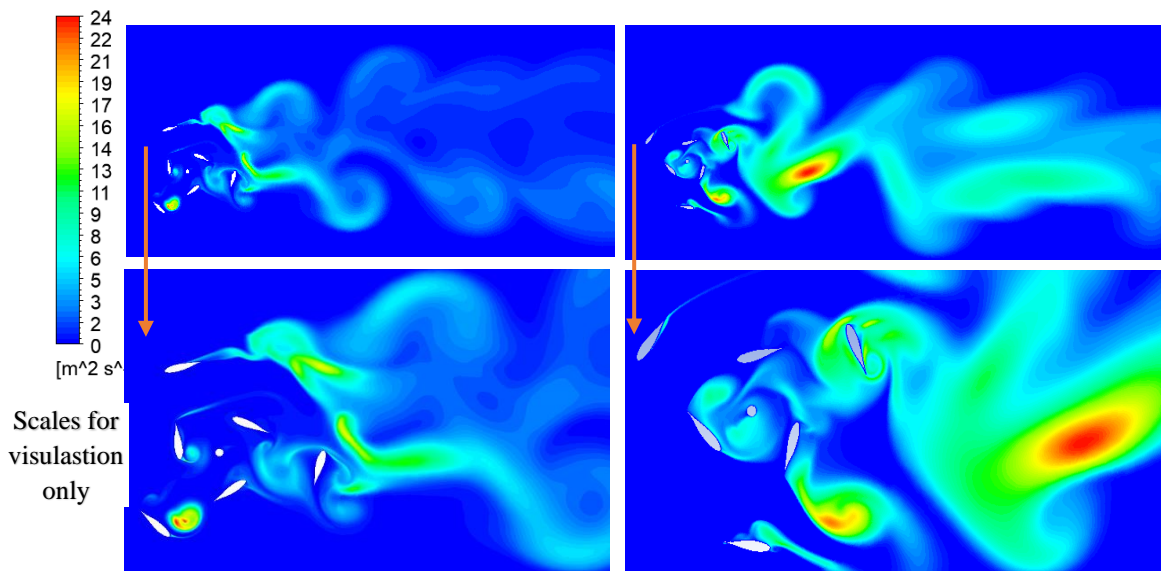
Left: Uniform WSP

Right: Non-uniform WSP

Figure 4.37. Turbulent kinetic energy contour after four cycles for Design 3.

Design 3, When TSR (Tip Speed Ratio) is equal to 3.25, the turbulent kinetic energy in the case of a Darius wind turbine with a uniform wind speed profile (WSP) has a maximum value of $19 \text{ m}^2/\text{s}^2$. On the other hand, when non-uniform WSP is used, the maximum value of turbulent kinetic energy is $101 \text{ m}^2/\text{s}^2$.

Figure 4.38 contains various random contours observed during Design 4.



Left: Uniform WSP

Right: Non-uniform WSP

Figure 4.38. Turbulent kinetic energy contour after four cycle Design1.

At $TSR = 1$, the turbulent kinetic energy in Darius wind turbine Design 4 with uniform wasp has a maximum value of $24 \text{ m}^2/\text{s}^2$ and when non-uniform wasp has a maximum value of $37 \text{ m}^2/\text{s}^2$.

Designs. in Figs. 4.35 to 4.38 for all Designs at uniform WSP and non-uniform WSP. Figure 4.35 shows the turbulent kinetic energy contour after four cycles for Design 1 and $TSR = 5$, with a maximum value of $35 \text{ m}^2/\text{s}^2$ for uniform and $31 \text{ m}^2/\text{s}^2$ for non-uniform. Reversing flow and turbulent eddies are very clear, and a high value of TKE occurred around the blade geometry.

In Figure 4.36, the van Karmen vortex is shown in the wake region with a maximum turbulent kinetic energy of $15 \text{ m}^2/\text{s}^2$ for uniform during Design 2 and $TSR = 3.25$. The same behaviour can be seen in Figure 3.37 for Design 3 and $TSR = 3.25$, with a maximum turbulent kinetic energy of $19 \text{ m}^2/\text{s}^2$ for uniform and $101 \text{ m}^2/\text{s}^2$ for non-uniform. Random contours can be found in Figure 3.38 during Design 4 and $TSR = 1$, with a maximum turbulent kinetic energy of $24 \text{ m}^2/\text{s}^2$ for uniform and $37 \text{ m}^2/\text{s}^2$ for non-uniform, respectively.

4.3.6. Turbulence Intensity

Turbulence Intensity, indicates the intensity of fluctuations in airflow. Low intensity can signify a more regular flow and higher efficiency.

Figures 4.39 to 4.42 display contour plots of the turbulence intensity in the flow direction around the wind turbine for uniform WSP and non-uniform WSP. The turbulence intensity (IT) is dependent on the turbulent kinetic energy. From the figures, the wind turbine wakes in shear flows have a high turbulence intensity, which is connected with the extreme manufacture of TKE related to the vigorous shear in that zone. Nevertheless, the flow was a forced situation via wind, with a large turbulence quantity being conveyed far from the wake centre owing to the side wind shear created via the Coriolis force. Also, it's noted that the intensity of the turbulence of the arriving wind is the same in all situations. This higher level of turbulence in the zone of wake contributes to bigger entrainment of flow and, as a result, quicker wake retrieval than

beneath unidirectional pressure-gradient forcing. In general low-turbulence intensity (5%), the field of flow is comprised of an average and changing constituent, where the peak vector norm values of the changing constituents (u) stay within the restrictions of (5%) in comparison with the vector norm of the entire field of velocity (u). Generally, this is the mean intensity level of turbulence at which offshore wind turbines usually work. But, for the medium intensity of turbulence (15%), the field of flow is further irregular and chaotic. And the torque is anticipated to reduce even further compared with the laminar situation as well as the augmented turbine's structural vibrations. Finally, for the high intensity of turbulence (25%), the systems of arriving flow are estimated in storms and gusts. Such mostly disturbed fields of flow are projected to result in lower torques in addition to higher turbine blade degradation and backing construction.

Figure 4.39 portrays the turbulent kinetic energy contour after four cycles for Design 1. The reverse flow and turbulent eddies are very clear, and a high value of TKE occurred around the blade geometry.

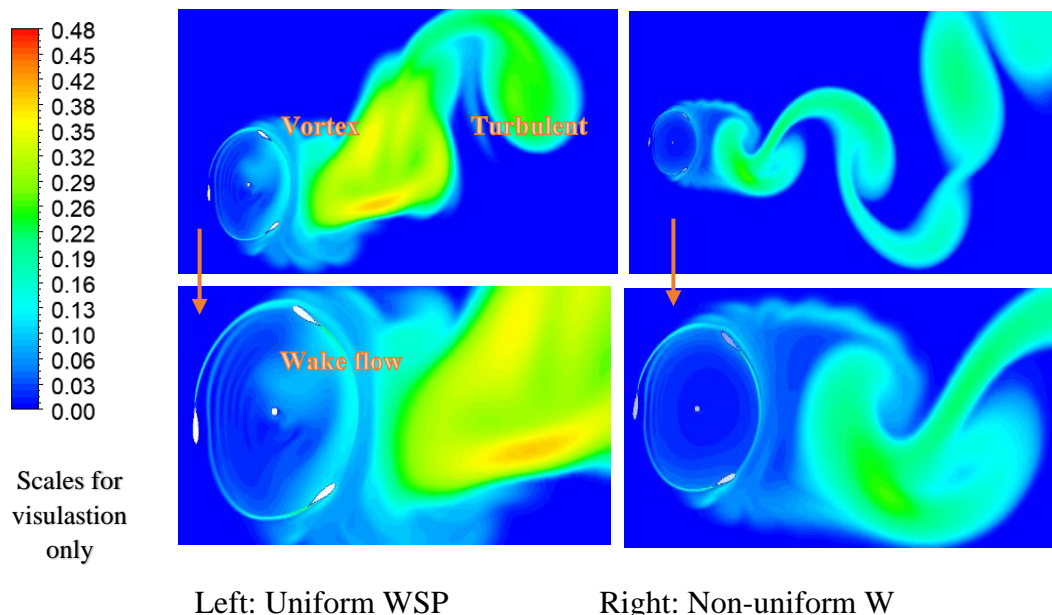


Figure 4.39. Turbulence intensity contour after four cycles Design 1.

In Design 1, when the turbulent intensity and TSR are both 5, the maximum value for a uniform wind speed profile is 0.48, while for a non-uniform wind speed profile, the maximum value is 0.46.

In Figure 4.40, which represents Design 2, the turbulence intensity contour is shown on the double blades when they are 1 m apart.

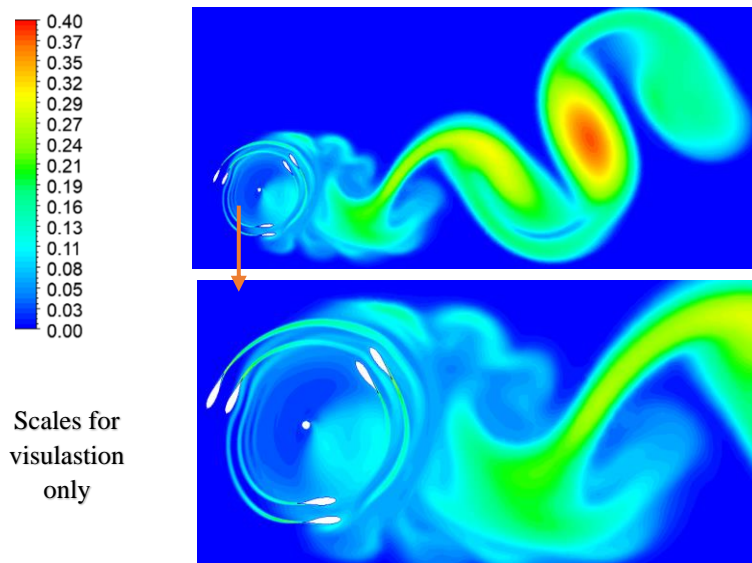
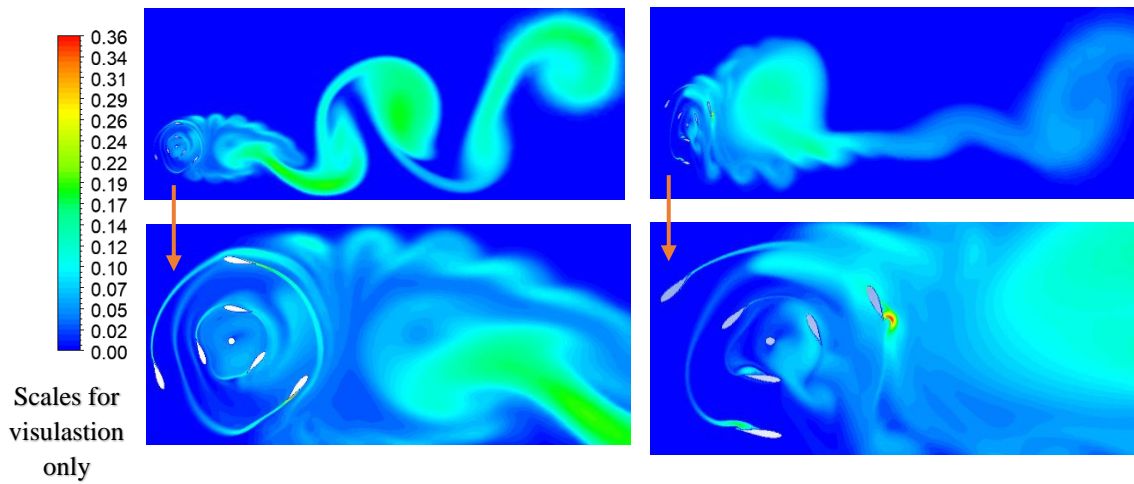


Figure 4.40. Turbulence intensity contour after four cycles Design 2.

In Design 2, when the turbulence intensity and TSR are both 3.25, the maximum value for a uniform wind speed profile is 0.40.

In Figure 4.41, which represents Design 3, the contour of the turbulence intensity on the double blades when the distance between them is 3 m is shown.

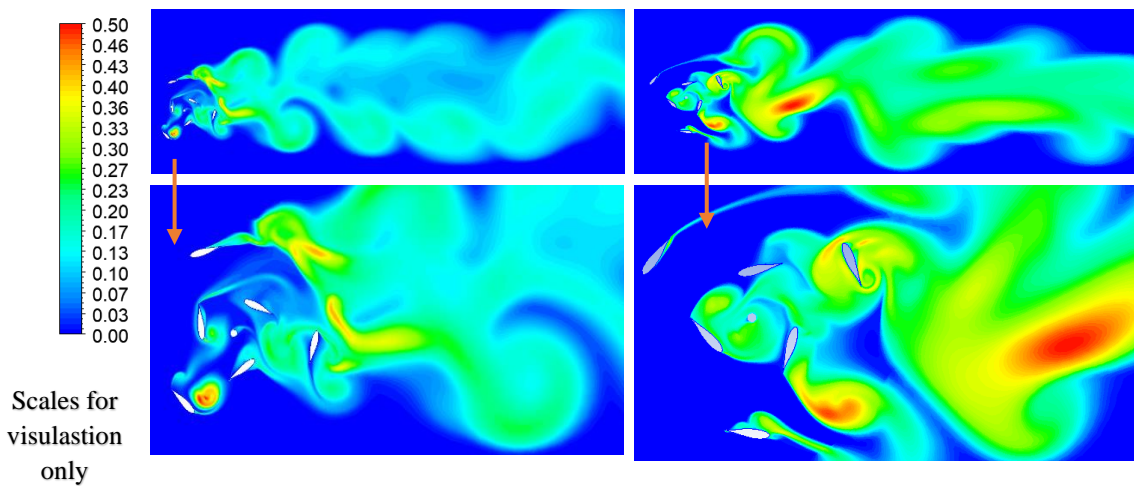


Left: Uniform WSP

Right: Non-uniform WSP

Figure 4.41. Turbulence intensity contour after four cycles Design 3.

In Design 3, when the turbulent intensity and TSR are both 3.25, the maximum value for a uniform wind speed profile is 0.36, while for a non-uniform wind speed profile, the maximum value is 0.85.



Left: uniform WSP

Right: non uniform WSP

Figure 4.42. Turbulence intensity contour after four cycles Design 4.

In design 4, when the value of Tip = 1, the maximum value of the disturbance intensity for a uniform WSP is 0.5, and for a non-uniform WSP, the maximum value is 0.6.

Where the max. turbulence intensity value for uniform wind speed equals (0.48), (0.4), (0.36), and (0.5) for Designs 1, 2, 3, and 4, respectively. And for non-uniform wind speeds equal (0.46), (0.85), (0.6, 0), for Designs 1, 3, and 4, respectively. From results, The turbulence intensity in Designs 1, 3, and 4 has a value in non-uniform WSP greater than in uniform WSP; otherwise, in Design 2.

4.3.7. Total Pressure Distribution

Total Pressure, this indicates the total pressure in the airflow around the turbine. High pressure can assist the turbine in generating more power.

Figures 4.43 to 4.46 depict the contour plots of total pressure distribution in a computational domain for uniform WSP and non-uniform WSP. Total pressure in a wind turbine refers to the sum of static pressure and dynamic pressure. Static pressure is the pressure exerted by the air on the blades when the blades are stationary, while dynamic pressure is the pressure exerted by the air on the blades when they are rotating.

The total pressure in a wind turbine is affected by various factors, including wind speed. Generally, as the wind speed increases, the total pressure also increases. This is because the kinetic energy of the wind increases with wind speed, resulting in a higher velocity and increased pressure. However, it's important to note that the relationship between wind speed and total pressure is not linear. At a certain point, the increase in wind speed may not result in a proportional increase in total pressure due to factors such as turbulence and air resistance. Additionally, the design of the wind turbine and its components can also affect the total pressure. For example, the shape and size of the blades can impact the amount of pressure generated by the wind. Overall, while wind speed is a significant factor in determining total pressure in a wind turbine, other factors must also be considered to fully understand the relationship between these variables. The total pressure is an important parameter in wind turbine design as it helps to determine the amount of energy that can be extracted from the wind. In wind turbine design, total pressure is used to calculate the power output of the turbine. The power output of a wind turbine is proportional to the cube of the wind speed and the

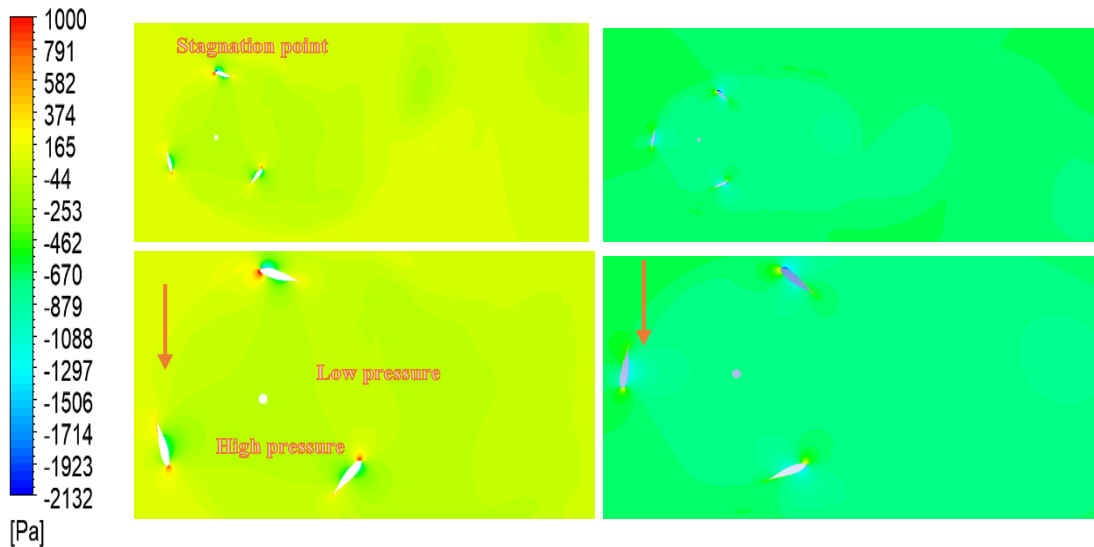
total pressure of the wind. Therefore, a higher total pressure means that more power can be generated by the turbine.

As well, the total pressure is also used to determine the aerodynamic performance of the turbine blades. The shape and size of the blades are designed to optimize the conversion of wind energy into electrical power. The total pressure of the wind affects the drag and lift forces that act upon the blades, which in turn affect their performance. Overall, understanding the significance of total pressure in wind turbine design is crucial for optimizing the efficiency and power output of wind turbines. According to the figures, the high- and low-pressure regions around the blades are very clear in all cases, especially for the wake flow in Figure 4.46.

As a result, the nearby zone gets narrower, and the wake extends as the streamlines are shifted externally. And, at the nearby streamlines, there's no important variation in the entire pressure. Thus, the velocity reduces if the static pressure rises. Generally, the prevailing phenomenon of the rotor downstream is the blending of wake with freestream. The velocity shortfall at the close wake recovers more downstream, and the flow gets further even.

For calculating the distributions of pressure as well as the incorporated torque and thrust, the model of $k-\omega$ -based shear-stress-transport (SST) is designed to give the most precise forecast of the start and the flow separation quantity beneath the adverse gradients of pressure via the insertion of the influences of transport into the eddy viscosity formulation. Because the geometries of WTs are possible for causing the separation of flow, the model of SST with an automatic wall task was motivated for modelling the fields of flow.

Figure 4.43 for the first Design shows the effect of total pressure on the three blades, as shown in areas where there is high pressure or low pressure.



Left: uniform WSP Right: non uniform WSP

Figure 4.43. Total pressure contour after four cycles Design 1.

In Design 1, the total pressure contour and TSR are 5, while for uniform WSP, the maximum value is 2449 Pa and the minimum value is -2132 Pa. For non-uniform WSP, the maximum value is 2380 Pa, and the minimum is -1933Pa.

Figure 4.44 for Design 2 shows the total pressure effect on the double blades, shown in the interaction effect area.

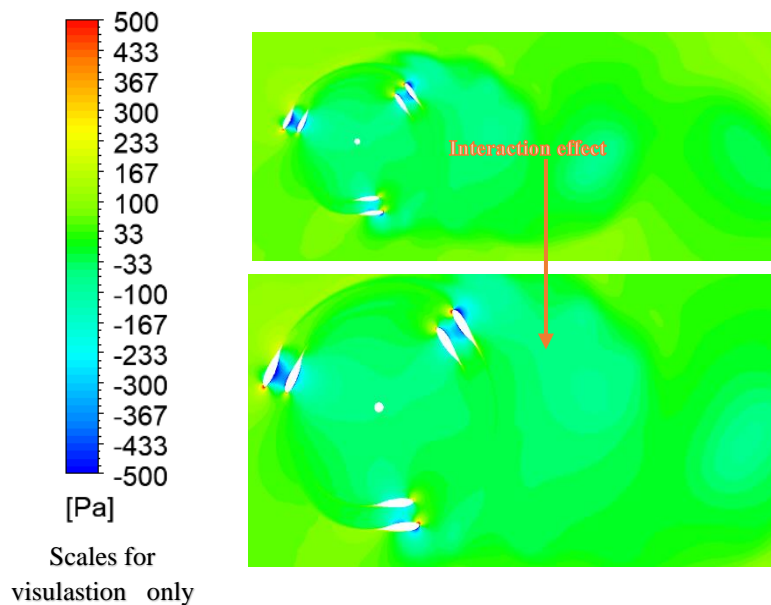
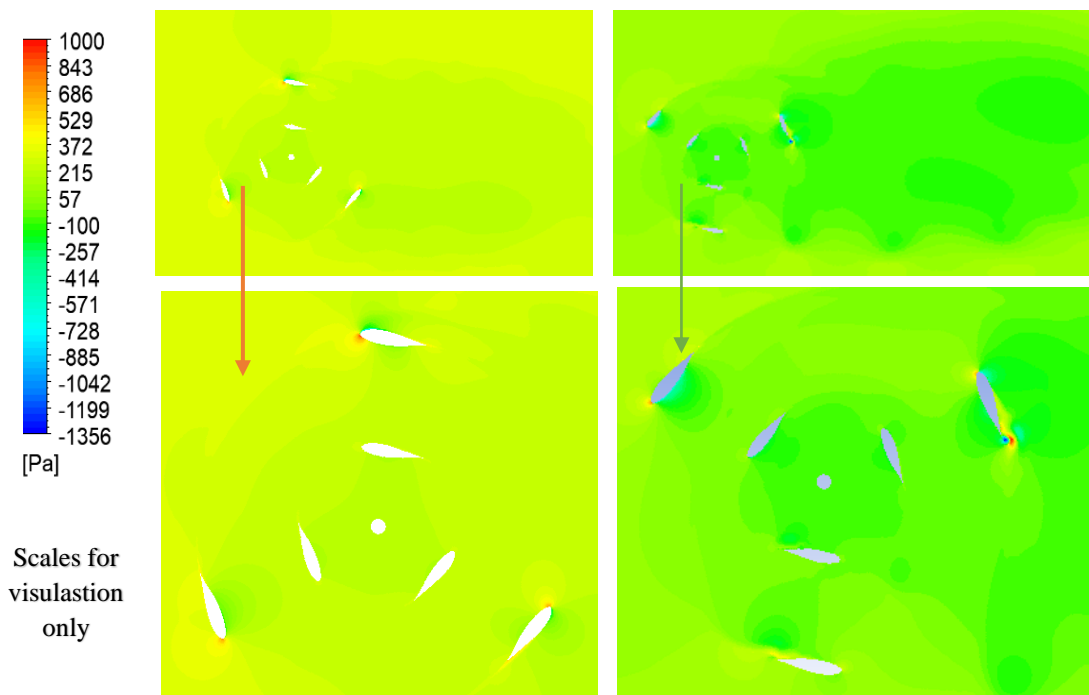


Figure 4.44. Total pressure contour after four cycles Design 2.

For Design 2, when the total pressure contour is analyzed, the TSR value is 3.25. When the wind speed profile is uniform, the maximum pressure is 1000 Pa, and the minimum pressure is -1029 Pa.

Figure 4.45 for Design 3 shows the effect of the total pressure at the double blades and the effect of the pressure on the front and rear edges of the blade.



Left: uniform WSP

Right: non uniform WSP

Figure 4.45. Total pressure contour after four cycles Design 3.

In design 3, the total pressure contour and TSR are 3.25, while for uniform WSP, the maximum value is 1179 Pa and the minimum value is -1356 Pa. For non-uniform WSP, the maximum value is 1259 Pa and the minimum is -1589 Pa

Figure 4.46 for Design 4 shows the increased effect of the total pressure rise at the double blades.

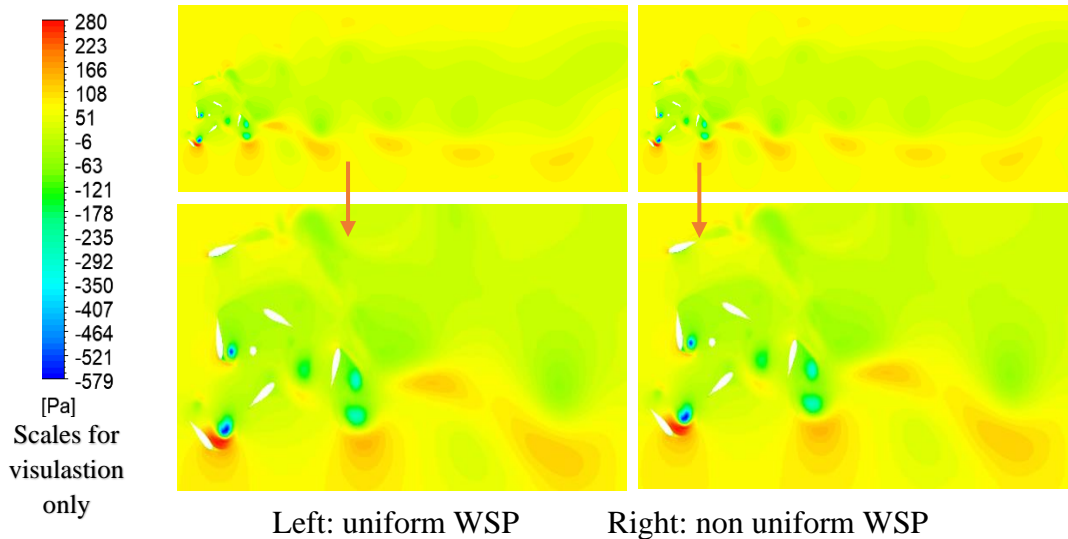


Figure 4.46. Total pressure contour after four cycles, Design 4.

In Design 4, the total pressure contour and TSR are 1, while for uniform WSP, the maximum value is 280 Pa and the minimum value is -578 Pa. For non-uniform WSP, the maximum value is 280 Pa and the minimum is -578 Pa.

When Figs. 4.43, 4.44, 4.45, and 4.46 are examined, it is seen that in the case of uniform velocity, the positive maximum values of the total pressure values for Design1, Design2, Design3, Design4 are 2449, 1000, 1179 and 280 pascals, respectively. Similarly, it can be said that negative values are -2132, -1029, -1356 and -578 pascals, respectively. According to these results, when the positive and negative value differences are examined, it is understood that the highest difference is in Design 1 and the least difference is in Design 4. It can be concluded that this difference is proportional to the power performance value.

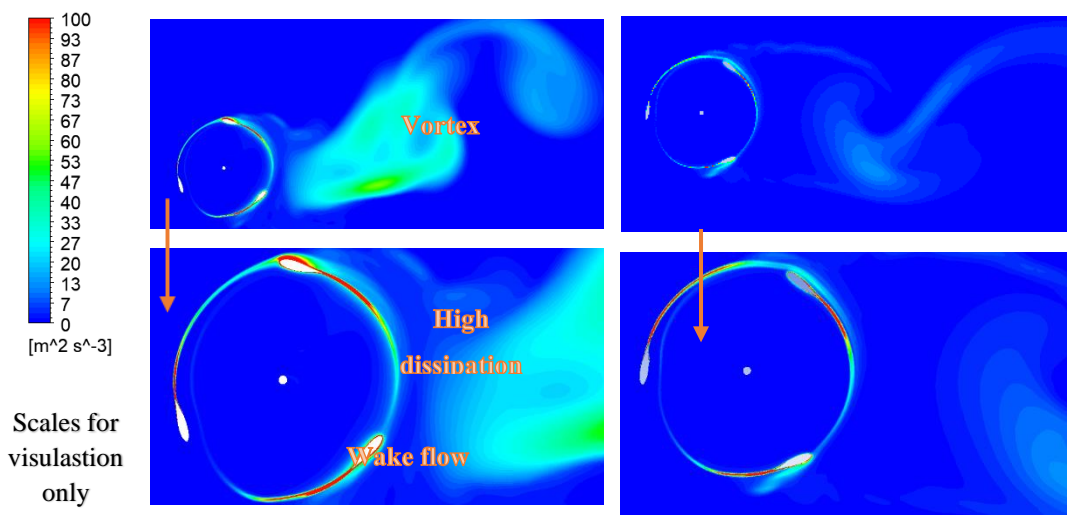
4.3.8. Turbulence Eddy Dissipation

Turbulence Eddy Dissipation, represents the rate at which vortices in the airflow around the turbine dissipate. Low vortex dissipation can lead to a more regular flow and more efficient energy collection.

Figures 4.47 to 4.50 demonstrate the contour plots of the turbulence eddy dissipation distribution in the computational domain for uniform WSP and non-uniform WSP.

Turbulence Eddy Dissipation Contour (TEDC) is a graphical representation of the turbulence intensity distribution around a wind turbine. It shows the rate of dissipation of turbulent kinetic energy owing to the turbine's presence. Eddy turbulence dissipation in wind turbines refers to the process of converting the kinetic energy of turbulent eddies into heat through viscous dissipation. This phenomenon occurs within the boundary layer of the wind turbine blades and has a significant impact on the aerodynamic performance and structural integrity of the blades.

Figure 4.47 shows, for the first Design, the effect of the turbulent vortex dissipation contour on the three blades. After four cycles, we observe the amplitude of the vortex resulting from the rotation of the blades and the length of the wake flow effect on the trailing edge.



Left: Uniform WSP Right: Non-uniform WSP

Figure 4.47. Turbulence eddy dissipation contour after four cycles Design 1.

In Design 1, for uniform WSP, the maximum value is $2 \cdot 10^6 \text{ m}^2/\text{s}^3$, and for non-uniform WSP, the maximum value is $2 \cdot 10^6 \text{ m}^2/\text{s}^3$.

Figure 4.48, for the second design, shows the effect of the turbulent vortex dissipation contour on the coupled blades. After four cycles, we notice a clear, high-dispersion effect behind the bleeds.

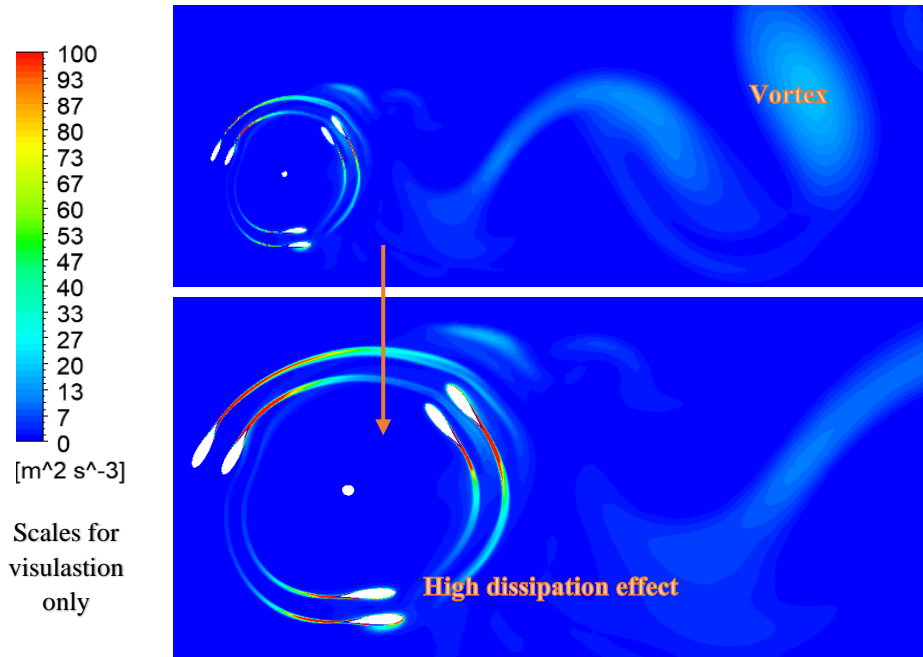
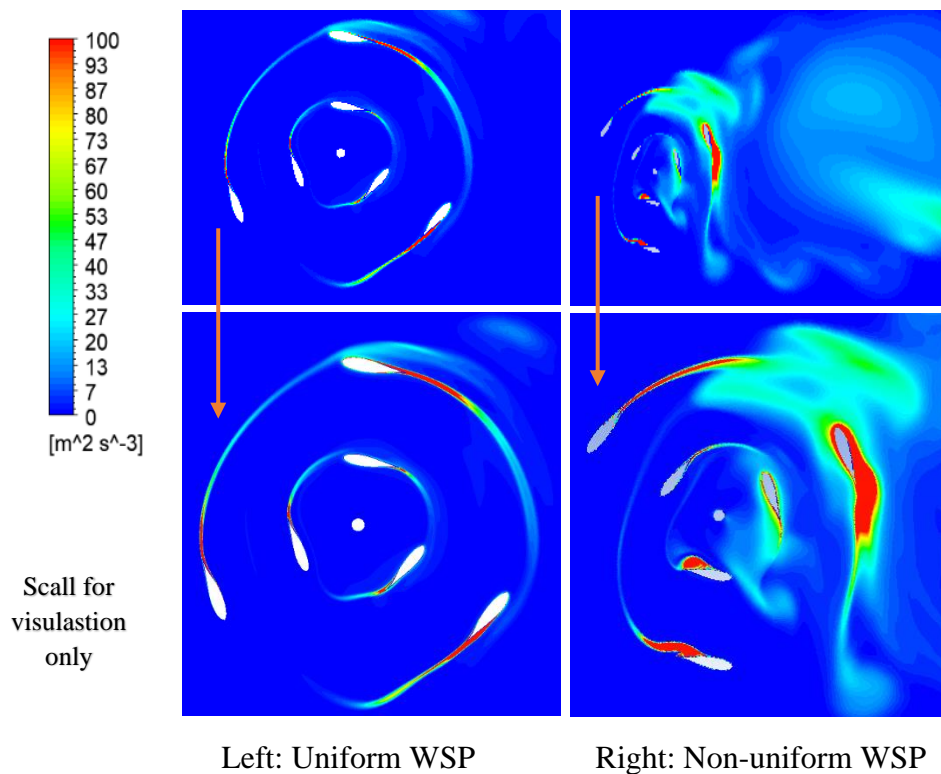


Figure 4.48. Turbulence eddy dissipation contour after four cycles.

In Design 2, when TSR is 3.25, the maximum value for uniform WSP is $5 \cdot 10^5 \text{ m}^2/\text{s}^3$. Figure 4.49, the third design, shows the significant effect of the turbulent vortex dissipation contour on the double blades.



Left: Uniform WSP

Right: Non-uniform WSP

Figure 4.49. Turbulence eddy dissipation contour after four cycles Design 3.

In Design 3, when TSR is 3.25, the maximum value for uniform WSP is $7 \cdot 10^5 \text{ m}^2/\text{s}^{-3}$, and for non-uniform WSP, the maximum value is $5 \cdot 10^6 \text{ m}^2/\text{s}^{-3}$.

Figure 4.50, the fourth Design, shows the large effect of the turbulent vortex dissipation contour on the double blades in particular. In non-uniform.

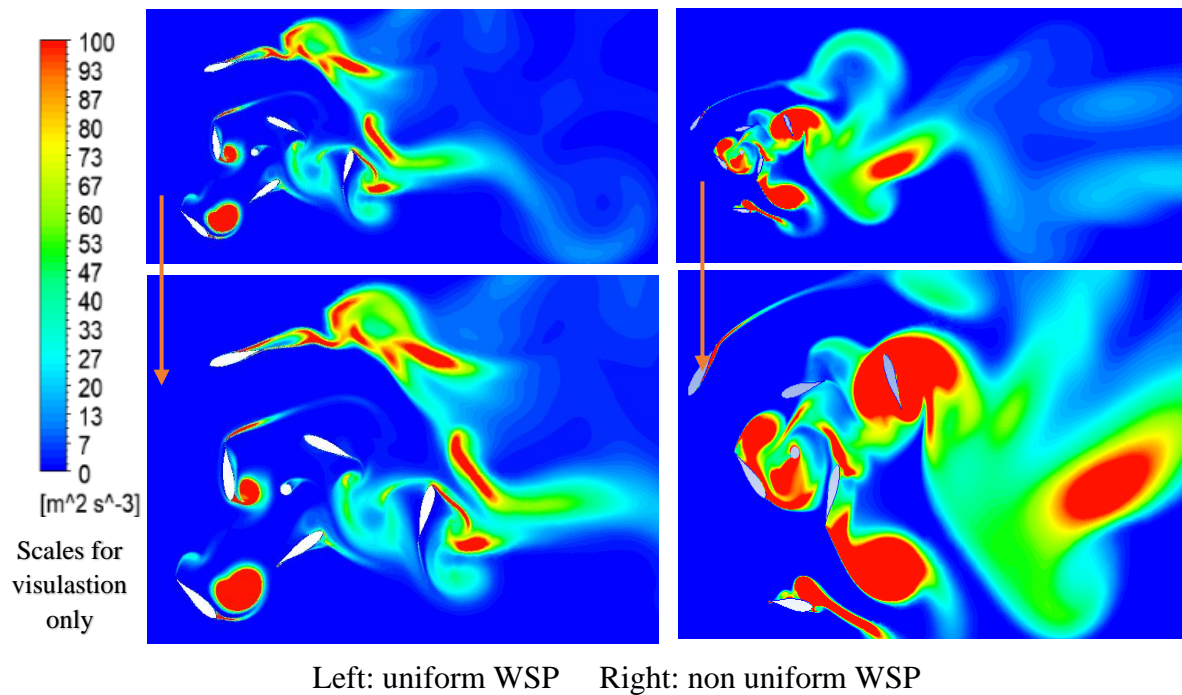


Figure 4.50. Turbulence eddy dissipation contour after four cycle Design 4.

In Design 4, when TSR is 1, the maximum value for uniform WSP is $2 \cdot 10^4 \text{ m}^2/\text{s}^{-3}$ and In non-uniform WSP, the maximum value is $1.2 \cdot 10^6 \text{ m}^2/\text{s}^{-3}$.

Turbulence eddy dissipation can have a significant impact on the power output of a wind turbine. Turbulence is a natural occurrence in the atmosphere and can cause fluctuations in wind speed and direction. These fluctuations can result in changes in the angle of attack of the wind turbine blades, which can affect the blades' aerodynamic efficiency as well as, ultimately, the turbine's power output. Eddy dissipation is a process that occurs when turbulent energy is converted into heat through frictional forces. This process can reduce the amount of kinetic energy available to the wind turbine, resulting in a decrease in power output. However, some wind turbine designs are better equipped to handle turbulence and eddy dissipation than others, and modern turbines often incorporate advanced control systems to optimize power output under

turbulent conditions. Overall, turbulence eddy dissipation can have a complex and variable effect on wind turbine performance, and the specific impact will depend on factors such as wind speed, turbulence intensity, and blade design. Therefore, the figures show that effect for all designs.

Where the max. and min. turbulence eddy values for uniform equal $(2 \cdot 10^6)$, $(5 \cdot 10^5)$, $(7 \cdot 10^5)$, and $(2 \cdot 10^4)$ for Designs 1, 2, 3, and 4, respectively. And for non-uniform wind speed, equal $(2 \cdot 10^6)$, $(5 \cdot 10^6)$, and $(1.2 \cdot 10^6)$ for Designs 1, 3, and 4, respectively. From the results, the turbulence eddy value in Designs 1 and 3 has a value in non-uniform WSP greater than in uniform WSP. The major reason is the decrease in the TSR value between the designs and the distance between the double blades.

4.3.9. Velocity Invariant Q

Velocity Invariant Q, this expresses the degree to which speed remains constant. Consistent speed can stabilize the turbine's performance and enhance its efficiency.

Velocity invariant Q is a control strategy used in wind turbines to maintain a constant power output at varying wind speeds. It adjusts the blade pitch angle to maintain a constant rotor speed, which in turn keeps the power output constant. Velocity invariant Q is a control strategy used in wind turbines to regulate the power output by adjusting the pitch angle of the blades. Unlike other control strategies, such as tip speed ratio and torque control, velocity invariant Q is not dependent on the wind speed. Instead, it maintains a constant ratio between the blade pitch angle and the rotor speed, resulting in a more stable and predictable power output.

One of the advantages of velocity-invariant Q is that it can operate over a wide range of wind speeds, making it suitable for use in variable wind conditions. It also provides better control over the power output, which can help reduce wear and tear on the turbine components and improve overall efficiency. However, velocity-invariant Q may not be the best control strategy for all wind turbine applications. Other control strategies may be more effective in certain wind conditions or for specific turbine designs. Ultimately, the choice of control strategy will depend on a variety of factors,

including the turbine's operating environment, performance requirements, and cost considerations. The benefit of using velocity invariant Q is that it allows for a constant power output regardless of the wind speed. This means that the turbine can operate efficiently over a wider range of wind speeds, resulting in increased energy production and reduced wear and tear on the turbine components. Additionally, velocity invariant Q can improve the stability of the turbine during turbulent wind conditions, leading to a more reliable and safer operation.

Therefore, figures 4.51 to 4.54 show that effect for all cases for uniform WSP, non-uniform WSP, and Q values.

In Figure 4.51, Design 1, the movement of three blades and the effect of Velocity invariant Q on the blades are shown.

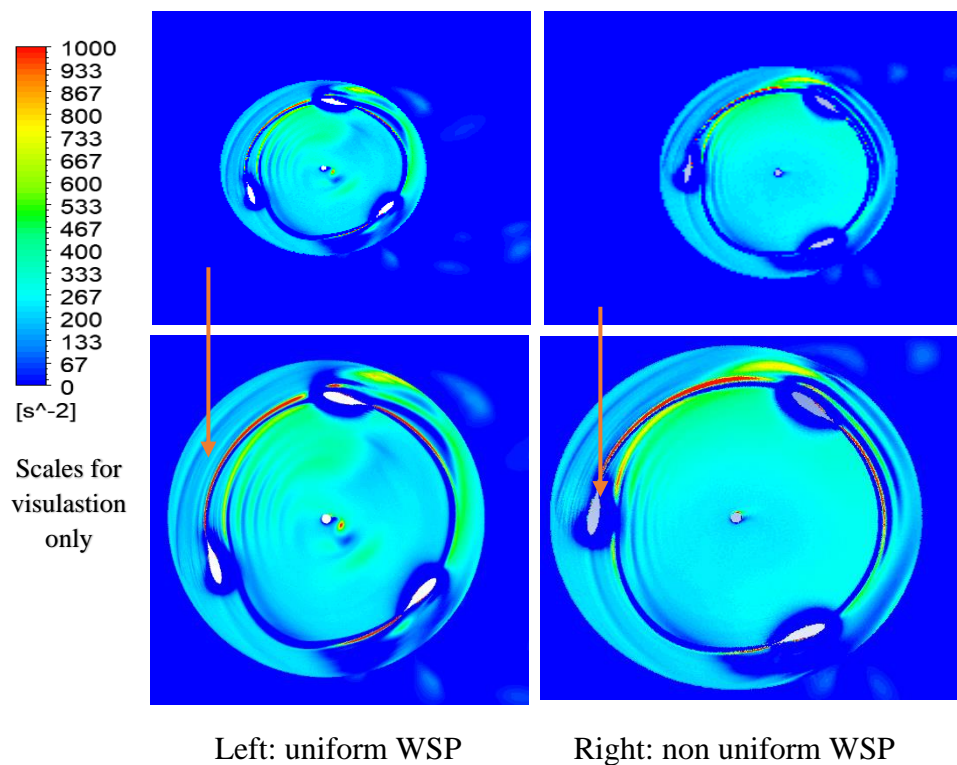


Figure 4.51. Velocity invariant Q contour after four cycles Design 1.

The Velocity invariant in Darius wind turbine design 1 with uniform WSP has a maximum value of $3.3 * 10^{10} \text{ s}^{-2}$ and a minimum value of $-1.5 * 10^{10} \text{ s}^{-2}$ and when

non-uniform WSP, values are maximum is $1.2 \cdot 10^{10} \text{s}^{-2}$, the minimum is $-4.3 \cdot 10^9 \text{s}^{-2}$ At $\text{TSR} = 5$. This indicates that the blade's base and tip are moving at different speeds.

In Figure 4.52, Design 2, the distance between the double blades is 1 meter, There is high Q and vortex separation.

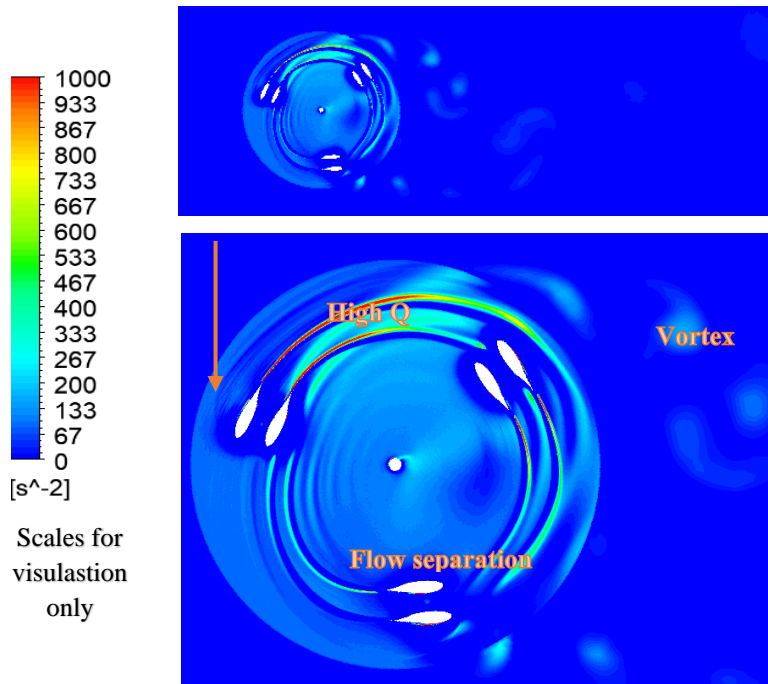
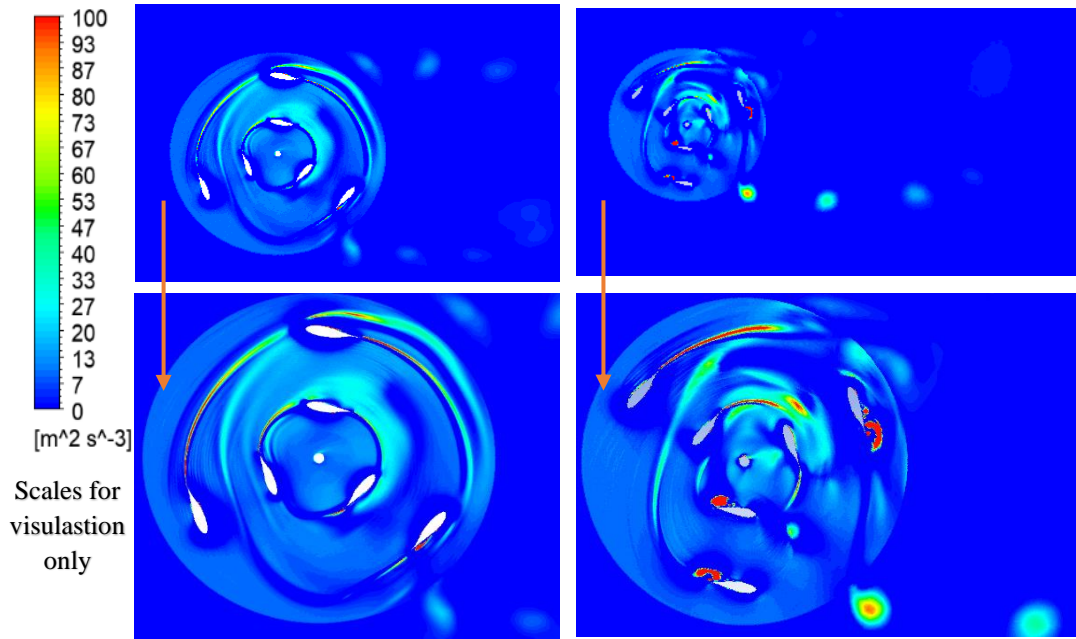


Figure 4.52. Velocity invariant Q contour after four cycles Design 2.

In Design 2, the velocity invariant has a minimum value of $-9 \cdot 10^9 \text{s}^{-2}$ and a maximum value of $8 \cdot 10^9 \text{s}^{-2}$. At TSR of 3.25. This suggests that there is a difference in speed between the blade's base and tip.

In Figure 4.53, Design 3, we notice the great clarity of the effect velocity invariant Q.

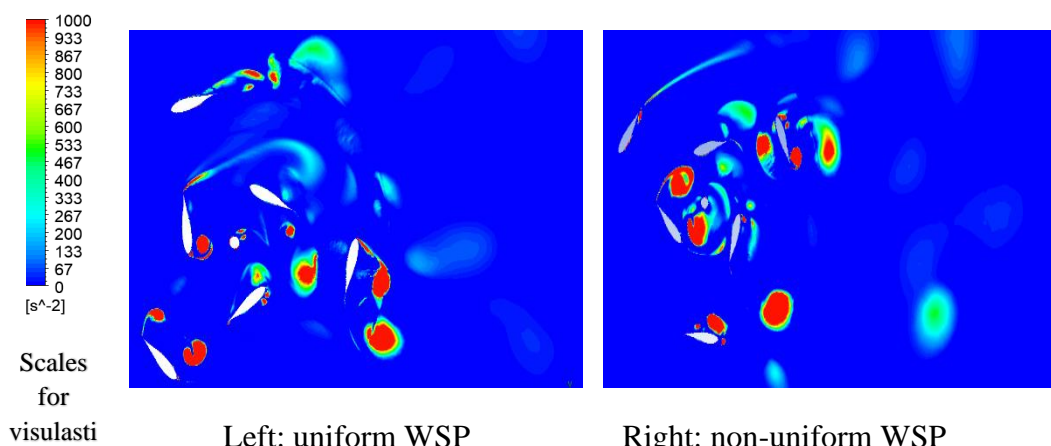


Left: uniform WSP Right: non uniform WSP

Figure 4.53. Velocity invariant Q contour after four cycles Design 3.

The velocity invariant Design 3, uniform WSP has a maximum value of $9 \cdot 10^9 \text{ s}^{-2}$ and a minimum value of $-1.5 \cdot 10^9 \text{ s}^{-2}$, and when non-uniform WSP has a maximum value of $2.5 \cdot 10^{10} \text{ s}^{-2}$, the minimum value is $-4.3 \cdot 10^{10} \text{ s}^{-2}$. At $\text{TSR} = 3.25$, this indicates that the blade's base and tip are moving at different speeds.

In Figure 4.54, Design 4, we notice the great clarity of the effect velocity invariant Q.



Left: uniform WSP

Right: non-uniform WSP

Figure 4.54. Velocity invariant Q contour after four cycles design 4.

The Velocity invariant Design 4, uniform WSP has a maximum value of $8 * 10^8 \text{ s}^{-2}$ and a minimum value of $-8 * 10^8 \text{ s}^{-2}$ and when non-uniform WSP has a maximum value of $1.3 * 10^{10} \text{ s}^{-2}$, the minimum value is $-8 * 10^9 \text{ s}^{-2}$. At $\text{TSR} = 1$, this indicates that the blade's base and tip are moving at different speeds.

Designs 1, 3, and 4, respectively. From the results, the turbulence eddy value in Design 1 has a value in uniform WSP greater than in non-uniform WSP; otherwise, in Designs 3 and 4, the major reason for that is the decrease in the TSR value between the Designs is 1, 3, and 4, respectively. From the results, the turbulence eddy value in Design 1 has a value in uniform WSP greater than in non-uniform WSP; otherwise, in Designs 3 and 4, the major reason for that is the decrease in the TSR value between the Designs.

4.3.10. Velocity Swirling Strength

Velocity Swirling Strength: This term indicates the intensity of rotational motion at speed. High swirling strength shows how the speed around the turbine changes with a rotating tendency. Rotation can positively affect the turbine's performance by providing a more even distribution of speed. It seems to be a combination of two concepts: velocity and swirling strength. Let's break down these terms individually:

- **Velocity:** Velocity refers to the speed and direction of an object's motion in a specific direction. In fluid dynamics, velocity describes how fast a fluid (liquid or gas) is moving at a particular point in space and time. Velocity is typically represented as a vector quantity, meaning it has both magnitude (speed) and direction.
- **Swirling Strength:** Swirling strength, also known as vorticity, is a measure of the local rotation or circulation of a fluid element. It describes the tendency of a fluid to rotate or form vortices. In the context of fluid dynamics, vorticity is a vector field defined as the curl of the velocity vector.

So, "velocity swirling strength" would likely refer to the level or magnitude of swirling or rotational motion of a fluid at a particular point in space. In other words, it quantifies how much the fluid is rotating or swirling at that location.

In more technical terms, the swirling strength (vorticity) is mathematically expressed as the curl of the velocity vector field. If one denotes the velocity vector as

$$V = V_{xi} + V_{yj} + V_{zk} \quad (4.2)$$

In three-dimensional space (where i , j , and k are unit vectors along the x , y , and z axes, respectively). ∇ is the del operator (gradient) and represents the cross product.

$$\nabla = \left(\frac{\partial}{\partial x}, \frac{\partial}{\partial y}, \frac{\partial}{\partial z} \right) \quad (4.3)$$

where the partial derivatives concerning the x , y , and z coordinates are represented by the variables $\frac{\partial}{\partial x}$, $\frac{\partial}{\partial y}$, and $\frac{\partial}{\partial z}$, respectively. then the vorticity vector (Ω) is given by:

$$\Omega = \nabla * V \quad (4.4)$$

Understanding swirling strength and its variations in fluid flow is essential in various fields such as aerodynamics, where the behaviour of fluids is of significant interest. Scientists and engineers study swirling strength to better understand fluid behaviour, turbulence, and vortices, which have implications for the design of aircraft, weather prediction, and various engineering applications. Velocity-swirling strength refers to the rotational motion of air particles around the axis of a wind turbine. It is typically measured in radians per second.

The relationship between velocity swirling strength and wind speed is complex and can vary depending on factors such as the design of the wind turbine and the atmospheric conditions. Generally, as wind speed increases, so does the velocity-swirling strength. However, there is a limit to how fast the air can swirl around the turbine blade before it becomes unstable and loses efficiency. It is also worth noting that the velocity-swirling strength is just one factor that contributes to the overall performance of a wind turbine. Other factors, such as blade design, generator efficiency, and control systems, also play important roles in determining the amount of energy that can be extracted from the wind.

The velocity-swirling strength, also known as turbulence intensity, can have an impact on the power output of a wind turbine

In general, higher turbulence intensity can lead to a reduction in power output. This is because the turbulence in the wind can cause the blades of the turbine to stall, which reduces the amount of energy that can be extracted from the wind. However, it's important to observe that some WT's are designed to work well in high-turbulence environments. These turbines are often equipped with advanced control systems that can adjust the blade pitch or other parameters in response to changes in wind conditions.

In summary, the impact of velocity swirling strength on wind turbine power output depends on the specific design of the turbine and its control system.

Therefore, figures 4.55 to 4.58 show that effect for all cases for uniform WSP and non-uniform WSP.

Figure 4.55, which represents the design 1, shows the velocity swirling strength contour of the force of the rapid vortex on the three blades after four rotations.

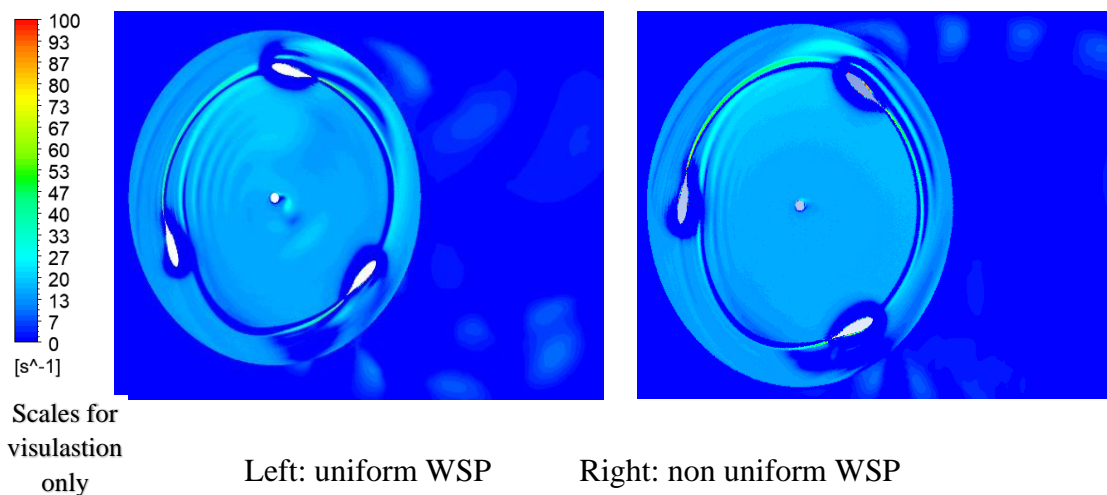


Figure 4.55. Velocity swirling strength contour, Design1.

There is a very strong vortex in Design 1, at the blade tip, when uniform the maximum speed rotation force value is 140199 s^{-1} and non-uniform the value is 102895 s^{-1} at the

TSR value is 5 in both uniform and non-uniform scenarios. The performance of the blades with this vortex may result in instability and noise.

Figure 4.56, In Design 2, we observe the effect of the force-velocity swirling strength contour in the area of wake flow and vortex.

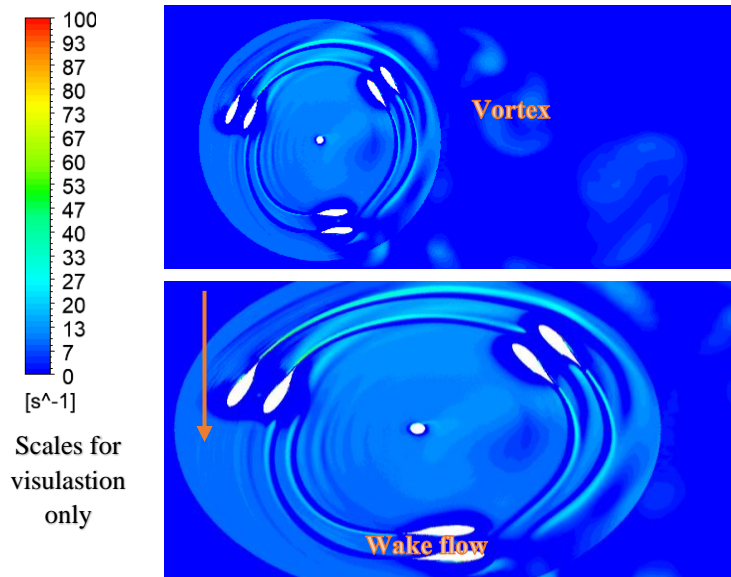


Figure 4.56. Velocity swirling strength contour Design 2.

In Design 2, the value of velocity swirling strength after four cycles is maximum $\approx 140199 \text{ s}^{-1}$, at $\text{TSR} = 3.25$ in both cases (uniform and non-uniform).

Figure 4.57, in Design 3, we observe the effect of velocity swirling strength contour force on the double blades when the distance between them is 3 meters.

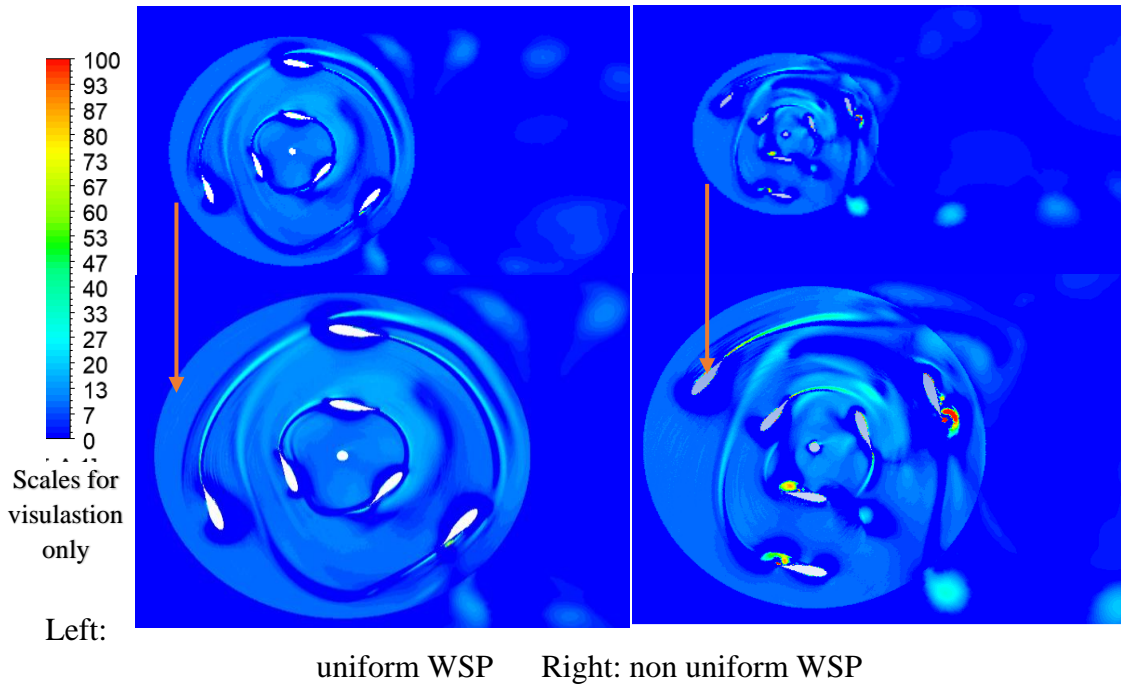


Figure 4.57. Velocity swirling strength contour Design 3.

In this Design 3, at TSR = 3.25, the maximum value of the velocity swirling strength after four cycles is as follows: when the case is uniform, the result is 97344 s^{-1} , and when the case is non-uniform, the result is 158829 s^{-1} .

Figure 4.58. In Design 4, we observe the effect of Velocity swirling strength contour force on the double blades when the distance between them is 3 meters. When the outer blades deviate from the corresponding inner blades.

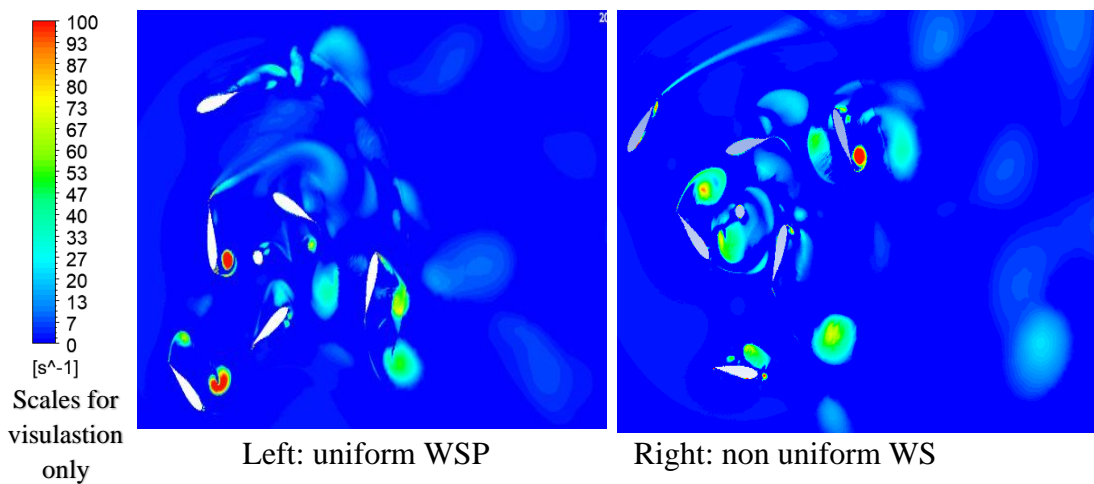


Figure 4.58. Velocity swirling strength contour Design 4.

In this Design 4, at TSR is equal to 1, the maximum value of the velocity swirling strength after four cycles is as follows: when the case is uniform, the result is 28078 s^{-1} , and when the case is non-uniform, the result is 116077 s^{-1} .

Where the maximum velocity invariant Q values for uniform wind speed equal 140199, 89498, 97344 and 28078 for Designs 1, 2, 3, and 4, respectively. And for non-uniform wind speed, equal 102895, 158829, and 116077 for Designs 1, 3, and 4, respectively. From the results, the turbulence eddy value in Designs 1 and 3 has a value in uniform WSP greater than in non-uniform WSP; otherwise, Design 4. The major reason is the decrease in the TSR value between the Designs.

PART 5

CONCLUSIONS AND RECOMMENDATIONS

5.1. CONCLUSIONS

This study presents numerically the double-blade effects of DVAWT performance. Different blade configurations are used in the rotor to enhance wind turbine efficiency. Moreover, to study the wind profile effects on wind turbine operation conditions. The main conclusions from the results are:

- A properly discretized border layer close to the surface of the rotor is critical to obtain precise outcomes of calculations in the CFD mesh study.
- C_p rises if TSR is augmented to a given value, and after that, this value reduces with the TSR rise for the whole model.
- The turbine rotation speed (N) increases with increasing TSR and the wind speed remains 10 m/s.
- Design 1, at TSR equal to 5 can be applied with high efficiency with $C_p=0.272$.
- Design 2 has a high turbulence effect due to the interaction effect between the blades so, it is not a successful design.
- Design 3, at TSR equal to 3.25 can be applied with high efficiency with $C_p=0.213$.
- Design 4, at TSR equal to 1 can be applied with high efficiency with $C_p=0.110$.
- From the results, CFD tools have a good performance in capturing the turbulence eddies, vortices, and separation around the blades.
- When four different design results are evaluated, design 1 has the highest power performance. Design 2 was a failed design due to the interaction effect between double blade and too near together. Although design 3 is a successful

design, it does not have as high-power performance as design 1. design4 has some power performance, It is noteworthy that it works, especially in the low TSR value range.

- It can be said that the ideal TSR value at which the maximum power is obtained is 5 for Design 1, for Design 3, it is 3.25, and for Design 4, it is 1.

Another conclusion that can be drawn from this study is that contours and torque history graph CFD results will be very useful to analyze the flow on Darrieus designs, measure their performance, and thus improve the designs.

5.2. RECOMMENDATIONS

Depending upon the works concealed via the current investigation, the subsequent recommendations being proposed for the experimental and numerical upcoming work are:

- Investigate the variation in the airfoil kind to find out the enhancement in DWT in circumstances similar to the current work.
- Study the variation in the preliminary attack angle for DWT to find out the enhancement in the hybrid wind turbine under similar circumstances to the present work.
- Extend the present study into 3D CFD simulation to predict the helical profile effect on WT efficiency.
- Extend the present study to include the experimental part of double-blade DWT.
- For future studies, there are suggestions for different designs that could be considered, such as assuming different distances between the coupled blades, using more TSR values, using different wind speed values, and performing more detailed analyses to optimize new designs and 3D CFD analysis.

REFERENCES

1. KOHILO, “201: Wind Energy Benefits & Challenges – KOHILO Wind Turbines, (n.d).” <https://kohilowind.com/kohilo-university/201-wind-energy-benefits-challenges>, (2015)
2. I. Dincer and A. Abu-Rayash, “Energy sources,” *Energy Sustainability*, 19–58 (2020).
3. C. K. Kannan, V. Kamaraj, and S. R. Paranjothi, “Renewable Energy from Induced Airflow Generated by Cruising Ground Vehicles in Tandem using RANS,” *Energy Procedia*, 14: 1877–1882 (2012).
4. N. E. Chowdhury, M. A. Shakib, F. Xu, S. Salehin, M. R. Islam, and A. A. Bhuiyan, “Adverse environmental impacts of wind farm installations and alternative research pathways to their mitigation,” *Clean Eng Technol*, 7: 100-415 (2022).
5. mar D. L. M. L. D.Velasco’s, “Numerical simulations of active flow control with synthetic jets in a Darrieus turbine”, *Renewable Energy*, 113: 129-140 (2017).
6. M. P. Yunus Celika, b*, Derek Inghama, Lin Maa, “Design and aerodynamic performance analyses of the self-starting H-type VAWT having J-shaped aerofoils considering various design parameters using”, *Energy*, 251: (2022).
7. R. Kumar, K. Raahemifar, and A. S. Fung, “A critical review of vertical axis wind turbines for urban applications,” *Renewable and Sustainable Energy Reviews*, 89: 281–291 (2018).
8. V. Sharma, S. Sharma, and G. Sharma, “Recent development in the field of wind turbine,” *Mater Today Proc*, 64: 1512–1520 (2022).
9. M. Jafari, A. Razavi, and M. Mirhosseini, “Effect of airfoil profile on aerodynamic performance and economic assessment of H-rotor vertical axis wind turbines,” *Energy*, 165: 792–810 (2018).
10. H. Huang, J. Luo, and G. Li, “Study on the optimal design of vertical axis wind turbine with novel variable solidity type for self-starting capability and aerodynamic performance,” *Energy*, 271: 127-131 (2023).
11. R. Whittlesey, “Vertical Axis Wind Turbines: Farm and Turbine Design,” *Wind Energy Engineering: A Handbook for Onshore and Offshore Wind Turbines*, 185–202 (2017).
12. T. Wilberforce and A. Alaswad, “Performance analysis of a vertical axis wind turbine using computational fluid dynamics,” *Energy*, 263: 125892 (2023).

13. M. Zemamou, M. Aggour, and A. Toumi, "Review of savonius wind turbine design and performance," *Energy Procedia*, 141: 383–388 (2017).
14. S.-M. L.-M. J. Ali, "Lift and Drag Forces with Respect to Azimuth Position of a Darrieus Wind Turbine", *American Society of Mechanical Engineers*, 1: (2018).
15. O. S. Mohamed, A. A. Ibrahim, A. K. Etman, A. A. Abdelfatah, and A. M. R. Elbaz, "Numerical investigation of Darrieus wind turbine with slotted airfoil blades," *Energy Conversion and Management: X*, 5: 100026 (2020).
16. S. ed D. Fertahi, A. Samaouali, and I. Kadiri, "CFD comparison of 2D and 3D aerodynamics in H-Darrieus prototype wake," *e-Prime - Advances in Electrical Engineering, Electronics and Energy*, 4: 100178 (2023).
17. R. Quispe-Abad and N. Müller, "Finding an absolute maximum theoretical power coefficient for ducted wind turbines," *Journal of Wind Engineering and Industrial Aerodynamics*, 236: 105335, (2023).
18. A. A. Ibrahim, A. M. R. Elbaz, P. F. Melani, O. S. Mohamed, and A. Bianchini, "Power augmentation of Darrieus wind turbine blades using trapped vortex cavity," *Journal of Wind Engineering and Industrial Aerodynamics*, 223, 104949 (2022).
19. P. Ghiasi, G. Najafi, B. Ghobadian, A. Jafari, R. Mamat, and M. Fairusham Ghazali, "CFD-Study of the H-Rotor Darrius wind turbine performance in Drag-Lift and lift Regime: Impact of Type, thickness and chord length of blades," *Alexandria Engineering Journal*, 67: 51–64 (2023).
20. W. Km. M J Jamanun¹, M S Misaran², M Rahman, "Performance Investigation of A Mix Wind Turbine Using A Clutch Mechanism At Low Wind Speed Condition", *Materials Science and Engineering*, 217 (1): (2017).
21. M. M. Aslam Bhutta, N. Hayat, A. U. Farooq, Z. Ali, S. R. Jamil, and Z. Hussain, "Vertical axis wind turbine – A review of various configurations and design techniques," *Renewable and Sustainable Energy Reviews*, 16 (4): 1926–1939 (2012).
22. B. Hand, A. Cashman, and G. Kelly, "A Low-Order Model for Offshore Floating Vertical Axis Wind Turbine Aerodynamics," *IEEE Trans Ind Appl*, 53(1): 512–520 (2017).
23. M. Islam, D. S. K. Ting, and A. Fartaj, "Desirable Airfoil Features for Smaller-Capacity Straight-Bladed VAWT," <http://dx.doi.org/10.1260/030952407781998800>, 31 (3): 165–196 (2007).
24. F. Balduzzi, A. Bianchini, E. A. Carnevale, L. Ferrari, and S. Magnani, "Feasibility analysis of a Darrieus vertical-axis wind turbine installation in the rooftop of a building," *Appl Energy*, 97: 921–929 (2012).

25. S. Mertens, G. Van Kuik, and G. Van Bussel, "Performance of an H-Darrieus in the Skewed Flow on a Roof," *J Sol Energy Eng*, 125 (4): 433–440 (2003).
26. C. J. S. Ferreira, G. J. W. Van Bussel, and G. A. M. Van Kuik, "Wind Tunnel Hotwire Measurements, Flow Visualization and Thrust Measurement of a VAWT in Skew," *J Sol Energy Eng*, 128 (4): 487–497 (2006).
27. M. H. Mohamed, "Aero-acoustics noise evaluation of H-rotor Darrieus wind turbines," *Energy*, 65 596–604 (2014).
28. "Book Review: Wind Energy in the Built Environment — Concentrator Effects of Buildings," <http://dx.doi.org/10.1260/030952406779502623>, 30 (5): 451–452 (2006).
29. B. Hand and A. Cashman, "A review on the historical development of the lift-type vertical axis wind turbine: From onshore to offshore floating application," *Sustainable Energy Technologies and Assessments*, 38: 100646 (2020).
30. B. Hand, A. Cashman, and G. Kelly, "Aerodynamic analysis of a 5 mw stall-regulated offshore vertical axis wind turbine using computational fluid dynamics," *Lecture Notes in Civil Engineering*, 18: 485–491 (2019).
31. B. Hand and A. Cashman, "Conceptual design of a large-scale floating offshore vertical axis wind turbine," *Energy Procedia*, 142: 83–88 (2017).
32. B. Hand, G. Kelly, and A. Cashman, "Numerical simulation of a vertical axis wind turbine airfoil experiencing dynamic stall at high Reynolds numbers," *Comput Fluids*, 149: 12–30 (2017).
33. S. ERIKSSON, H. BERNHOFF, and M. LEIJON, "Evaluation of different turbine concepts for wind power," *Renewable and Sustainable Energy Reviews*, 12 (5): 1419–1434 (2008).
34. M. ISLAM, D. TING, and A. FARTAJ, "Aerodynamic models for Darrieus-type straight-bladed vertical axis wind turbines," *Renewable and Sustainable Energy Reviews*, 12 (4): 1087–1109 (2008).
35. B. Hand, A. Cashman, and G. Kelly, "An aerodynamic modelling methodology for an offshore floating vertical axis wind turbine," *2015 International Conference on Renewable Energy Research and Applications, ICRERA*, 273–277 (2015).
36. S.Schettini, F.Saeed, "Wind turbine design with emphasis on Darrieus Concept," <https://www.perlego.com/book/2802110/wind-turbine-design-with-emphasis-on-darrieus-concept-pdf>, (2002).
37. M. R. Islam, S. Mekhilef, and R. Saidur, "Progress and recent trends of wind energy technology," *Renewable and Sustainable Energy Reviews*, 21: 456–468 (2013).

38. P. J. Tavner, J. Xiang, and F. Spinato, "Reliability analysis for wind turbines," *Wind Energy*, 10 (1): 1–18 (2007).
39. H. Arabian-Hoseynabadi, H. Oraee, and P. J. Tavner, "Failure Modes and Effects Analysis (FMEA) for wind turbines," *International Journal of Electrical Power & Energy Systems*, 32 (7): 817–824 (2010).
40. J. Kjellin, S. Eriksson, and H. Bernhoff, "Electric Control Substituting Pitch Control for Large Wind Turbines," *Journal of Wind Energy*, 2013, 1–4 (2013).
41. G. Marsh and S. Peace, "Tilting at windmills," *Refocus*, 6 (5): 37–42 (2005).
42. C. Li , S. Songye, Y. Lin "2.5D large eddy simulation of vertical axis wind turbine in consideration of high angle of attack flow," *Renew Energy*, 51: 317-330 (2013).
43. S. Apelfröjd, S. Eriksson, and H. Bernhoff, "A Review of Research on Large Scale Modern Vertical Axis Wind Turbines at Uppsala University," *Energies* 2016, 9 (7): 570 (2016).
44. D. W. Wekesa, C. Wang, Y. Wei, and L. A. M. Danao, "Influence of operating conditions on unsteady wind performance of vertical axis wind turbines operating within a fluctuating free-stream: A numerical study," *Journal of Wind Engineering and Industrial Aerodynamics*, 135: 76–89 (2014).
45. F. Scheurich and R. E. Brown, "Modelling the aerodynamics of vertical-axis wind turbines in unsteady wind conditions," *Wind Energy*, 16 (1): 91–107 (2013).
46. L. Du, G. Ingram, and R. G. Dominy, "A review of H-Darrieus wind turbine aerodynamic research," *Proc Inst Mech Eng C J Mech Eng Sci*, 233 (23-24): 7590–7616 (2019).
47. O. S. Mohamed, A. A. Ibrahim, A. K. Etman, A. A. Abdelfatah, and A. M. R. Elbaz, "Numerical investigation of Darrieus wind turbine with slotted airfoil blades," *Energy Conversion and Management: X*, 5: 100026 (2020).
48. P. Mohan Kumar, K. Sivalingam, T.-C. Lim, S. Ramakrishna, and H. Wei, "Strategies for Enhancing the Low Wind Speed Performance of H-Darrieus Wind Turbine—Part 1," *Clean Technologies*, 1 (1): 185–204 (2019).
49. B. C. Owens and D. T. Griffith, "Aeroelastic Stability Investigations for Large-scale Vertical Axis Wind Turbines," *J Phys Conf Ser*, 524: 012092 (2014).
50. J. Zhu, H. Huang, and H. Shen, "Self-starting aerodynamics analysis of vertical axis wind turbine," *Advances in Mechanical Engineering*, 7 (12): 168781401562096 (2015).
51. M. Douak, Z. Aouachria, R. Rabehi, and N. Allam, "Wind energy systems: Analysis of the self-starting physics of vertical axis wind turbine," *Renewable and Sustainable Energy Reviews*, 81: 1602–1610 (2018).

52. W. Tian, X. Ni, B. Li, G. Yang, and Z. Mao, "Improving the efficiency of Darrieus turbines through a gear-like turbine layout," *Energy*, 267: 126580 (2023).
53. "Wind Turbine Blade Design, Flat, Bent or Curved," <https://www.alternative-energy-tutorials.com/wind-energy/wind-turbine-blade-design.html>, (2023)
54. K. M. Almohammadi, D. B. Ingham, L. Ma, and M. Pourkashan, "Computational fluid dynamics (CFD) mesh independency techniques for a straight blade vertical axis wind turbine," *Energy*, 58: 483–493 (2013).
55. A. Bianchini, G. Ferrara, and L. Ferrari, "Design guidelines for H-Darrieus wind turbines: Optimization of the annual energy yield," *Energy Convers Manag*, 89: 690–707 (2015).
56. T. Ashwill, H. Sutherland, and D. Berg, "A retrospective of VAWT technology." Office of Scientific and Technical Information (OSTI), *SAND 2012-03040TRN: USA* (2012).
57. Dr. Stuart Scott, "Wind Turbine Design Exercise," http://en.wikipedia.org/wiki/Wind_turbine_design, (2023).
58. S. Armstrong, A. Fiedler, and S. Tullis, "Flow separation on a high Reynolds number, high solidity vertical axis wind turbine with straight and canted blades and canted blades with fences," *Renew Energy*, 41: 13–22 (2012).
59. M. Baghdadi, S. Elkoush, B. Akle, and M. Elkhoury, "Dynamic shape optimization of a vertical-axis wind turbine via blade morphing technique," *Renew Energy*, 154: 239–251 (2020).
60. F. Balduzzi, A. Bianchini, R. Maleci, G. Ferrara, and L. Ferrari, "Critical issues in the CFD simulation of Darrieus wind turbines," *Renew Energy*, 85: 419–435 (2016).
61. E. Dayan, "Wind energy in buildings: Power generation from wind in the urban environment - where it is needed most," *Refocus*, 7 (2): 33–38 (2006).
62. T. Wilberforce and A. Alaswad, "Performance analysis of a vertical axis wind turbine using computational fluid dynamics," *Energy*, 263: 125892 (2023).
63. S. M. H. Karimian and A. Abdolahifar, "Performance investigation of a new Darrieus Vertical Axis Wind Turbine," *Energy*, 191: 116551 (2020).
64. "A Simple, Robust Design Saves Money." <https://www.huyett.com/resources/case-studies/case-study-simple-robust-design>, (2023)
65. "SeaTwirl – The future of offshore wind", Available: <https://seatwirl.com/>, (2023).

66. “Gwind Company Profile - Powrbot list of companies”, Available: <https://powrbot.com/companies/profile/gwind/>, (2023).
67. A. Alaimo, A. Esposito, A. Messineo, C. Orlando, and D. Tumino, “3D CFD Analysis of a Vertical Axis Wind Turbine,” *Energies (Basel)*, 8 (4): 3013–3033 (2015).
68. Z. Wang, Y. Wang, and M. Zhuang, “Improvement of the aerodynamic performance of vertical axis wind turbines with leading-edge serrations and helical blades using CFD and Taguchi method,” *Energy Convers Manag*, 177: 107–121 (2018.)
69. L. Battisti, A. Brighenti, E. Benini, and M. R. Castelli, “Analysis of Different Blade Architectures on small VAWT Performance,” *J Phys Conf Ser*, 753: 062009 (2016).
70. M. R. Castelli and E. Benini, “Effect of Blade Inclination Angle on a Darrieus Wind Turbine,” *J Turbomach*, 134 (3), (2011).
71. P. Marsh, D. Ranmuthugala, I. Penesis, and G. Thomas, “Numerical investigation of the influence of blade helicity on the performance characteristics of vertical axis tidal turbines,” *Renew Energy*, 81: 926–935 (2015).
72. Y. Guo, L. Liu, X. Lv, and Y. Tang, “The Aerodynamic Analysis of Helical-Type VAWT With Semi Empirical and CFD Method,” *Proceedings of the International Conference on Offshore Mechanics and Arctic Engineering - OMAE*, 10, (2019).
73. B. Hand, G. Kelly, and A. Cashman, “Aerodynamic design and performance parameters of a lift-type vertical axis wind turbine: A comprehensive review,” *Renewable and Sustainable Energy Reviews*, 139: 110699 (2021).
74. A. S. Alexander and A. Santhanakrishnan, “Trapped Cylindrical Flow with Multiple Inlets for Savonius Vertical Axis Wind Turbines,” *Journal of Fluids Engineering, Transactions of the ASME*, 140 (4), (2018).
75. B. F. Blackwell, R. E. Sheldahl, and L. V Feltz, “Wind tunnel performance data for the Darrieus wind turbine with NACA 0012 blades,” Office of Scientific and Technical Information (OSTI), *SAND 1976-0130: USA* (1976).
76. X. Sun, Y. Wang, Q. An, Y. Cao, G. Wu, and D. Huang, “Aerodynamic performance and characteristic of vortex structures for Darrieus wind turbine. II. The relationship between vortex structure and aerodynamic performance,” *Journal of Renewable and Sustainable Energy*, 6 (4), (2014).
77. G. Bedon, U. Schmidt Paulsen, H. Aagaard Madsen, F. Belloni, M. Raciti Castelli, and E. Benini, “Computational assessment of the DeepWind aerodynamic performance with different blade and airfoil configurations,” *Appl Energy*, 185: 1100–1108 (2017).

78. Dr. Stuart Scott, “Wind Turbine Design Exercise,” http://en.wikipedia.org/wiki/Wind_turbine_design, (2023).
79. Q. Li, T. Maeda, Y. Kamada, J. Murata, K. Furukawa, and M. Yamamoto, “Effect of number of blades on aerodynamic forces on a straight-bladed Vertical Axis Wind Turbine,” *Energy*, 90: 784–795 (2015).
80. M. Shiono, K. Suzuki, and S. Kiho, “An experimental study of the characteristics of a Darrieus turbine for tidal power generation,” *Electrical Engineering in Japan*, 132 (3): 38–47 (2000).
81. R. Dominy, P. Lunt, A. Bickerdyke, and J. Dominy, “Self-starting capability of a Darrieus turbine,” *Proceedings of the Institution of Mechanical Engineers, Part A: Journal of Power and Energy*, 221 (1): 111–120 (2007).
82. N. Hill, R. Dominy, G. Ingram, and J. Dominy, “Darrieus turbines: The physics of self-starting,” <http://dx.doi.org/10.1243/09576509JPE615>, 223 (1): 21–29 (2008).
83. B. Hand, G. Kelly, and A. Cashman, “Aerodynamic design and performance parameters of a lift-type vertical axis wind turbine: A comprehensive review,” *Renewable and Sustainable Energy Reviews*, 139: (2021).
84. N. J. Wei, I. D. Brownstein, J. L. Cardona, M. F. Howland, and J. O. Dabiri, “Near-wake structure of full-scale vertical-axis wind turbines,” *J Fluid Mech*, 914: (2019).
85. “Numerical Simulation of Vertical Axis Wind Turbine at Low Speed Ratios.” <https://globaljournals.org/item/3521-numerical-simulation-of-vertical-axis-wind-turbine-at-low-speed-ratios>, (2023).
86. P. Wernert, W. Geissler, M. Raffel, and J. Kompenhans, “Experimental and numerical investigations of dynamic stall on a pitching airfoil,” *AIAA Journal*, 34 (5): 982–989 (1996).
87. G. Brochier, P. Fraunie, C. Beguier, and I. Paraschivoiu, “Water channel experiments of dynamic stall on Darrieus wind turbine blades,” *J Propuls Power*, 2 (5): 445–449 (1986).
88. C. Simão Ferreira, G. van Kuik, G. van Bussel, and F. Scarano, “Visualization by PIV of dynamic stall on a vertical axis wind turbine,” *Exp Fluids*, 46(1):97–108 (2008).
89. D. B. Araya and J. O. Dabiri, “A comparison of wake measurements in motor-driven and flow-driven turbine experiments,” *Exp Fluids*, 56(7), (2015).
90. Q. Li, T. Maeda, Y. Kamada, J. Murata, K. Furukawa, and M. Yamamoto, “Measurement of the flow field around straight-bladed vertical axis wind turbine,” *Journal of Wind Engineering and Industrial Aerodynamics*, 151: 70–78 (2016).

91. C. M. Parker and M. C. Leftwich, "The effect of tip speed ratio on a vertical axis wind turbine at high Reynolds numbers," *Exp Fluids*, 57(5), (2016).
92. K. J. Ryan, F. Coletti, C. J. Elkins, J. O. Dabiri, and J. K. Eaton, "Three-dimensional flow field around and downstream of a subscale model rotating vertical axis wind turbine," *Exp Fluids*, 57 (3), (2016).
93. C. M. Parker, D. B. Araya, and M. C. Leftwich, "Effect of chord-to-diameter ratio on vertical-axis wind turbine wake development," *Exp Fluids*, 58 (12), (2017).
94. L. Battisti *et al.*, "Experimental benchmark data for H-shaped and troposkien VAWT architectures," *Renew Energy*, 125: 425–444 (2018).
95. A.-J. Buchner, J. Soria, D. Honnery, and A. J. Smits, "Dynamic stall in vertical axis wind turbines: scaling and topological considerations," *J Fluid Mech*, 841: 746–766 (2018).
96. T. C. Hohman, L. Martinelli, and A. J. Smits, "The effects of inflow conditions on vertical axis wind turbine wake structure and performance," *Journal of Wind Engineering and Industrial Aerodynamics*, 183: 1–18 (2018).
97. S. Zanforlin and T. Nishino, "Fluid dynamic mechanisms of enhanced power generation by closely spaced vertical axis wind turbines," *Renew Energy*, 99: 1213–1226 (2016).
98. S. Nazari, M. Zamani, and S. A. Moshizi, "Comparison between two-dimensional and three-dimensional computational fluid dynamics techniques for two straight-bladed vertical-axis wind turbines in inline arrangement," *Wind Engineering*, 42(6): 647–664 (2018).
99. A. Rezaeiha, H. Montazeri, and B. Blocken, "Characterization of aerodynamic performance of vertical axis wind turbines: Impact of operational parameters," *Energy Convers Manag*, 169: 45–77 (2018).
100. A. Rezaeiha, H. Montazeri, and B. Blocken, "Towards optimal aerodynamic design of vertical axis wind turbines: Impact of solidity and number of blades," *Energy*, 165: 1129–1148 (2018).
101. S. Brusca, R. Lanzafame, and M. Messina, "Design of a vertical-axis wind turbine: how the aspect ratio affects the turbine's performance," *International Journal of Energy and Environmental Engineering*, 5 (4): 333–340 (2014).
102. S. Zanforlin and S. Deluca, "Effects of the Reynolds number and the tip losses on the optimal aspect ratio of straight-bladed Vertical Axis Wind Turbines," *Energy*, 148: 179–195 (2018).
103. "Theory of Wing Sections, Including a Summary of Airfoil Data - Ira Herbert Abbott, Albert Edward Von Doenhoff -Google." Available: https://books.google.iq/books/about/Theory_of_Wing_Sections_Including_a_Summ.html?id=DPZYUGNyuboC&redir_esc=y, (2023).

104. F. Balduzzi, J. Drofelnik, A. Bianchini, G. Ferrara, L. Ferrari, and M. S. Campobasso, "Darrieus wind turbine blade unsteady aerodynamics: a three-dimensional Navier-Stokes CFD assessment," *Energy*, 128: 550–563 (2017).
105. Q. Li *et al.*, "Wind tunnel and numerical study of a straight-bladed vertical axis wind turbine in three-dimensional analysis (Part I: For predicting aerodynamic loads and performance)," *Energy*, 106: 443–452 (2016).
106. Q. Li *et al.*, "Effect of rotor aspect ratio and solidity on a straight-bladed vertical axis wind turbine in three-dimensional analysis by the panel method," *Energy*, 121: 1–9 (2017).
107. Y. Li, N. Karri, and Q. Wang, "Three-dimensional numerical analysis on blade response of a vertical-axis tidal current turbine under operational conditions," *Journal of Renewable and Sustainable Energy*, 6 (4): (2014).
108. S. Lee, K. Kim, W. Choi, and S. Lee, "Annoyance caused by amplitude modulation of wind turbine noise," *Noise Control Eng J*, 59 (1): 38 (2011).
109. E. P. TORRANCE and K. GOFF, "A Quiet Revolution," *J Creat Behav*, 23 (2): 136–145 (1989).
110. E. Pedersen, "Health aspects associated with wind turbine noise—Results from three field studies," *Noise Control Eng J*, 59 (1): 47 (2011).
111. "Punch, J et al, Wind Turbine Noise, What Audiologists Should Know | Waubra Foundation." Available: <https://waubrafoundation.org.au/resources/punch-j-et-al-wind-turbine-noise-what-audiologists-should-know/>, (2023).
112. E. Son, H. Kim, H. Kim, W. Choi, and S. Lee, "Integrated numerical method for the prediction of wind turbine noise and the long range propagation," *Current Applied Physics*, 10 (2): S316–S319 (2010).
113. S. Oerlemans, M. Fisher, T. Maeder, and K. Kögler, "Reduction of Wind Turbine Noise Using Optimized Airfoils and Trailing-Edge Serrations," *AIAA Journal*, 47 (6): 1470–1481 (2009).
114. A. Tabassum, T. Abbasi, and S.A. Abbasi "Wind Energy Increasing Deployment Rising Environmental Concerns": Noise Emissions," *Sustain Energy Rev.*, 31:270-288 (2014).
115. "Wind farms are not only beautiful, they're absolutely necessary | Simon Gourlay | The Guardian." Available:<https://www.theguardian.com/commentisfree/2008/aug/12/windpower.alternativeenergy>, (2023).
116. E. Hau, "Wind turbines: Fundamentals, technologies, application, economics", *SPRING*, U.K., 1–783 (2013).

117. “The Aesthetics of Wind Energy - Nexus Media News.”, Available: <https://nexusmedianews.com/the-aesthetics-of-wind-energy-7a610c1e5b0a/>, (2023).
118. B. Möller, “Changing wind-power landscapes: regional assessment of visual impact on land use and population in Northern Jutland, Denmark,” *Appl Energy*, 83 (5): 477–494 (2006).
119. T. Tsoutsos, A. Tsouchlaraki, M. Tsiropoulos, and M. Serpetsidakis, “Visual impact evaluation of a wind park in a Greek island,” *Appl Energy*, 86 (4): 546–553 (2009).
120. “Texas Wind Farm Uses NASA Radar to Prevent Bird Deaths – Impact Lab.”, Available: <https://www.impactlab.com/2009/05/02/texas-wind-farm-uses-nasa-radar-to-prevent-bird-deaths/>, (2023).
121. W. Tesfahunegny, D. Datiko, M. Wale, G. E. Hailay, and T. Hunduma, “Impact of wind energy development on birds and bats: the case of Adama wind farm, Central Ethiopia,” *The Journal of Basic and Applied Zoology*, 81 (1): 1–9 (2020).
122. “Effects of offshore wind farm noise on marine mammals and fish. | IOGP EIA Tool - International Association of Oil & Gas Producers.”, Available: <https://usrd.iogp.org/resource/effects-of-offshore-wind-farm-noise-on-marine-mammals-and-fish/>, (2023).
123. “Are wind farms changing the weather? | South China Morning Post.”, Available: <https://www.scmp.com/article/731506/are-wind-farms-changing-weather>, (2023).
124. “How Wind Turbines Affect Your (Very) Local Weather | Scientific American.”, Available: <https://www.scientificamerican.com/article/how-wind-turbines-affect-temperature>, (2023).
125. D. W. Keith *et al.*, “The influence of large-scale wind power on global climate,” *Proc Natl Acad Sci U S A*, 101 (46): 16115–16120 (2004).
126. M. Premalatha, T. Abbasi, and S. Abbasi, “Wind energy: Increasing deployment, rising environmental concerns,” 31: 270-288 (2014).
127. M. C. Claessens, “The Design and Testing of Airfoils for Application in Small Vertical Axis Wind Turbines.” <https://repository.tudelft.nl/islandora/object/uuid%3Afe4a7ae3-103e-40f3-a1f1-ae6d910d8c71>, (2023).
128. L. A. Danao, N. Qin, and R. Howell, “A numerical study of blade thickness and camber effects on vertical axis wind turbines,” *Proceedings of the Institution of Mechanical Engineers, Part A: Journal of Power and Energy*, 226 (7): 867–881 (2012).

129. C. S. Ferreira and B. Geurts, “Aerofoil optimization for vertical-axis wind turbines,” *Wind Energy*, 18 (8): 1371–1385 (2015).
130. M. Zamani, M. J. Maghrebi, and S. R. Varedi, “Starting torque improvement using J-shaped straight-bladed Darrieus vertical axis wind turbine by means of numerical simulation,” *Renew Energy*, 95: 109–126 (2016).
131. Z. Wang, Y. Wang, and M. Zhuang, “Improvement of the aerodynamic performance of vertical axis wind turbines with leading-edge serrations and helical blades using CFD and Taguchi method,” *Energy Convers Manag*, 177: 107–121, (2018).
132. A. Bianchini, F. Balduzzi, D. Di Rosa, and G. Ferrara, “On the use of Gurney Flaps for the aerodynamic performance augmentation of Darrieus wind turbines,” *Energy Convers Manag*, 184: 402–415 (2019).
133. F. Balduzzi *et al.*, “Understanding the Aerodynamic Behavior and Energy Conversion Capability of Small Darrieus Vertical Axis Wind Turbines in Turbulent Flows,” *Energies (Basel)*, 13 (11): 2936, (2020).
134. S. Das Karmakar and H. Chattopadhyay, “A review of augmentation methods to enhance the performance of vertical axis wind turbine,” *Sustainable Energy Technologies and Assessments*, 53: 102469 (2022).
135. I. F. Zidane, H. M. Ali, G. Swadener, Y. A. Eldrainy, and A. I. Shehata, “Effect of upstream deflector utilization on H-Darrieus wind turbine performance: An optimization study,” *Alexandria Engineering Journal*, 63: 175–189 (2023).
136. Internet: “DU 06-W-200 VAWT airfoil (du06-w-200-dt).” <http://airfoiltools.com/airfoil/details?airfoil=du06-w-200-dt>, (2023).
137. J. F. Manwell, J. G. McGowan, and A. L. Rogers, “Wind Energy Explained: Theory, Design and Application”, *DNV- Global Energy Concepts*, Washington, USA (2010).
138. T. Burton, D. Sharpe, N. Jenkins, and E. Bossanyi, “Wind Energy Handbook”, *Wiley*, U.K., (2011).
139. Q. Li, T. Maeda, Y. Kamada, J. Murata, K. Furukawa, and M. Yamamoto, “Effect of number of blades on aerodynamic forces on a straight-bladed Vertical Axis Wind Turbine,” *Energy*, 90:784–795 (2015).
140. S. Kulkarni, “Design study of a horizontal axis tidal turbine blade”, Phd Thesis, *Birmingham City University*, United kingdom, 31–32(2016).
141. D. Han Y. Gun, N. Joon and S. Hyun, “Design, Fabrication, and Performance Test of a 100-W Helical-Blade Vertical-Axis Wind Turbine at Low Tip-Speed Ratio”, *MDPI Journal Energies*, 11(6): 1517 (2018).
142. D. Zhao, N. Han, E. Goh, J. Cater, and A. Reinecke, “Wind turbines and aerodynamics energy harvesters”, *ELSEVIER*, U.K. , 1–530 (2019).

143. I. Paraschivoiu, "Aerodynamic Loads and Performance of the Darrieus Rotor", *Journal of Energy*, 6 (6): 406–412 (1982).
144. Newman BG, "Actuator-disc theory for vertical-axis wind turbines," *Journal of Wind Engineering and Industrial Aerodynamics*, (1983).
145. G. Bangga, A. Dessoky, T. Lutz, and E. Krämer, "Improved double-multiple-streamtube approach for H-Darrieus vertical axis wind turbine computations," *Energy*, 182: 673–688, (2019).
146. M. T. Brahim, A. Allet, and I. Paraschivoiu, "Aerodynamic Analysis Models for Vertical-Axis Wind Turbines," *International Journal of Rotating Machinery*, 2 (1): 15–21 (1995).
147. L. M. Milne Thomson, "Theoretical aerodynamics", <https://search.worldcat.org/title/theoretical-aerodynamics-by-lm-milne-thomson/oclc/859841764#goodreads>, (2023).
148. J. N. Sorensen, "Aerodynamic Analysis of Wind Turbines," *Compr. Renew Energy*, 2: 225-241 (2012).
149. N. M. Ali, a. H. A. K., and s. Aljabair, "the effect of darrieus and savonius wind turbines position on the performance of the hybrid wind turbine at low wind speed," *international journal of mechanical engineering and technology (ijmet)*, 11 (2), (2020).
150. S. Aljabair, N. M. Ali, and A. A. Hassan, "An Experimental and Numerical Investigation on Darrieus Vertical Axis Wind Turbine Types at Low Wind speed <https://www.researchgate.net/publication/339271837>, (2023).
151. N. M. Ali, Dr. A. K. A. Hassan, and Dr. S. Aljabair, "Effect of Conventional Multistage Savonius wind Turbines on the Performance of the Turbine at Low Wind Velocity," *Journal of Advanced Research in Dynamical and Control Systems*, 11 (11): 229–239 (2019).
152. M. Zamani, S. Nazari, S. A. Moshizi, and M. J. Maghrebi, "Three dimensional simulation of J-shaped Darrieus vertical axis wind turbine," *Energy*, 116: 1243–1255 (2016).
153. J. Králik, L. Konečná, D. Lavrinčíková, "Experimental Validation of Computer Fluid Dynamics Simulation aimed on Pressure Distribution on Gable Roof of Low-rise Building," *Procedia Engineering*, 190: 377–384 (2017).
154. "Menter's Shear Stress Transport-Wikipedia." https://en.m.wikipedia.org/wiki/Menter%27s_Shear_Stress_Transport, (2023).
155. S. Shukla, C. J. Ramanan, B. Jyoti Bora, A. Deo, and N. Alom, "Numerical analysis of vertical axis wind turbine blades in ANSYS Fluent," *Mater Today Proc*, 59: 1781–1785 (2022).

APPENDIX A.

TABLES

Airfoil DU06W200 details.

X**	Y**	X	Y	X	Y
10.00030	0.00330	5.55676	0.76339	1.07876	0.81772
9.95071	0.00991	5.43792	0.78282	0.97863	0.78610
9.88745	0.01790	5.31879	0.80195	0.88085	0.75175
9.80844	0.02821	5.19984	0.82060	0.78586	0.71484
9.71354	0.04134	5.08056	0.83885	0.69402	0.67515
9.60703	0.05676	4.96115	0.85679	0.60586	0.63284
9.49361	0.07380	4.84187	0.87431	0.52175	0.58794
9.37673	0.09188	4.72242	0.89147	0.44254	0.54063
9.25781	0.11064	4.60354	0.90814	0.36871	0.49124
9.13799	0.12967	4.48446	0.92426	0.30107	0.44037
9.01782	0.14892	4.36599	0.93990	0.24057	0.38898
8.89754	0.16828	4.24787	0.95466	0.18781	0.33816
8.77727	0.18779	4.13003	0.96877	0.14332	0.28930
8.65704	0.20741	4.01290	0.98182	0.10681	0.24359
8.53697	0.22719	3.89595	0.99392	0.07756	0.20195
8.41679	0.24714	3.77963	1.00483	0.05460	0.16479
8.29686	0.26717	3.66361	1.01453	0.03720	0.13151
8.17740	0.28741	3.54814	1.02282	0.02419	0.10168
8.05771	0.30796	3.43266	1.02969	0.01446	0.07489
7.93799	0.32857	3.31726	1.03514	0.00702	0.05102
7.81854	0.34939	3.20178	1.03912	0.00259	0.02932
7.69889	0.37053	3.08593	1.04180	0.00038	0.00944
7.57924	0.39180	2.97054	1.04309	0.00046	-0.00911
7.46007	0.41327	2.85489	1.04290	0.00385	-0.02855
7.34077	0.43511	2.73928	1.04142	0.00980	-0.04968
7.22128	0.45716	2.62419	1.03851	0.01862	-0.07256
7.10225	0.47936	2.50920	1.03406	0.03065	-0.09755
6.98325	0.50176	2.39441	1.02815	0.04630	-0.12507
6.86453	0.52417	2.28016	1.02074	0.06653	-0.15533
6.74589	0.54685	2.16637	1.01172	0.09224	-0.18871
6.62687	0.56949	2.05318	1.00103	0.12477	-0.22518
6.50773	0.59221	1.94052	0.98861	0.16534	-0.26484
6.38859	0.61480	1.82866	0.97447	0.21456	-0.30740
6.26934	0.63716	1.71792	0.95845	0.27288	-0.35182
6.15006	0.65934	1.60792	0.94042	0.33970	-0.39704
6.03147	0.68109	1.49938	0.92038	0.41417	-0.44177
5.91292	0.70229	1.39170	0.89806	0.49507	-0.48508
5.79430	0.72307	1.28563	0.87366	0.58159	-0.52655
5.67547	0.74343	1.18128	0.84689	0.67244	-0.56572

X	Y	X	Y	X	Y
0.76717	-0.60244	4.05087	-0.91739	7.42078	-0.34463
0.86510	-0.63669	4.16892	-0.91073	7.53726	-0.31815
0.96591	-0.66865	4.28714	-0.90318	7.65344	-0.29234
1.06888	-0.69816	4.40534	-0.89484	7.76960	-0.26740
1.17402	-0.72555	4.52348	-0.88562	7.88585	-0.24315
1.28085	-0.75067	4.64176	-0.87561	8.00182	-0.21981
1.38941	-0.77391	4.75993	-0.86480	8.11752	-0.19742
1.49918	-0.79520	4.87811	-0.85322	8.23301	-0.17617
1.61017	-0.81472	4.99605	-0.84091	8.34860	-0.15593
1.72199	-0.83251	5.11354	-0.82780	8.46387	-0.13685
1.83459	-0.84857	5.23068	-0.81386	8.57897	-0.11903
1.94835	-0.86310	5.34692	-0.79904	8.69394	-0.10249
2.06246	-0.87627	5.46245	-0.78317	8.80860	-0.08731
2.17718	-0.88783	5.57686	-0.76620	8.92291	-0.07367
2.29267	-0.89822	5.69025	-0.74781	9.03719	-0.06160
2.40824	-0.90722	5.80320	-0.72781	9.15150	-0.05108
2.52445	-0.91498	5.91592	-0.70620	9.26586	-0.04214
2.64104	-0.92160	6.02880	-0.68293	9.38030	-0.03470
2.75771	-0.92709	6.14212	-0.65812	9.49424	-0.02872
2.87455	-0.93136	6.25585	-0.63191	9.60662	-0.02393
2.99179	-0.93459	6.37030	-0.60434	9.71321	-0.01989
3.10901	-0.93673	6.48597	-0.57558	9.80723	-0.01708
3.22646	-0.93783	6.60268	-0.54610	9.88627	-0.01544
3.34386	-0.93785	6.71981	-0.51627	9.94978	-0.01364
3.46164	-0.93688	6.83701	-0.48657	9.99970	-0.01169
3.57917	-0.93494	6.95430	-0.45719		
3.69702	-0.93194	7.07153	-0.42807		
3.81483	-0.92805	7.18795	-0.39964		
3.93277	-0.92315	7.30458	-0.37180		

* <http://airfoiltools.com/airfoil/details?airfoil=du06-w-200-dt>.

- ** Dimensions of X and Y (cm).
- *** Details of DU 06-W-200 airfoil:
 - Max thickness 19.8% at 31.1% chord.
 - Max camber 0.5% at 84.6% chord.

APPENDIX B.

CONTOUR FIGURES FOR DESIGNS.

1, 2, and 3 show the streamlines contours for Designs 1, 3, and 4, respectively, for non-uniform And Figures 4, 5, and 6 show the time step contours for Design 4, respectively, for non-uniform

B.1.Show the streamlines contours for Designs

Design 1 streamlines contours at TSR, which is equal to 5 for non-uniform.

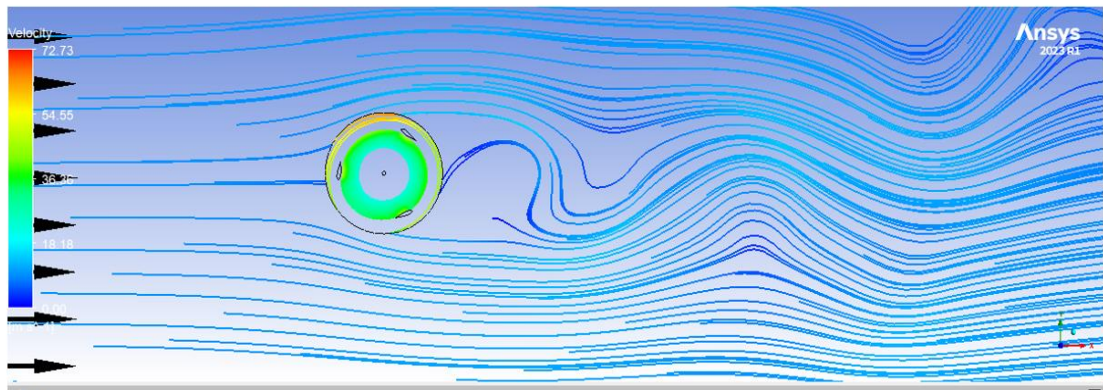


Figure Appendix B1. Streamlines contours, Design 1.

Design 3 streamlines contours at TSR, which is equal to 3.25 for non-uniform.

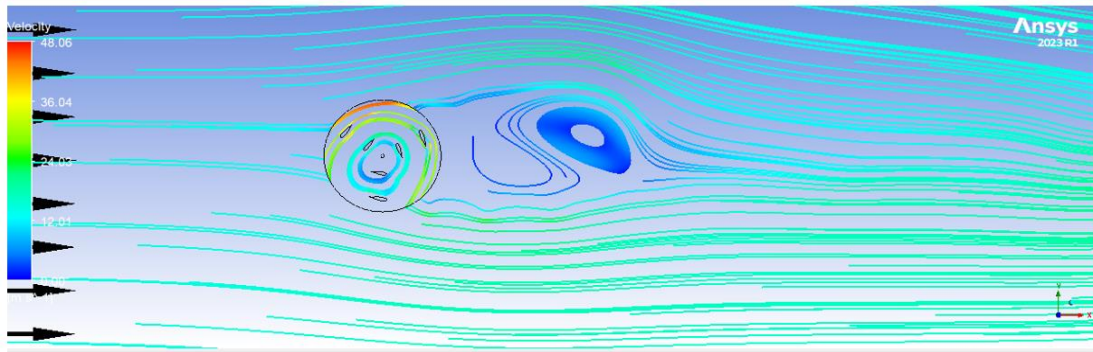


Figure Appendix B2. Streamlines contours, Design 3.

Design 4 streamlines contours at TSR, which is equal to 1 for non-uniform.

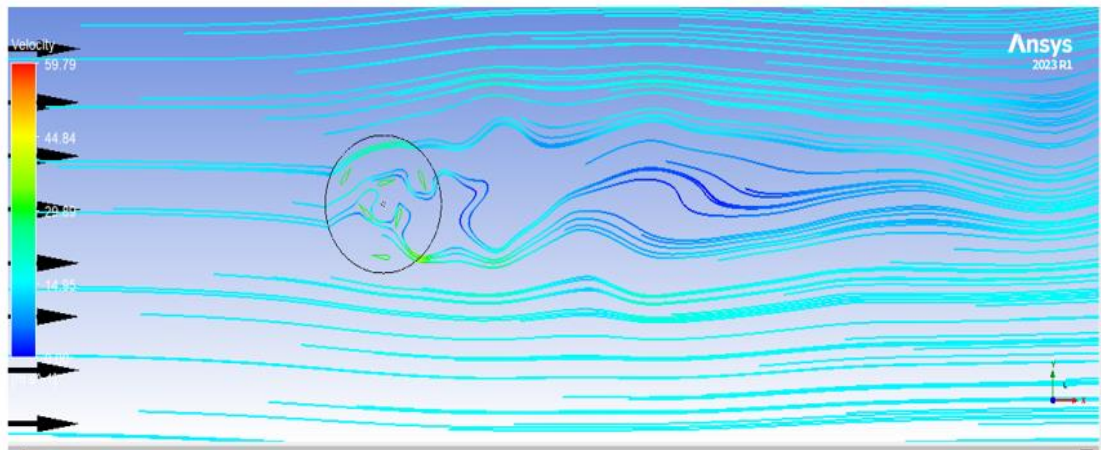


Figure Appendix B3. Streamlines contours, Design 4.

B.2. Show The Time Step Contours For Design 4

Design 4, time step contour at 1.02102 seconds and TSR equal to 1

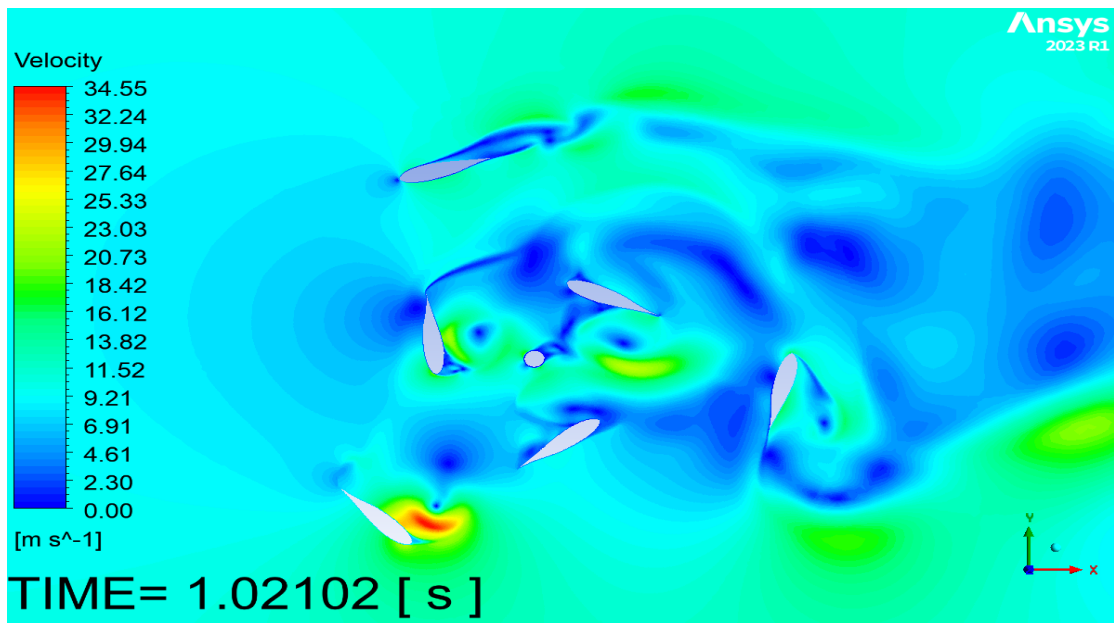


Figure Appendix B4. Time step contour at 1.02102 seconds, Design 4.

Design 4, time step contour at 3.06305 seconds and TSR equal to 1

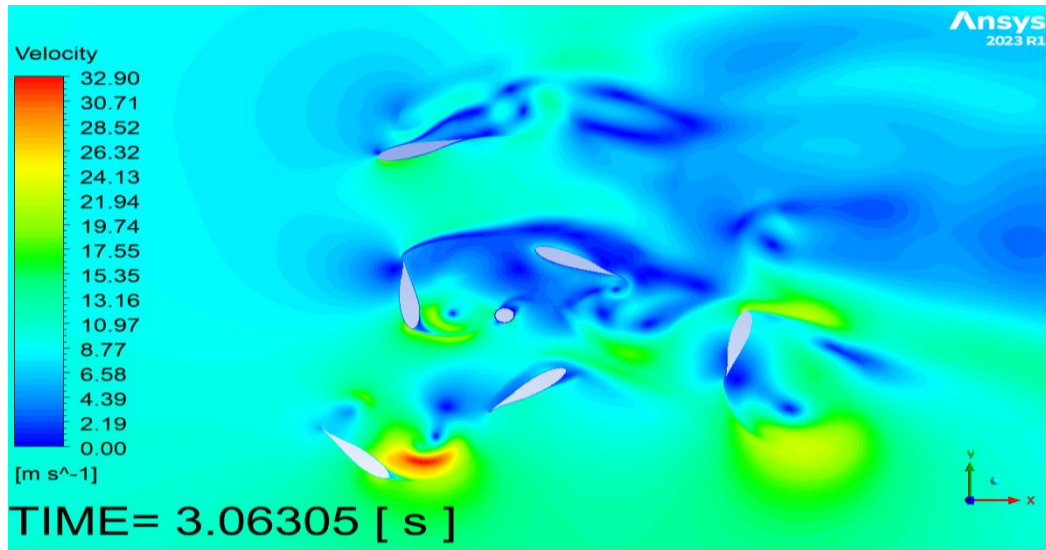


Figure Appendix B5. Time step contour at 3.06305 seconds, Design 4.

Design 4, time step contour at 7.85049 seconds and TSR equal to 1

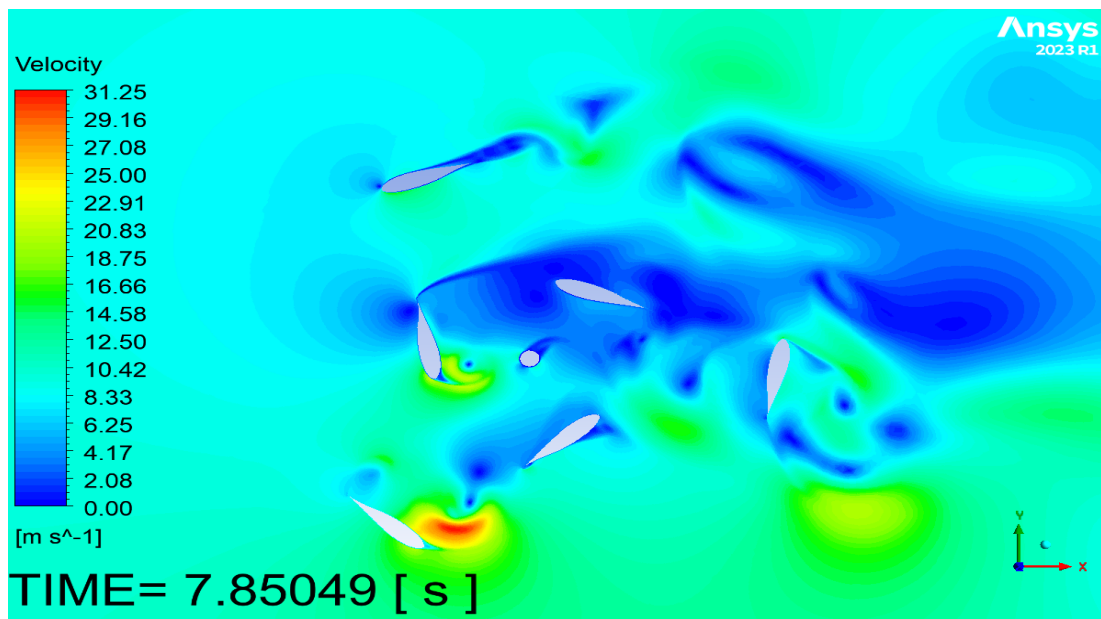


Figure Appendix B6. Time step contour at 7.85049 seconds, Design 4.

RESUME

Yasser Abbas Ali AL-SUDANI he received his primary, middle, and secondary education, then joined the College of Engineering / Al-Mustansiriya University's Department of Mechanical Engineering in 1996 and graduated in 2001. He worked in the field of engineering design for Water pumping stations, compressed air systems, and firefighting systems; then, he worked in the field of energy. For oil refineries for several years. In 2022, he started his academic career as a graduate student at Karabük University Higher Education Institute for his master's degree.